Hydrogen Production via Simultaneous Methane Reforming and Water Splitting Processes using Membrane Reactor

By

Sureena binti Abdullah

A Thesis Submitted for the Degree of Doctor of Philosophy (PhD) in Chemical Engineering at Newcastle University, United Kingdom

School of Chemical Engineering and Advanced Material

November 2014

Abstract

The main objective of this study is to investigate on the ability of a perovskite-based membrane reactor to produce hydrogen via simultaneous reforming and water splitting processes. Being able to perform such processes will confirm on the ability of the membrane system in performing an autothermal production of hydrogen. Initial experiments were conducted to evaluate the ability of two different types of hollow fibre membrane namely $La_{0.6}Sr_{0.4}Co_{0.2}Fe_{0.8}O_{3-\delta}$ (LSCF6428) and $Ba_{0.5}Sr_{0.5}Co_{0.8}Fe_{0.2}O_{3-\delta}$ (BSCF5582) in permeating oxygen in three different inlet configurations. All of the experiments were conducted at 900^{o}C. The LSCF6428 membrane gives lower oxygen permeation rate comparing to BSCF5582 when inert gas argon was used as the sweep gas on the shell side of the membrane. The oxygen permeation rate into the shell side of LSCF6428 membrane reactor was at 0.24μmol$O.s^{-1}$ whereas for BSCF5582 was at 1.50μmol $O.s^{-1}$. The trend is similar when the shell sides were fed with 5% methane and the lumen sides were fed with 10% oxygen. In these experiments, both membranes were stable enough to perform oxygen permeation up to more than 100 hours of operation. BSCF5582 membrane however shows instability in performing oxygen permeation when the lumen side was fed with 4% water and shell side was fed with 5% methane. BSCF5582 membrane was only able to perform oxygen permeation for less than two hours before showing substantial amount of leaks upon breaking. In contrast, the

LSCF6428 membrane shows good stability in the same condition with the shell side oxygen permeation rate of 0.04±0.01μmolO.s^{-1}. The experiment operating time lasted for more than 90 hours. Based on its stability in performing oxygen permeation in the combination of highly reducing and highly oxidising environment, the LSCF6428 membranes were chosen to perform the simultaneous methane reforming and water splitting process in a multiple-membrane based reactor. The results obtained from this experiment proved that simultaneous methane reforming and water splitting can be achieved using a membrane reactor.

Acknowledgements

In the name of Allah, the most beneficent, the most merciful

First of all, I would like to express my gratitude to my supervisor, Professor Ian S. Metcalfe for his endless support, enthusiasm and kindness in helping me to get going and finally finishing my PhD. My appreciation goes to Prof Kang Li and his group from Imperial College London for the supply of the membranes used in this study, without it I wouldn't have learnt how to be a patient and determined person I am today. I am also thankful to the other CEAM staff members; Justine, Simon, Stewart, Bryan, Jamie and Ian Ditchburn for the help that they have given to me along the years of my study. No doubt it is a pleasant time working with all of you in CEAM and things are much easier and faster with the help from all of you.

I wish to thank my entire colleagues in the Applied Catalysis Group, especially to the members of room C501, Claire, Callum, Yousef, Selgin, Henry, Mas, Cristina, Samuel and Vangelis. Thank you for always brighten up my day with jokes, lunches, cakes and presents. I am forever indebted to my family especially my mom, Rohana Cheah Abdullah, abah, Abdullah Ismail and my three brothers, Mohd Hannif, Abu Hannifa and Muhammad Hannafiah. Thanks for your encouragements and advices along the years of my study. The cheerful video conferencing sessions and laughter to cheer me up when I am down. Not forgetting all of my Malaysian friends in Newcastle who

are always there for me through ups and downs, Nas, Baizah, Naimah, Rozi, Min, Nabilah and others who are close to my heart. Last but not least, I would like to thank all of UMP and KPM staffs for the scholarship and helps.

Table of Contents

Nomenclature

List of acronyms

ATR	Autothermal Reforming of Methane
BSCF5582	$Ba_{0.5}Sr_{0.5}Co_{0.8}Fe_{0.2}O_{\delta-3}$
CPO	Catalytic Partial Oxidation
EDX	Energy Dispersive X-Ray Analysis
GC	Gas Chromatography
HEX	Heat Exchanger
HTS	High Temperature Shift
IGCC	Integrated Gasification Combined Cycle
LSCF6428	$La_{0.6}Sr_{0.4}Co_{0.2}Fe_{0.8}O_{\delta-3}$
LTS	Low Temperature Shift
MFC	Mass Flow Controller
MIEC	Mixed Ionic and Electronic Conductor
OTM	Oxygen transport Membrane
PEM	Polymer Electrolytes Membrane
POM	Partial Oxidation of Methane
POX	Partial Oxidation
SEM	Scanning Electron Microscopy
SMR	Steam Methane Reforming
SOFC	Solid Oxide Fuel Cells
STP	Standard temperature and pressure (273.15 K, 1 atm)

TCD	Thermal Conductivity Detector
WGS	Water Gas Shift
YSZ	Yttrium Stabilised Zirconia

List of symbols

ABO_3	Perovskite structure
$CaTiO_3$	Calcium titanium oxide
F	Faraday constant (9.648 70 x 10^4 $Cmol^{-1}$)
F	Flowrate ($mlmin^{-1}$)
J_{O_2}	Oxygen permeation rate define by modified Wagner equation
L	Thickness of membrane
P_A	Permeability of A
P_B	Permeability of B
$p_{O_2(feed)}$	Oxygen partial pressure of feed side
$p_{O_2(perm)}$	Oxygen partial pressure of the permeated side
r_A	radius of the A-site cation
r_B	radius of the B-site cation
r_O	radius of the lattice oxygen anion
R	Ideal gas constant (8.314 J K^{-1} mol^{-1})
T	Temperature (^oC)
V_m	Molar volume of gas at STP (24 465 $mlmol^{-1}$ at 25 °C)
ΔH	Heat of reaction (J mol^{-1})
$\alpha_{A/B}$	Selectivity
σ_{el}	Electronic conductivity
σ_{ion}	Ionic conductivity

Kröger-Vink notation

$V_{\ddot{O}}$	Oxygen vacancy site
O_o^x	Oxygen occupying site
δ	Oxygen vacancies/deficiencies
e^-	electron
h·	Electron holes

Material balance notation

OP_{SS}	Oxygen permeation on the shell side
OP_{LS}	Oxygen permeation on the lumen side
$n_T^{L(x)}$	Total flowrate of lumen side x, where x is the number of lumen used in the experiment; x = 1 or 2
$n_T^{SS(y)}$	Total flowrate of shell side y, where y is the number of reactor; y= 1, 2 or 3
$CH_{4(in)}^{LS(x)/SS(y)}$	The inlet mole fraction of methane on lumen side x or on shell side y, where x is the number of lumen used; x= 1 or 2 and y is the number of reactor used in the experiment; y = 1,2 or 3
$CH_{4(out)}^{LS(x)/SS(y)}$	The outlet mole fraction of methane on lumen side x or on shell side y, where x is the number of lumen used; x= 1 or 2 and y is the number of reactor used in the experiment; y = 1,2 or 3
$CO_{(in)}^{LS(x)/SS(y)}$	The inlet mole fraction of carbon monoxide on lumen side x or on shell side y, where x is the number of lumen used; x= 1 or 2 and y is the number of reactor used in the experiment; y = 1,2 or 3
$CO_{(out)}^{LS(x)/SS(y)}$	The outlet mole fraction of carbon monoxide on lumen side x or on shell side y, where x is the number of lumen used; x= 1 or 2 and y is the number of reactor used in the experiment; y = 1,2 or 3
$CO_{2(in)}^{LS(x)/SS(y)}$	The inlet mole fraction of carbon dioxide on lumen side x or on shell side y, where x is the number of lumen used; x= 1 or 2 and y is the number of reactor used in the experiment; y = 1,2 or 3
$CO_{2(out)}^{LS(x)/SS(y)}$	The outlet mole fraction of carbon dioxide on lumen side x or on shell side y, where x is the number of lumen used; x= 1 or 2

	and y is the number of reactor used in the experiment; y = 1,2 or 3
$H_{2(in)}^{LS(x)/SS(y)}$	The inlet mole fraction of hydrogen on lumen side x or on shell side y, where x is the number of lumen used; x= 1 or 2 and y is the number of reactor used in the experiment; y = 1,2 or 3
$H_{2(out)}^{LS(x)/SS(y)}$	The outlet mole fraction of hydrogen on lumen side x or on shell side y, where x is the number of lumen used; x= 1 or 2 and y is the number of reactor used in the experiment; y = 1,2 or 3
$H_2O_{(out)}^{LS(x)/SS(y)}$	The inlet mole fraction of water on lumen side x or on shell side y, where x is the number of lumen used; x= 1 or 2 and y is the number of reactor used in the experiment; y = 1,2 or 3
$H_2O_{(out)}^{LS(x)/SS(y)}$	The outlet mole fraction of water on lumen side x or on shell side y, where x is the number of lumen used; x= 1 or 2 and y is the number of reactor used in the experiment; y = 1,2 or 3
$O_{2(in)}^{LS(x)/SS(y)}$	The inlet mole fraction of oxygen on lumen side x or on shell side y, where x is the number of lumen used; x= 1 or 2 and y is the number of reactor used in the experiment; y = 1,2 or 3
$O_{2(out)}^{LS(x)/SS(y)}$	The outlet mole fraction of oxygen on lumen side x or on shell side y, where x is the number of lumen used; x= 1 or 2 and y is the number of reactor used in the experiment; y = 1,2 or 3

List of Figures

List of Tables

Chapter 1 Introduction

1.1 Background of the Research

Hydrogen is the lightest substance in the periodic table. It is mainly being used in the production of ammonia, and as the reducing gas in stainless steel production, as a feedstock to the petrochemical industries and as the hydrogenation agent in the food processing industries [1]. It has the highest energy density with nearly three times the energy yield than other hydrocarbon fuels [2]. The fact that hydrogen when burned in air only produces water coupled with high amount of energy makes it easy to claim hydrogen is the cleanest, renewable alternative fuel available to date [3-5].

Globally the largest hydrogen production source is from natural gas followed by fossil fuels and coal [6]. Conventional hydrogen production processes that are widely used in the industries are the steam methane reforming, water gas shift and partial oxidation of methane processes[7]. As these processes are relying too much on the use of fossil fuels, efforts need to be made to find other alternatives for producing hydrogen in a cleaner environment and at a cheaper cost.

Perovskites-type mixed ionic and electronic conductor (MIEC) membranes were claimed to have great potential to be used in hydrogen production membrane

reactors because of their stability and good oxygen permeation attributes[8]. This hydrogen production system relies on the MIEC membranes' ability to separate oxygen from air and/or from other mixtures of gases only through partial pressure differences in the inlet streams.

Recently most of the studies on hydrogen production using MIEC membranes are focussed on the partial oxidation process [9, 10]. This kind of reaction is highly exothermic and energy intensive. It is only recently that a MIEC membrane was seen to have the potential to be used in a direct water splitting process[11]. Studies on combining both water splitting and methane oxidation in a MIEC membrane reactor however, are limited and not well described.

1.2 Scope of the Research

The scope of the research will remain focussed on the ability of oxygen permeation using hollow fibre perovskites membranes to perform water splitting, partial oxidation of methane and full combustion of methane. The main aim of this thesis is to combine the methane oxidation and water splitting processes in the same reactor.

1.3 Objectives of the Research

The objectives of this study are:

1. To solve membrane stability issues by redesigning the membrane reactor; having individual inlets and outlets for better gas analysis and monitoring purposes.
2. To investigate the performance of LSCF6428, BSCF5582 in performing oxygen permeation with and without reducing gas.
3. To investigate the ability of LSCF6428, BSCF5582 to perform the water splitting process with reducing gas on the other side of the membrane.
4. To combine the best membrane that can withstand (2) and (3) in a multiple membrane reactor for a simultaneous methane reforming and water splitting processes.

1.4 Thesis Outline

This thesis is divided into six chapters. The first chapter discusses on the problem statement, the background of the research and scope of the research. Chapter 2 reviews on the use of alternative methods in hydrogen production starting from the early days of hydrogen being produced until the advancement in these methods. State of the art research for the design of the membrane reactor involving an oxygen transport membrane will also be discussed in detail. Further description on the theory and the advancement this study will contribute to the body of knowledge in the membrane reactor field will also be looked at in detail.

Chapter 3 deals with the preliminary results run for individual membrane for (i) oxygen permeation without reducing gas on the shell side (ii) oxygen permeation with methane reforming reactions on the shell side and (iii) oxygen permeation performance having methane reforming reactions on the shell side and water splitting processes on the lumen side. These three types of experiments were run on two different membrane materials namely $La_{0.6}Sr_{0.4}Co_{0.2}Fe_{0.8}O_{3-\delta}$ (LSCF6428) and $Ba_{0.5}Sr_{0.5}Co_{0.8}Fe_{0.2}O_{3-\delta}$ (BSCF5582). Thorough explanations are made on the experimental techniques, membrane characterisation, reactor setup, leak tests and gas analysis in this chapter. The calculation techniques and error propagation applied in the calculations will also be discussed.

Chapter 4 will discuss the preliminary experiment of an autothermal process. In this chapter only one type of selected hollow fibre was used; the LSCF6428 membrane. The membrane was used to perform (i) oxygen permeation from oxygen feed stream and (ii) water splitting processes in the both the different lumens. The shell was fed with methane to assist the oxygen permeation and simultaneously perform methane reforming processes. Further analysis from the results obtained from this chapter revealed that the amount of oxygen permeated into the shell increased the oxygen partial pressure in the shell side and halted the water splitting in the lumen of the second LSCF6428 membrane. Determining the cause led to several modifications aiming to increase the oxygen utilisation in the shell side. Only one of them showed good results.

In Chapter 5 the processes conducted in and discussed previously in Chapter 4 were separated into three reactors namely Reactor 1 (R1), Reactor 2 (R2) and Reactor 3 (R3). Three reactors were used to separate the processes; R1 is specifically aimed for full combustion and partial oxidation of methane reactions in the shell side and

oxygen permeation in the lumen side. R2 is used to further improve the selectivity of CO over CO_2 in the product stream of the shell side from R1 and R3 is for methane reforming in the shell side and water splitting processes in the lumen side of the membrane. Results are discussed in terms of the total oxygen permeation rates throughout the whole system, selectivity of CO in R2 and hydrogen production rates from the water splitting process in R3.

The summary and conclusions achieved in the experiments conducted in this study are presented in Chapter 6.

Chapter 2 Literature Review

2.1 Introduction

The very first hydrogen production process was said to be discovered by Sir William Grove in 1839 through a simple steam decomposition reaction experiment. It was also documented that hydrogen has been used as an energy carrier particularly for heating purposes in most parts of Europe prior to the discovery of fossil fuel. The production and use of hydrogen however slowly declined with the discovery of fossil fuel.

Currently there are more than 30 variations of the methods used by the researcher to produce hydrogen. The feedstock used in the process of hydrogen production can be from unrenewable resources such as natural gas[12], coal[13, 14] and hydrocarbons from petroleum oil[15]. Other sources can also be from renewable resources such as biomass[16], ethanol[17] and water[18] assisted by heat, sunlight[19, 20], electricity and winds.

This chapter will provide an overview of the commercially available hydrogen production methods with some of the state-of-the-art improvements made on the readily available methods. This is followed by an introduction of the membrane system used in hydrogen production studies, the use a perovskite-type mixed ionic and electronic conductor (MIEC) membrane in processes such as partial oxidation of methane and water splitting as part of a hydrogen production system.

2.2 Commercial Hydrogen Production Processes

The most common type of reactions involved in hydrogen production processes that are currently used in industry are the steam methane reforming, water gas shift, partial oxidation of methane and autothermal reforming. These processes are not independent but are used together in most of the hydrogen production plants.

2.2.1 Steam Methane Reforming (SMR)

Steam methane reforming is the most common process used for the production of hydrogen in industry [21, 22]. In this process the feed gas, normally natural gas is reacted with steam in a catalytic environment (normally nickel-based) to produce carbon monoxide, carbon dioxide and hydrogen. This process is highly endothermic (refer Equation 2.1 and Equation 2.2). In this reforming stage methane is reacted with steam at high temperature normally ranging from 850°C to 1000°C and operating pressure between 15 to 20bar [23].

$$CH_4 + 2H_2O \rightleftharpoons CO_2 + 4H_2 \qquad \Delta H^{o}_{298} = +165 kJmol^{-1} \qquad \text{Equation 2.1}$$

$$CH_4 + H_2O \leftrightarrow CO + 3H_2 \qquad \Delta H^{o} = +206 kJmol^{-1} \qquad \text{Equation 2.2}$$

Further products in the steam reforming process are then transferred to another reactor to perform the water gas shift reaction to increase the production of hydrogen; refer Equation 2.3.

$$CO + H_2O \leftrightarrow CO_2 + H_2 \qquad \Delta H^o = -41 kJmol^{-1} \qquad \text{Equation 2.3}$$

Figure 2.1 shows the process flow diagram of a conventional SMR process.

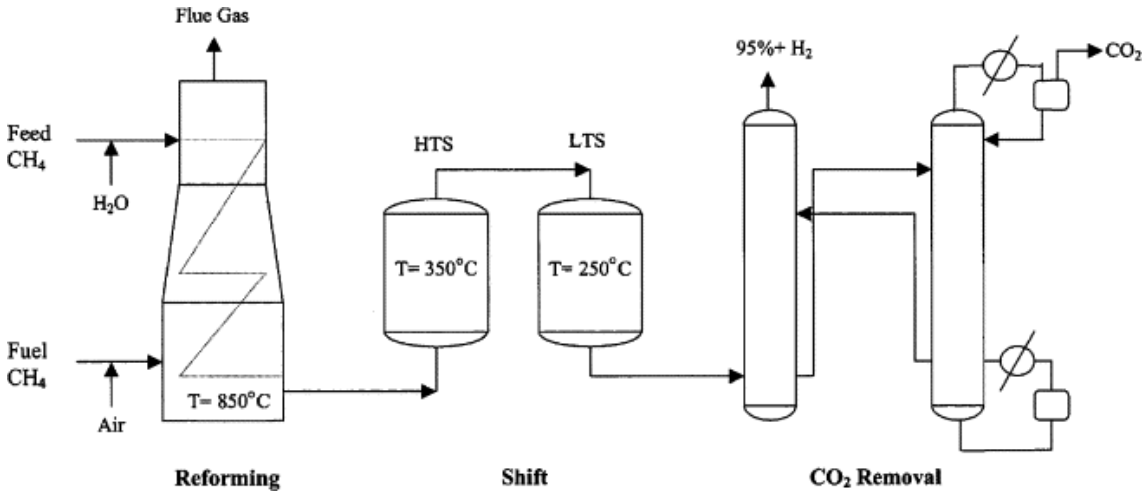

Figure 2.1: The schematic diagram of SMR process [24]

After the reaction process the product stream containing carbon dioxide, carbon monoxide and hydrogen need to go through hydrogen purification process. The main technology that is being used in this step can normally be cryogenic distillation or pressure swing adsorption (PSA)[25, 26].

The main drawbacks of SMR process is that the overall reactions are highly endothermic[27] and low conversion of methane at moderate temperature[28]. Furthermore the separation processes involved are energy intensive[29]. In this case, to maintain the production selectivity towards producing hydrogen the system temperature needs to be maintained at high temperature and to do that a higher energy input is needed.

Current research to improve the production and purity of hydrogen is more focussed on the use of new catalysts. Different types of catalyst were studied by the researchers in order to increase the selectivity of hydrogen production in the reformer. Among them are nickel, platinum, ruthenium, rhodium and others [30, 31]. On the separation part, improvements include changes in design of the separation unit for example, the use of sorption material for the removal of carbon dioxide [32] and changes in bed volume in the PSA unit [33, 34]. Lately studies on the improvement of the downstream process of the steam methane reforming plant started to incorporate the use of a membrane reactor; the membrane of interest is the palladium membrane.

The role of membrane systems are normally focussed on the separation unit used for carbon dioxide removal. The first hydrogen transport membranes to be associated with the hydrogen production processing technique that have been studied over the past decades are metallic membranes; primarily focussed on palladium (Pd) alloy membranes [35]. Palladium, a metal from group 10 of periodic table, finds its use in the ultra-pure hydrogen recoveries because of its ability to bind with the hydrogen atoms at elevated temperature [36, 37]. The hydrogen separation process via a palladium membrane involves seven steps [38]; (i)External diffusion (ii)Dissociation (iii)Dissolution (iv)Internal Diffusion (v)Association (vi)Desorption and (vii) External diffusion. Figure 2.2 demonstrates the seven hydrogen separation steps in Pd membrane.

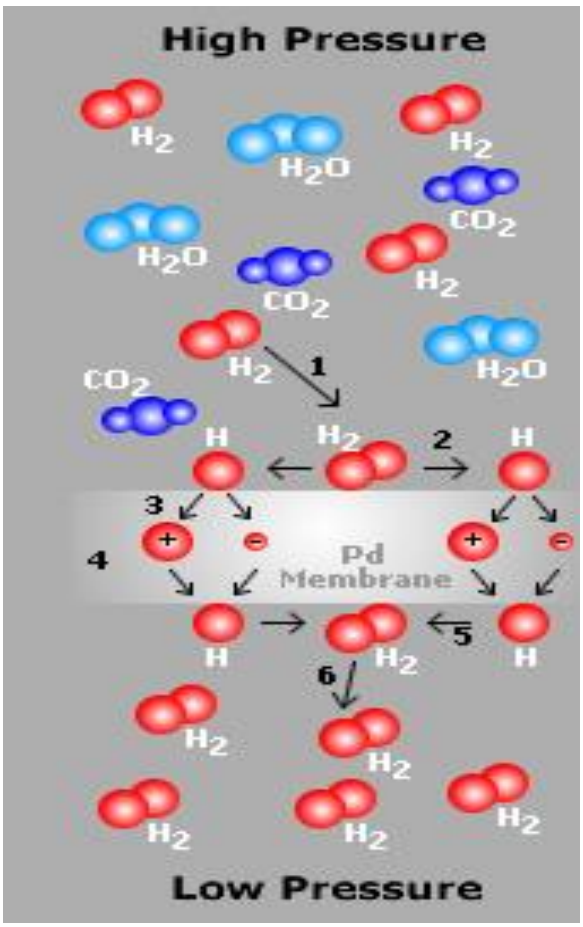

Figure 2.2: Hydrogen permeation activity with Pd membrane[14]

Currently Pd membranes are still being studied by researchers and are more focussed on combining another material to form a hybrid membrane to improve the hydrogen separation for the products of the WGS reaction and its stability in the operating conditions after the hydrogen production units [39].

2.2.2 Partial Oxidation (POX)

Partial oxidation is another process preferred in the hydrogen production industries. In a partial oxidation process, a small amount of air is mixed with a light

hydrocarbon (usually methane) to be partially oxidised or combusted in a chamber [40]. Refer Equation 2.4.

$$CH_4 + \frac{1}{2}O_2 \leftrightarrow CO + 2H_2 \qquad \Delta H^o = -36 kJmol^{-1} \qquad \text{Equation 2.4}$$

The conversion of methane for this process is more than 90% operating at temperature higher than 750^{o}C [41]. The reaction is slightly exothermic but requires an operating temperature of between 1300 – 1500^{o}C although studies have shown that the best conversion can be achieved at *ca* 730^{o}C [42]. This is particularly to avoid the Boudouard Reaction; a reaction that will cause carbon deposition and methane decomposition, resulting in an incomplete conversion of methane [43].

Meanwhile studies have shown that the same yield and selectivity of hydrogen can be maintained at a lower operating temperature by using catalysts such as nickel and cobalt [44] . This started the interest in Catalytic Partial Oxidation (CPO) among researchers. Currently the interest in CPO research is more focussed on the improvement of the process operating parameters such as temperature, pressure and reactant compositions. The type of catalyst of interest in the CPO studies ranges from noble- catalysts such as nickel, platinum, cobalt to the less common ones such as copper and YSZ [45, 46] [47].

Similar to the SMR process, the conventional POM process needs either air or pure oxygen as reactant in producing hydrogen. By using air as the reactant, the final products of POM need to be further purified by using a series of costly separation processes. Likewise in the case of using pure oxygen as reactant, oxygen production

will still need those costly and energy intensive separation units like PSA and cryogenic distillation units [48].

2.2.3 Autothermal Reforming of Methane (ATR)

ATR is a process that combines the CPO and SMR reaction. These reactions were combined to react in the same reactor. As reviewed previously, the CPO like the POM is an exothermic reaction while the SMR is an endothermic reaction.

Combining both of these reactions will counterbalance the energy needed and minimise the energy input to the hydrogen production process. The combined reaction equation is as follows;

$$4CH_4 + O_2 + 2H_2O \longrightarrow 10H_2 + 4CO \qquad \text{Equation 2.5}$$

ATR is considered an economical process because the heat from the CPO (the partial oxidation reaction) supplies most of the heat needed to drive the catalytic steam reforming. Figure 2.3 shows the differences between the ATR, POX and CPO.

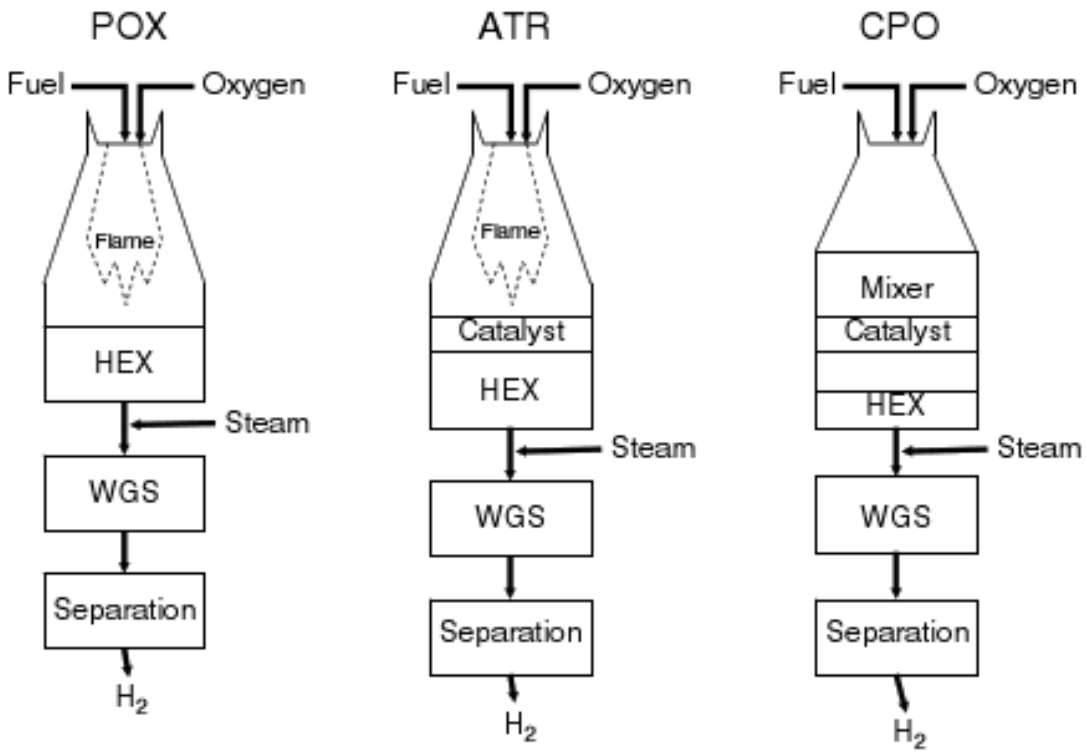

Figure 2.3: The difference in the furnace configurations used in partial oxidation of methane, autothermal reforming and catalytic partial oxidation of methane processes [49].

In an ATR reactor, fuel is mixed with oxygen to initiate CPO. Typically, normal operating temperature for the combustion furnace could start from 2000^{o}C and not less than 1000^{o}C for the catalytic zone [50]. As there is a great difference in operating temperature between these two zones, the catalyst needs to be selected from high thermal resistance materials [51]. Other advantages of the ATR process are lower operating pressure, low methane slip (unreacted methane found in the exhaust of the reactor) and produce higher yield of hydrogen [52] [53, 54].

Recently researchers started to develop a membrane-based ATR reactor with the aim to produce pure hydrogen[55]. Gallucci *et al* [56, 57] suggested the use of a hybrid system using the ATR process in a fluidized bed membrane reactor to

produce pure hydrogen as the product. Figure 2.4 shows the reactor design used for the study.

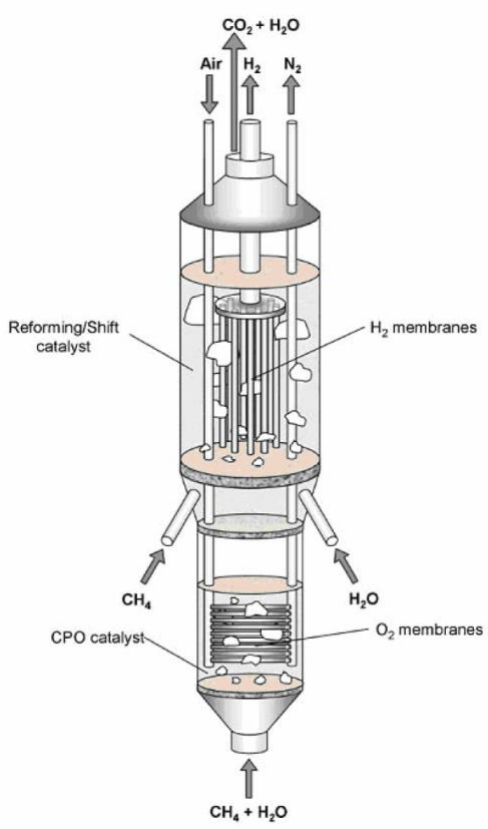

Figure 2.4: The schematic diagram for the autothermal reforming membrane integrated with Pd-membrane for hydrogen separation process [56].

The top part of the hybrid reactor was for the steam methane reforming reaction and the bottom part of the reactor was for the catalytic partial oxidation (CPO) reaction. Through simulation tests, the reactor design shows good results by achieving better conversion (up to 95% at 1 atm), higher hydrogen yields and good hydrogen separation ability (Pd membrane used for hydrogen separation) as compared to the normal autothermal reforming reactor.

The same group of researchers then conducted an experimental study on autothermal reforming of methane in an integrated reactor equipped with a Pd

membrane for better hydrogen recovery [58]. The study shows good methane conversion (more than 95 %) and higher hydrogen yield at high temperature, 903K. The Pd membrane used in the experiment shows good hydrogen separation ability with no trace of carbon monoxide found on the permeated side.

2.3 Other Methods of Hydrogen Production

There are also other methods of hydrogen production available on a lab-scale unit. Normally these methods were not preferred because they incur higher maintenance cost and/or have low product quality. Nevertheless there are still on-going researches made to these methods with the hope that they can be improved and get to the same level as of the aforementioned commercially available hydrogen production methods. Electrolysis is one of the methods used to produce hydrogen. In an electrolytic hydrogen production system, water is catalytically decomposed into hydrogen and oxygen with the help of an electricity supply [59]. Currently only 3.9% of the overall hydrogen production is from water electrolysis[60]. This method produces pure hydrogen but is not economical due to high energy requirements and the expensive electricity supply [61].

Hydrogen can also be produced through biological systems. In a bio-hydrogen system, hydrogen can be produced by bio-photolysis of water by algae [62, 63], pyrolysis of biomass specifically the lignocellulosic materials [64] and fermentation from food waste [65].

2.4 Membrane Systems

A membrane reactor is known as one of the systems that requires less energy to operate and is cost-effective yet still delivers the same quality as that of the costly, high maintenance conventional unit operations available today. Lately a palladium (Pd) membrane was proposed to be installed in several Integrated Gasification Combined Cycle (IGCC) plants for the purpose of separating hydrogen form carbon dioxide containing streams and to be further used to generate electricity within the plant[66, 67]. As reviewed earlier, major hydrogen production plants are also looking forward in the change in technology towards the use of membranes; mainly focussed on the use of membranes in the replacement of the separation units. This shows that membrane reactors are beginning to gain attention are making their way to be commissioned into industrial processes.

Basically a membrane is a dense barrier that may be made of polymer or other advanced materials to transport molecules through it by driving forces such as partial pressure difference and concentration difference. Figure 2.5 shows a typical membrane operating system. Classically a membrane system consists of one inlet and two outlets that are being named retentate and permeate.

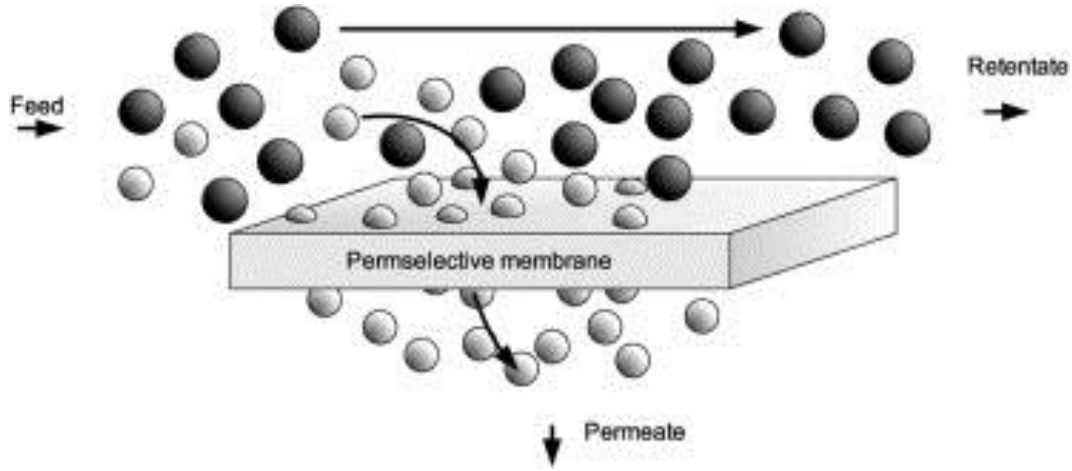

Figure 2.5: Basic principles of a working membrane [39]

Membrane performances are normally quantified by their permeation flux (J_x). Equation 2.6 shows how membrane flux can be calculated.

$$J_x = \frac{P}{t}\left(p^n_{x,feed} - p^n_{x,permeate}\right) \qquad \text{Equation 2.6}$$

Where P is the permeability ($molm^{-1}s^{-1}Pa^{-1}$), x is the species, t is the thickness of membrane, $p^n_{x,feed}$ is the partial pressure of x in the feed (kPa) and $p^n_{x,permeate}$ is the partial pressure of x in the permeate side (kPa).

Membrane performance can also be evaluated based on its selectivity. Selectivity ($\alpha_{A/B}$) can be derived by Equation 2.7.

$$\alpha_{A/B} = \frac{P_A}{P_B} \qquad \text{Equation 2.7}$$

Where P_A is the permeability of A and P_B is the permeability of B.

Hydrogen production via membrane systems usually operates on either Polymer Electrolyte Membranes (PEM) or the perovskite-type MIEC membranes (widely known as OTMs). This work focusses on the hydrogen production using the OTM membrane hence only the material associated with OTMs will be discussed in further detail.

2.4.1 Perovskite-type Mixed Ionic and Electronic Conductors (MIEC)

The perovskite mineral, calcium titanate ($CaTiO_3$), can be described by the general formula ABO_3 where A and B represent 12 and 6-cordinated metal cation sites[68]. Mixed ionic and electronic conductors primarily have been studied for the use in solid oxide fuel cell. Figure 2.6 shows the chemical structure of ABO_3 perovskites.

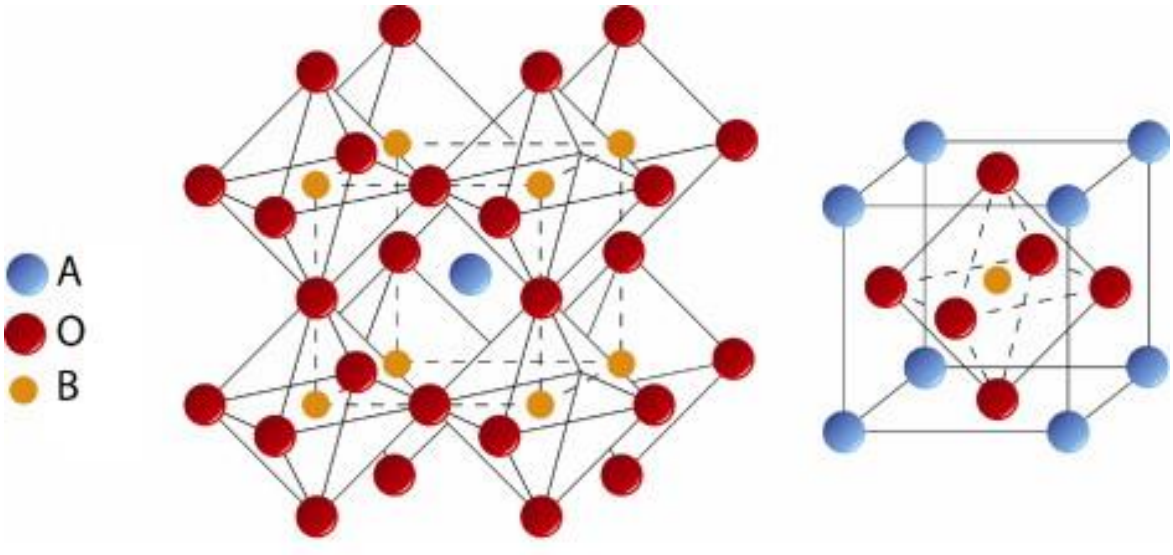

Figure 2.6: Perovskites ABO_3 structure [69]

The perovskite oxides are of particular interest as there are two cation sites to substitute different elements leading to a wide range of possible oxygen ion conducting materials[70]. The size limit of metal cation incorporation into the cubic crystal lattice is defined by the Goldschmit tolerance factor:

$$\text{Tolerance factor, } t = \frac{(r_A + r_O)}{\sqrt{2}(r_B + r_O)} \qquad \text{Equation 2.8}$$

Where r_A is the radius of the A-site cation, r_B is the radius of the B-site cation and r_O is the radius of the lattice oxygen anion. The A-site cation position is normally taken by the rare-earth (such as lanthanum) and alkaline earth metals (such as strontium) and the B-site is usually occupied by transition metals (such as cobalt and iron) although group III elements such as aluminium and gallium will also fit [71]. For perovskites the range of t is *ca* 0.75 to 1.05, where a value of 1 gives the ideal cubic structure. Outside of these limits severe distortion and segregation of cation will occur making the structure not stable. Hayashi et al [72] conducted a study on La and Nd-based materials to correlate between the ionic conductivity to the structural related parameters; specific free volume and tolerance factor. It is discovered that conductivity increases with the increase of specific free volume and that the best tolerance factor is 0.96. In this case the B-site cation needs to be chosen correctly depending on the radii to form a tolerance factor close to 0.96.

Stable perovskites are able to solvate a limited number of oxygen vacancies at elevated temperature over a range of oxygen activities. In Kröger-Vink notation, these vacancies are written as $V_{\ddot{O}}$ which indicates a vacancy at an oxygen sublattice site possessing a net +2 electrical charges [11]. The ionic mobility was assisted the

vacancies and the electronic conductivity happens when there is a state changes in the B-site cation[73]. The presence of oxygen vacancies is denotated by the symbol, δ; i.e., $ABO_{3-\delta}$ indicates oxygen deficiency. Several researchers have also studied on these perovskites properties in relation to the conductivity. These vacancies are mobile at elevated temperature, typically 700 to 1000^{o}C; it is this property which is of main interest in many applications. [74, 75].

With these abilities the MIEC materials were used as the main ceramic membrane material in the production of oxygen-enriched air, partial oxidation of light hydrocarbons and other applications [76]. The next section discusses the use of perovskite-type MIEC in gas-tight membrane structures.

2.4.2 Oxygen Transport Membrane (OTM)

The OTM systems normally consist of gastight MIEC materials that are able to transport oxygen ions through oxygen vacancies and the electronic conducting ability of the material [77]. OTM's ability in oxygen separation processes with less operating costs and at an atmospheric condition makes it easier to operate.

OTMs were claimed to be the most cost effective, clean and efficient system to be used for separating pure oxygen from air [8]. Several research groups have listed the potential and the advantages of OTM applications in oxygen permeation processes [78, 79]. Amongst the advantages mentioned were clean fuel processing, reduced capital cost and efficient performance in the oxygen separation step [80-82]. Furthermore OTMs were claimed to have the potential in reducing the production cost of oxygen processing process up to 35% [83-85].

Oxygen permeation ability of perovskite-type material was discovered in an early study conducted by Teraoka [86] where he observed a general trend in oxygen permeation in the $Ln_{1-x}\,AxCo_{1-y}B_yO_{3-\delta}$ (Ln = La, Pr, Nd, Sm,Gd; A = Sr, Ca, Ba; B= Mn, Cr, Fe, Co, Ni, Cu) type perovskites. Since then a number of studies have been conducted to observe the potential of the Lanthanum Strontium Cobalt Ferrites as oxygen transport membranes. Teraoka at. al [87] also concluded that the oxygen flux increased with the increased doping of Sr and Co. Further studies on $La_{1-x}Sr_xCo_{1-y}Fe_yO_{3-\delta}$ discovered that the material is able to exchange a large amount of oxygen from the oxygen sublattice on heating and cooling[86, 87]. It is believed that permeability and stability of the perovskite-type oxides are highly dependent on the dopant and oxygen pressure of the working environment [85,88, 89]. This is important so that the oxygen on the higher activity side can easily be reduced and solvate into the surface and be subsequently transported across the membrane. Further combinations between two oxygen species will release electrons to the membrane balancing the loss of electronic charges. Oxygen transport through the defects of MIEC materials can be divided into three steps[90]; (i) surface-exchange reaction at interface (ii)simultaneous bulk diffusion (iii)surface-exchange reaction on another interface.

In an oxygen permeation process, the performance of the MIEC membrane depends on the oxygen permeation rate J_{O_2} of the MIEC membrane can be calculated using the modified Wagner equation shown in Equation 2.9. However this equation only applies when bulk diffusion is the rate determining step in the membrane reactor system.

$$J_{O_2} = -\frac{RT}{16F^2L}\int_{\ln p_{O_2}(feed)}^{\ln p_{O_2}(perm)} \frac{\sigma_{el}\sigma_{ion}}{\sigma_{el}+\sigma_{ion}}\partial \ln p_{O_2} \qquad \text{Equation 2.9}$$

Where R, T, F, L are the gas constant, temperature, Faraday constant and membrane thickness respectively. σ_{el}, σ_{ion}, $p_{O_2(feed)}$, $p_{O_2(perm)}$ are the electronic conductivity, ionic conductivity oxygen partial pressure of feed side and oxygen partial pressure of the permeated side respectively.

Studies on the oxygen permeation ability by perovskite membranes have been performed by several groups of researchers. Perovskite membranes were used in the study of oxygen permeation. Common areas covered by the researchers in this field were the performances of the perovskites membrane to permeate oxygen in different temperature. Typical results showed that highest oxygen permeation rate was in the temperature range of 900°C to 1100°C.

The studies were more focussed on assessing the mobility of the oxygen vacancies when different doping materials were used and their stability at elevated temperatures [91-93]. Lanthanum-doped perovskites are the most common material used for the oxygen permeation experiments. This type of oxide was claimed to have high concentrations of vacancies in their structure [94]. Materials containing cobalt usually show higher oxygen permeability. Kuhn et al. [95] made a study on the degradation on the $La_{0.6}Sr_{0.4}Co_yFe_{1-y}O_{3-\delta}$ by varying y between 0 to 1. The results showed that the permeation of oxygen decreased with higher amount of cobalt doping. This is because cobalt has smaller binding energy with oxygen and this facilitates oxygen diffusion within the oxide bulk. [85, 96, 97]. Table 2.1

summarises some of the oxygen permeation studies with perovskite materials for oxygen permeation with inert gas and reducing gas; methane.

Table 2.1: Oxygen permeation studies done on different OTM materials.

Oxides materials	Membrane geometry	catalyst	Membrane thickness (mm)	Gas composition		Operating temperature (^oC)	Maximum operating time reported (hour)	Highest oxygen permeation rate ($\mu molcm^{-2}s^{-1}$)	Post operation analysis method	Ref (s)
				pO_2	psweep					
$La_{0.6}Sr_{0.4}Fe_{0.8}Co_{0.2}O_{3-\delta}$	disc-shaped pellets	Pt film on the surface	8	Air	Ar	800-1000	none	$0.800x10^{-3}$	none	[98]
$Ba_{0.9}Co_{0.7}Fe_{0.2}Nb_{0.1}O_{3-\delta}$	disc-shaped pellets	NiO/MgO	1	Air	He	875	400	$0.804x10^{-3}$	SEM XRD EDX TGA	[99]
$BaCe_{0.85}Tb_{0.05}Co_{0.1}O_{3-\delta}$	Hollow fibre membrane	none	-	Air	He	1000	none	$0.028x10^{-3}$	XRD SEM	[100]
$La_{0.6}Sr_{0.4}Ti_{0.2}Fe_{0.8}O_{3-\delta}$	disc-shaped pellets	none	1.6	Air	He	700-1000	none	$0.013x10^{-3}$	XRD SEM	[101]
$Ba_{0.5}Sr_{0.5}Co_{0.8}Fe_{0.2}O_{3-\delta}$	Tube membrane	Thin layer $La_{0.6}Sr_{0.4}Ti_{0.3}Fe_{0.7}O_{3-\delta}$	-	Air	He	950	300	$0.223x10^{-3}$	SEM	[102]
$La_{0.7}Sr_{0.3}Ga_{0.6}Fe_{0.4}O_{3-\delta}$	disc-shaped pellets	$NiO/NiAl_2O_4$	-	Air	CH_4	850	1.7	$0.008x10^{-3}$	SEM	[103]
$La_{0.7}Sr_{0.3}FeO_{3-\delta}$	Hollow fibre membrane	none	-	Air	CH_4	850-1000	none	$0.086x10^{-3}$	SEM	[104]
$SrCo_{0.8}Fe_{0.1}Ga_{0.1}O_{3-\delta}$	Hollow fibre membrane	none	-	Air	CH_4	900	100	$0.025\ x10^{-3}$	XRD SEM	[105]
$BaBi_{0.05}Co_{0.8}Nb_{0.15}O_{3-\delta}$	hollow fibre membrane	none	-	Air	CH_4	950	150	$5.88x10^{-3}$	SEM EDX XPS	[106]

Other methods applied with the aim to increase the oxygen permeability of OTM material are by coating the membrane surfaces with catalysts [85, 107, 108]. This method was aimed to increase the permeability and decrease the risk of disintegration of the membrane although some of the studies have shown that the mechanical strength of the hollow fibre membrane is very much dependant on surface etching [107].

Hayamizu et al [108] reported that the oxygen permeation only increases with specific thickness of the coating on the surface of the membrane. Another effort was made by coating the surface of the membrane with catalyst to enhance the reforming process; hence increasing the oxygen permeation rates. Results for coating a BSCF membrane with Pt and Pd showed that there were no evidence of increase permeation in such cases [109].

Currently OTM have been used in a number of applications including as an oxygen separation membrane in the oxy-fuel power station, as the cathode in the solid oxide fuel cells and as the pre-treatment unit for the partial oxidation of methane process and as the hydrogen production membrane using different feedstock as the starting materials [110, 111]. The next section will discuss on the use and studies conducted on OTM for hydrogen production purposes.

2.4.1 Hydrogen production with OTM

Researchers begin to study hydrogen production using OTM materials since the early 1990s [9, 112, 113]. Several review papers were also published on the role of OTMs in the hydrogen production process and its importance in the hydrogen processing industries [7, 39, 114].

Generally studies on hydrogen production via OTMs are more focussed on the POM reaction. In a membrane system containing OTMs, air was fed on one side of the membrane and oxygen shows up on the other side of the membrane. In Kröger Vink notation (Equation 2.10);

$$\frac{1}{2}O_2 + V_O^{\cdot\cdot} \rightarrow O_O^x + 2e^- \qquad \text{Equation 2.10}$$

Where

$V_{\ddot{O}}$ indicates a vacancy at an oxygen sub-lattice site possessing a net +2 electrical charge, O_O^x is the oxygen occupying site at an oxygen sub-lattice and e^- is the electron.

In a classical hydrogen production OTM reactor, the permeated oxygen in the permeate side were then reacted with methane to POM resulting in the production of hydrogen and carbon monoxide (Equation 2.12).

$$CH_4 + O_O^x \rightarrow V_O^{\cdot\cdot} + 2e^- + 2H_2 + CO \qquad \text{Equation 2.11}$$

Studies on the use of OTMs in producing hydrogen are often conducted with the aim of looking at the OTM's ability to be applied as the cathode material in Solid Oxide Fuel Cells (SOFC) [115]. A number of studies were conducted by other researchers concentrating on the efficiency of OTM reactors in producing hydrogen in such a feasible manner. $Ba_{0.5}Sr_{0.5}Co_{0.8}Fe_{0.2}O_{3-\delta}$ was studied by several researchers to perform POM and shows good permeation results and potential to be used in the

syngas production process [10]. Shao et al [116] conducted a permeation test and POM reaction on the dense $Ba_{0.5}Sr_{0.5}Co_{0.8}Fe_{0.2}O_{3-\delta}$ and achieved 88% methane conversion with 95% selectivity towards carbon monoxide. In another study done by the same authors, a $Ba_{0.5}Sr_{0.5}Co_{0.8}Fe_{0.2}O_{3-\delta}$ disk membrane was used to perform POM with lower concentration of methane/helium on one side and air on the other side of the membrane. The experiment was conducted in two different reactor configurations; (A) without catalyst and (B) with catalyst packing. The conversion of methane in (A) achieved was 3.25% and 80% was achieved in (B) [117].

Lanthanum-based OTMs were also among the candidate materials that have been studied for hydrogen production ability. Thursfield and Metcalfe [118] conducted a study on a $La_{0.6}Sr_{0.4}Co_{0.2}Fe_{0.8}O_{3-\delta}$ membrane in performing methane oxidation at 860^{o}C. The results however showed the sign of total combustion; having water and carbon dioxide as products. A similar trend was also observed in a $La_{0.2}Sr_{0.8}Fe_{0.2}Co_{0.8}O_{3-\delta}$ membrane reported by Balachandran *et al* [119]. Upon exposure to methane for POM reactions, the permeation of oxygen to the reducing sides was too high giving 90% selectivity towards carbon dioxide. The authors however emphasised the good stability of the membrane if being able to withstand such an environment for *ca* 1000hours. A hydrogen production experiment was also conducted on a gas-tight cobalt-free $La_{0.7}Sr_{0.3}FeO_{3-\alpha}$ membrane, by feeding methane or hydrogen as the sweep gas. The maximum CO yield obtained was 1.2%. The authors also stressed the instability showed by the membrane upon exposure to a reducing environment. Serious segregations were discovered when the membrane is continuously exposed to methane and hydrogen. [104].

Currently researchers have also begun to slowly show interest in applying catalysts onto the OTMs in order to reduce the operating temperature and increase selectivity

toward hydrogen [120, 121]. Tsai *et al* [122] conducted a study on syngas production using $La_{0.2}$ $Ba_{0.8}$ $Fe_{0.8}$ $Co_{0.2}$ $O_{3-\delta}$ using three different types of disk-membrane reactor configurations. In the study the membrane was exposed to 4.6% of methane feed, having an operating temperature of 850°C. It was found out that all of the three configurations of membrane reactors are feasible in producing syngas. In the reactor that was packed with 5%Ni/Al_2O_3 catalyst, the oxygen permeation increased five times compared to the one that was not being assisted by the catalyst. Another study that uses Ni-based catalyst for the production of hydrogen via oxy-CO_2 reforming of methane was conducted on a $La_{0.6}Sr_{0.4}Co_{0.8}Ni_{0.2}O_{3-\delta}$ membrane and it was discovered that the highest hydrogen selectivity is 88% achieved at 700°C [123]. Similar studies on syngas production using OTM with a catalyst were also conducted by several researchers. Among the types of catalyst used were Pt/ZrO_2 [124], Ni/Al_2O_3 [125] and Pd-film [126].

Surface modifications give good response in increasing the permeation hence increasing the chance of higher concentration of hydrogen production. Recently Zhang et al [127] published a new type surface-modified membrane with the introduction of micro-channelled membranes. It is disclosed that the micro-channelled membrane increases the surface area of the membrane and provides a good platform to be the material used for further investigations on both bulk diffusion and surface exchange activities. Recently a surface-modified $BaCo_{0.7}Fe_{0.2}Nb_{0.1}O_{3-\delta}$ membrane was used in study of hydrogen production via partial oxidation reforming of coke oven gas (COG). The surface of the membrane was modified by a coating a layer of $Ce_{0.8}Re_{0.2}O_{2-\delta}$ onto the permeation side of the membrane. The experiment was conducted at 875°C and achieved 99.4% conversion of methane with 65.7% selectivity towards hydrogen.

2.4.2 Membrane-based Water Splitting Process

Water splitting via a membrane reactor is one of the reaction-separation techniques resulting from the ability of the MIEC materials to transport oxygen. In the process of membrane-based water splitting, oxygen is removed from water and transported across the membrane through the oxygen vacancies in the materials. In Kröger Vink notation;

$$H_2O + V_o^{\cdot\cdot} + 2e^- \rightarrow O_o^x + H_2 \qquad \text{Equation 2.12}$$

On the release of oxygen to the surface of the membrane, the oxygen forms molecules by accepting 2 electrons

$$O_o^x \rightarrow 2e^- + V_o^{\cdot\cdot} + \frac{1}{2}O_2 \qquad \text{Equation 2.13}$$

And in the cases where the reaction side was fed with methane and carbon monoxide, the release of the oxygen ion from the vacancies may results in the formation of other by-products as shown in Equation 2.14 and Equation 2.15.

$$CO + O_o^x \rightarrow V_o^{\cdot\cdot} + 2e^- + CO_2 \qquad \text{Equation 2.14}$$

$$CH_4 + O_o^x \rightarrow V_o^{\cdot\cdot} + 2e^- + 2H_2 + CO \qquad \text{Equation 2.15}$$

Balachandran *et al* [128] in a study of water separation using ceramic-metal composites investigated the possibility of water dissociation using Gd-doped CeO_2 MIEC and proved that there was water dissociation activity. The same authors re-examined the ability of Gd-doped CeO_2 membrane with the addition of Ni catalyst made into a dual-phase cermet membrane. They concluded that the improved membrane structure resulted in higher hydrogen production via dissociation of water [129]. Franca *et al* [11] reported on the stable hydrogen production via water splitting using a $La_{0.6}Sr_{0.4}Co_{0.2}Fe_{0.8}O_{3-\delta}$ membrane. In the study, hydrogen production via water splitting was conducted using two different dimensions of furnaces. An oxygen balance was conducted and the oxygen balance closes for both of the systems operating on different furnaces showing good consistency in oxygen permeation performance of the membranes.

Hydrogen production from water splitting needs higher energy and need reducing environment to show good performance. In order to increase the production of hydrogen via water splitting in a membrane system, Jiang et al [130] suggested the use of methane or ethane or a reducing gas as the sweep gas. In this case the water can only be split when the partial pressure of oxygen, pO_2 is low on one side of the membrane, Park et al. [131] used $La_{0.7}$ $Sr_{0.3}Cu_{0.2}Fe_{0.8}O_{3-\delta}$ (LSCF7328) material in three different geometries; (i) thin film (ii) disk membrane (iii) hollow fibre and demonstrated the water splitting process to happen in a membrane that was fed with steam on one side of the membrane and CO on the other side of the membrane.

The presence of cobalt can facilitate the water splitting process. In several studies done by previous researchers, it is concluded that some membranes without cobalt doping show severe segregation when it is exposed to hydrogen and methane containing feed [132]. However, Park et al. [133] conducted a coal-gas assisted

water–splitting process using on a cobalt-free material, $BaFe_{0.9}Zr_{0.1}O_{3-\delta}$,and discovered that the hydrogen production rate of thicker $BaFe_{0.9}Zr_{0.1}O_{3-\delta}$ membrane gives the same hydrogen production rate as that of a thinner $La_{0.7}Sr_{0.3}Cu_{0.2}Fe_{0.8}O_{3-\delta}$ membrane. This shows that the latter materials show better hydrogen production ability even in lower surface area as to compare to the earlier materials.

2.4.3 OTM and Reactor Design Limitations

Although OTMs were seen to give good possibility to be used as a working membrane for membrane-based hydrogen production processes, there are still some limitations of OTMs that need to be improved. In a study involving the use of OTMs, researchers have listed the limitations and challenges in dealing with OTMs such as chemical instabilities, physical instabilities and reactor sealing problems [134].

Chemical instability is one of the main issues faced by the OTM materials. Upon exposure to some reducing gases in oxygen permeation experiments, the OTM surface demonstrates cation diffusion resulting in material degradation through formation of carbonates hence the inactivation of the membrane. Van Doorn *et al* [135] conducted a study to evaluate the stability of $La_{0.3}Sr_{0.7}CoO_{3-\delta}$ in air and 4.1% of oxygen. The results showed that under extended duration of oxygen permeation study (more than 100h) and higher operating temperature (1000^{o}C), the surface of $La_{0.3}Sr_{0.7}CoO_{3-\delta}$ was covered with a thick layer of strontium carbonate, $SrCO_3$. As the cation diffusion is believed to be caused by kinetic decomposition and impurity segregation, Wang *et al* [136] investigated these criteria on hollow fibre $La_{0.6}Sr_{0.4}Co_{0.2}Fe_{0.8}O_{3-\delta}$ membranes. The results however concluded that the

decomposition and impurity segregation does not much affect the performance of the membrane. The same authors reconfirmed the results in another experiment done at longer operating time[137].

In another study conducted to investigate on the stability issue in OTM membranes, Iguchi *et al* [138] ran in-situ Raman Spectroscopy on the surface of a $La_{0.6}Sr_{0.4}Fe_{0.8}Co_{0.2}O_{3-\delta}$ membrane after the membrane was exposed to methane and air on different sides; the typical gas used for oxygen permeation studies. They found out that there were carbon depositions on the surface of the membrane that is exposed to air. This shows that carbon deposition also plays an important role in making the membrane stiff and hence breaking the membrane.

Secondly is the mechanical strength of the OTM itself. OTM materials that have good oxygen permeability are said to have high thermal expansion and lower structural strength when exposed to a gradient of oxygen partial pressure and high temperature [139]. Typically the mechanical strength of OTMs was being studied in terms of its three-point-bending and creep bending behaviour [140, 141].

Huang et al. [142], studied the effect of oxygen partial pressure difference in the gas inlet towards the mechanical strength of the $La_{0.58}Sr_{0.4}Co_{0.2}Fe_{0.8}O_{3-\delta}$ disk membrane. It was found out that the act of heating or cooling the membrane in atmospheric air after the membrane was exposed to long hours of annealing in different oxygen partial pressures might cause the membrane to disintegrate. The lifetime of $Ba_{0.5}Sr_{0.5}Co_{0.8}Fe_{0.2}O_{3-\delta}$ has been studied subjected to slow crack growth [143].

Another limitation faced when dealing with a membrane system is on the need of an air-tight OTM reactor design. In assembling a membrane reactor that will be

operating at a high temperature environment, the main challenge in the membrane reactor assembly is to secure the membrane on to a support and make it gas-tight. This is because normal commercial sealant would have low tolerance to high temperature operation; particularly at temperatures more than 600^{o}C (highest temperature where a high-temperature silicone sealant would work). Applying a cement or water-based sealant for example will only lead to a massive leak at the connection between membrane and the support. By far, this problem should be a limitation experienced by all of the groups dealing with high temperature membrane reactors but is not well documented in the literature. Nevertheless to date, a number of researchers have been making some efforts on improving and finding solutions to this sealing problem. Most of them however were aiming on applying this high-temperature sealant for SOFC application. Recently a study done by Sharma *et al* [144] revealed the ability of their in-house manufactured sealant, $Ba_3(PO_4)_2$ to maintain its sealant property up to 1000^{o}C. Similar claims on the same type of borosilicate glass ceramic sealant ability were reported by Zhang and Zou [145]. On the use of gold sealant for the membrane reactor performance, Vivet *et al.* [146] conducted a study on the influence of the sealant towards the performance of the oxygen permeation membrane reactor. The study concluded that gold sealant does not affect the permeation rates of the membrane. Qi *et al* [147] suggested a recipe to produce a glass sealant by using 40–50 wt.% membrane material powder, 20–50 wt.% Pyrex glass and 5–20 wt.% additives. A clever approach to solve on the need of high-temperature sealant problem is by fabricating a one-dead end membrane [148]. Having one end sealed reduces the chance of membrane breakage due to bending. This design gives the membrane to have a free bending direction and does not force the membrane to stay intact to the sealant at the other end that would normally causes the membrane to break. This design also enables the

membrane user to have the membrane mounted to the gas inlet using cold sealant and reduces the chance of leakages. Figure 2.7 depicts a one-dead end $Ba_{0.5}Sr_{0.5}Co_{0.8}Fe_{0.2}O_{3-\delta}$ tube membrane.

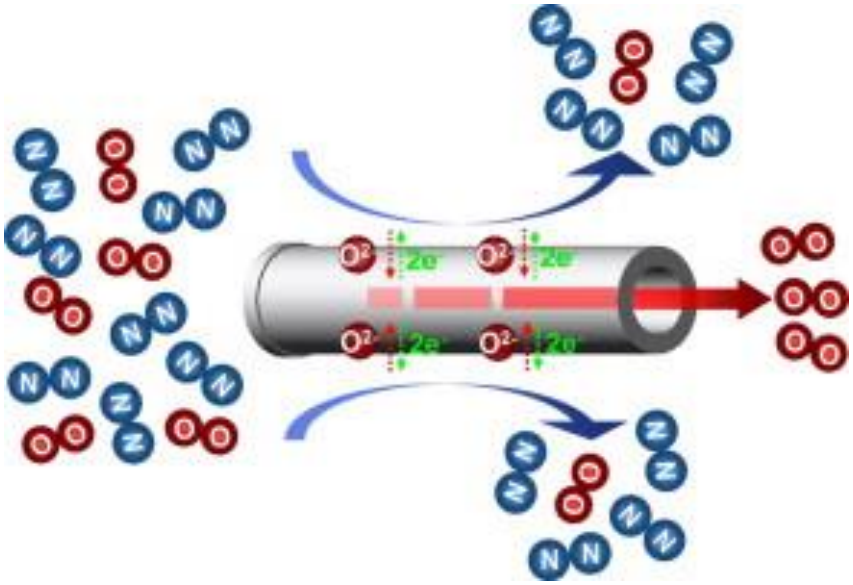

Figure 2.7: One dead-end membrane used in the study of high-purity oxygen production. Adapted from [148].

Another major concern in delivering information on the performance of the oxygen permeation ability of an OTM is that researchers in this field rarely report on the material balance of the system. Material balance, particularly oxygen balance is crucial for a claim to be made describing the efficiency of the membrane. This is because to be able to calculate the oxygen balance of the system, both inlets and outlets of lumen and shell sides of the membrane need to be analysed. Only by having this information could one confirm that permeation obtained through the experiment represents the oxygen permeation that is driven by the driving force of the membrane system, not by any other means such as through cracks and cross-chamber leaks

2.5 Summary

Earlier in this chapter we reviewed on the state-of-the-art advancement in the hydrogen production technology used either commercially or at lab-scale size. Membrane technology was seen to be given attention on the commercial scale because of its ability to give good hydrogen separation capability at a minimum energy requirement. Efforts have been made to combine the readily commercialised processes with membrane technology. As the demand of the hydrogen economy and green technology is increasing the potential of OTM to be used in the hydrogen production process needs to be observed and tapped.

A number of workers have proven on the ability of the OTM to produce hydrogen in a wide range of processes. Although there are still limitations in operating the OTM module, we believe that there is always room for improvements. Nevertheless, this research is aiming to produce hydrogen utilising the ability of OTM.

Chapter 3 Individual Membrane Reactor Performance for Oxygen Permeation and Water Splitting Process

3.1 Introduction

This chapter deals with the preliminary experiments with two different hollow fibre membranes; $La_{0.6}Sr_{0.4}Co_{0.2}Fe_{0.8}O_{\delta-3}$ (LSCF6428) and $Ba_{0.5}Sr_{0.5}Co_{0.8}Fe_{0.2}O_{\delta-3}$ (BSCF5582). Thorough descriptions of the overall experimental setup, membrane reactor design, calculation methods to determine the oxygen permeation rate and error propagation are included in section 3.2. Oxygen permeation rates for both of the membranes with different shell/lumen inlets are presented and discussed in section 3.3.

Prior to the simultaneous oxidation and water splitting experiments these membranes were tested with three oxygen permeation experiments having different inlet gases on the shell side as well as the on the lumen side. The results obtained in this chapter will be used as a reference to multiple-membrane reactor experiments to be presented in Chapter 4. Basically the membrane that shows stable performance in these three permeation tests conducted in this Chapter will be selected as the membrane to be used in the subsequent Chapters.

3.2 Methodology

The experimental setup for this study involves a system consisting of three main parts; (i) feed system (ii) membrane reactor and furnace and (iii) gas analyses. Figure 3.1 shows the basic process flow diagram of the experimental setup. Each main part consists of several instruments depending on the type of experiment to be conducted. Descriptions of the instruments involved will be discussed further in the latter section.

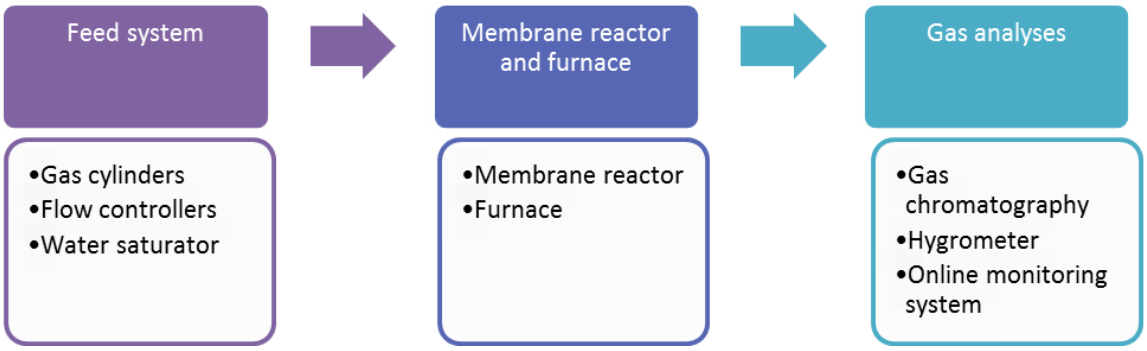

Figure 3.1: Process flow diagram for the experimental setup used in this study

3.2.1 Feed system

The feed system used in this system involves the use of four different gas cylinders, safety valves and an automated flow controller (Hastings, UK). Table 3.1 lists the provider for the gas cylinder and their content.

Table 3.1: Type of gases, the composition of each cylinder and the provider

MFC number	Gas	Composition	Provider company
MFC1	Argon	100% (Zero Grade)	BOC, UK
MFC2	Air	100% (Zero Grade)	BOC, UK
MFC3	Methane/Nitrogen	5% (99.5 % certification)	BOC, UK
MFC4	Air	100% (Zero Grade)	BOC, UK

For the water splitting experiment, water is supplied by a water saturator system, (Grant Scientific, UK). The water saturator system is equipped with a water pot that has one inlet, one outlet and a temperature controller to generate desired saturated water content. Figure 3.2 shows how the water pot inside the water saturator unit works.

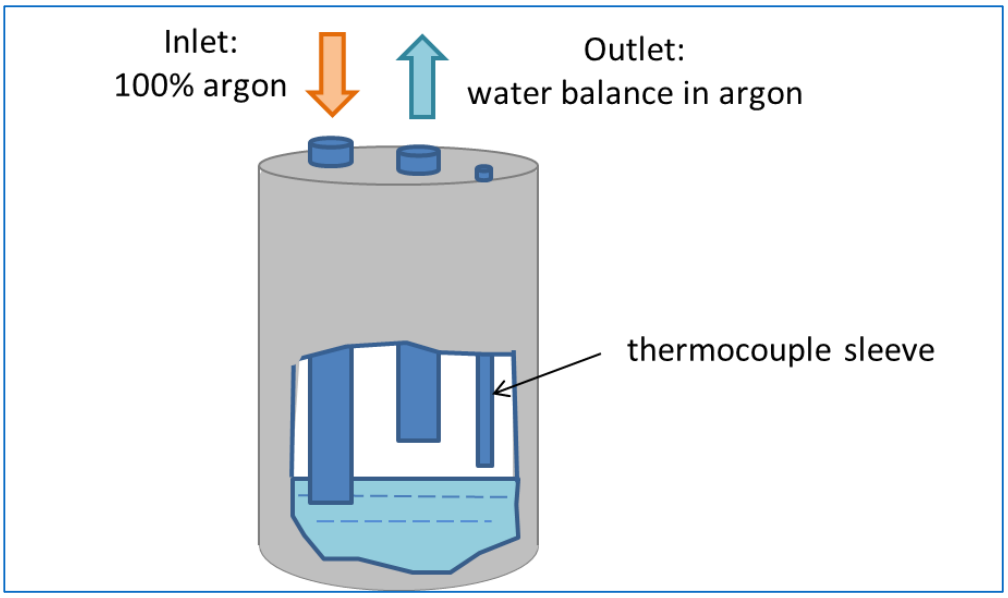

Figure 3.2: Water saturator system

In the water splitting/methane reforming experiment, the water was carried by the 30(STP) $mlmin^{-1}$ of zero grade argon. A simple experiment was conducted to determine the stability and the content deviation of the water supply to the reactor. In this simple experiment the flowrate of argon as the carrier was kept constant by the mass flow controller and double checked with the portable mass flow controller. The water bath is set at the desired temperature of an individual experiment. The maximum and minimum difference from the reading of the water content percentage were then recorded.

Figure 3.3 shows how the mole fraction of water varied with time when the temperature controller was set at 20°C, 30°C and 40°C respectively. The water content generated by the water saturator is stable and gives minimum deviation at 30°C although all of the other working temperature also does not show deviation more than 10%. In this study the concentration of water used as the feed to the lumen in water splitting experiment is set at 4.2 ±0.4% so the temperature set for the water generator is at 30°C.

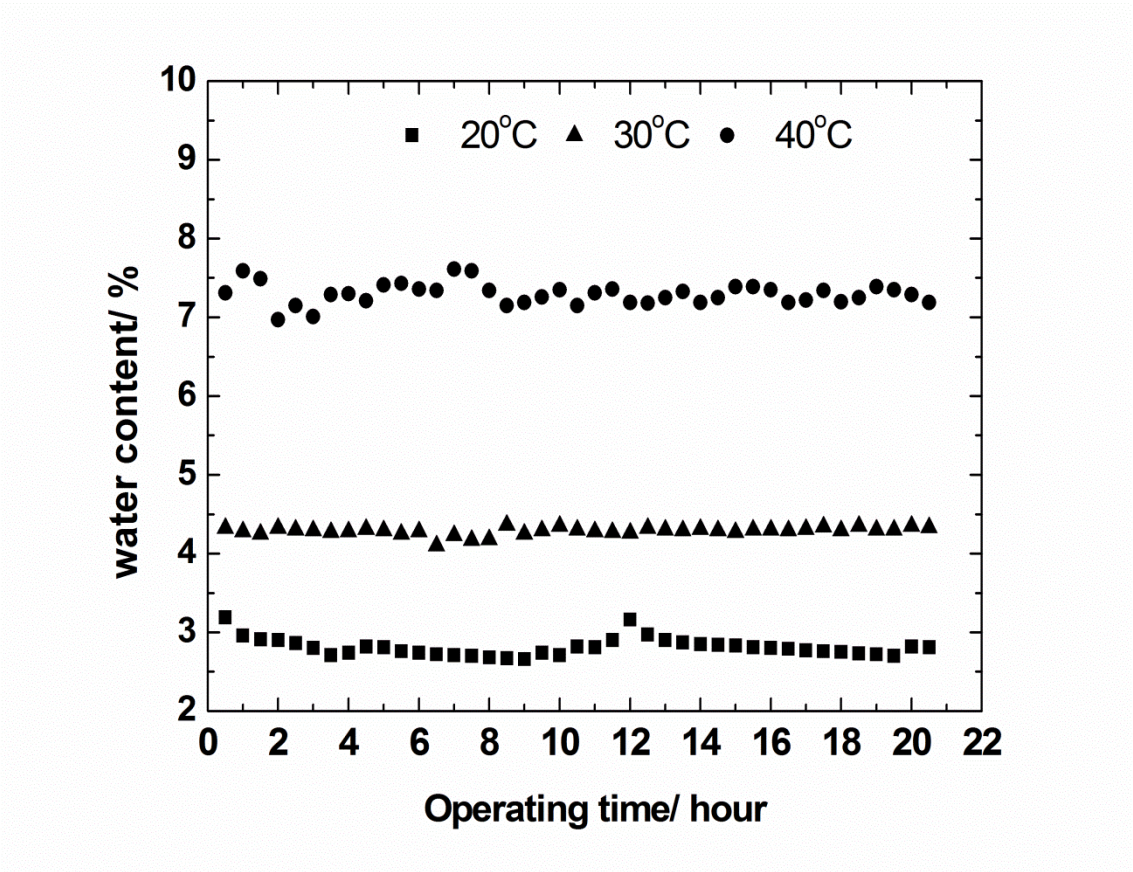

Figure 3.3: Water content generated by the water saturator according to the set temperature of the water pot located inside the waterbath.

3.2.2 Membrane materials and characterisation

This study uses hollow fibre membranes for both the LSCF6428 and BSCF55825 materials. The LSCF6428 membranes were supplied by Prof Kang Li's group from Imperial College of London. The LSCF6428 powder purchased from Praxair Ltd (USA) has an average particle diameter, d_{50} of 0.6μm and a surface area of 9.0 m^2g^{-1} The hollow fibres with an average dimension of 1.9mm OD x 1.4mm ID x 200mm L were fabricated using phase inversion/sintering technique as describe by Tan *et al* [149].

The BSCF5582 membranes were supplied by Cedric Buysse from the Flemish institute for Technological Research (VITO), Belgium. The membranes having an

average dimension of 3.5mm OD x 2.5mm ID x 250mm L were also fabricated using phase inversion/sintering technique described thoroughly by Buysse *et al.* [150].

Physically the structure for the BSCF5582 membrane is thinner and easier to break when handling the membrane in reactor setup. Figure 3.4(a) and Figure 3.4(b) show the SEM pictographs of the unused LSCF6428 and BSCF5582 membranes cross-sections.

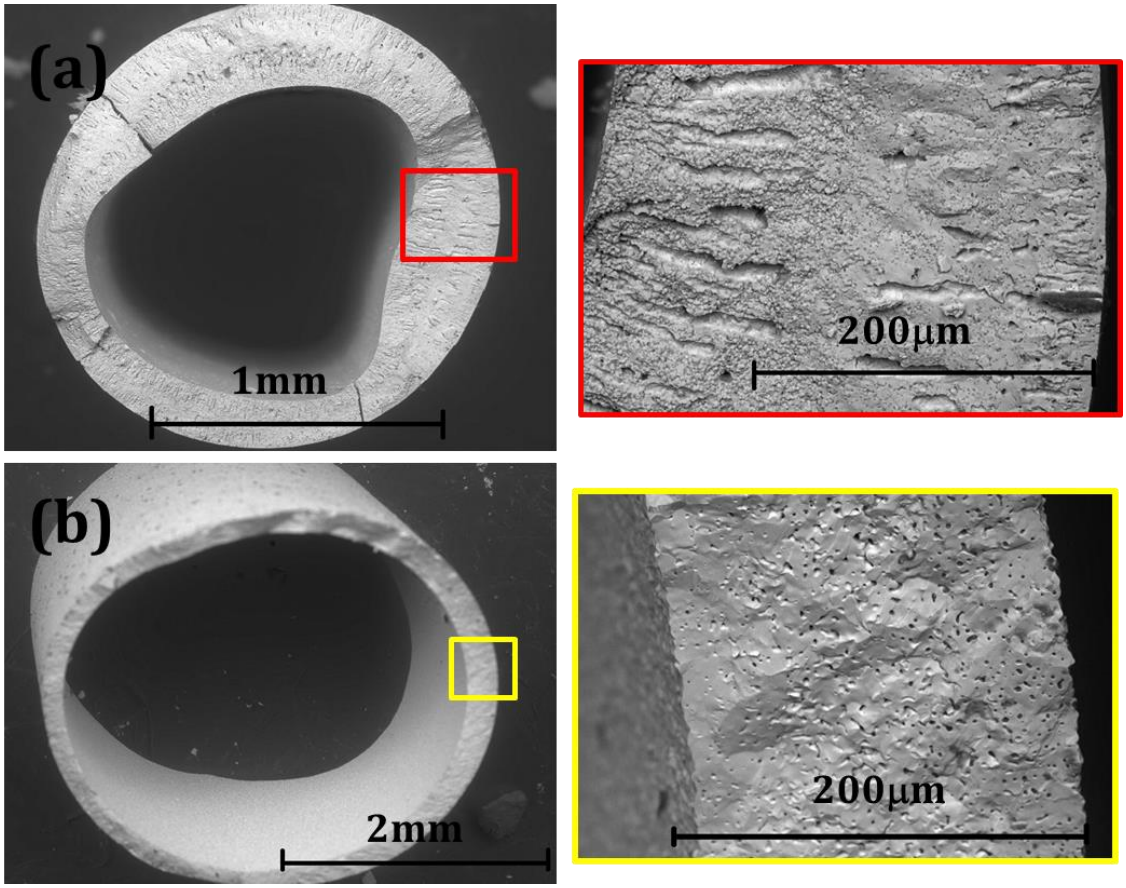

Figure 3.4: SEM micrographs for (a) LSCF6428 membrane and (b) for BSCF5582 membrane

Further elemental analysis EDX were made to observe the concentration of all the elements available on the surface of each membrane. Table 3.2 lists the EDX analysis of the surface of both membranes used in this study.

Table 3.2: Elemental analysis for the fresh membrane samples

Material	*Approximate atomic concentration (%)*				
	La	Ba	Sr	Co	Fe
LSCF6428	28.0	-	20.8	8.90	42.4
BSCF5582	-	20.1	25.6	41.9	12.4

The elemental analysis for both of the membranes are in the same range reported by Franca, [151] who used the same membrane materials for his study.

For the oxygen permeation studies, we used LSCF6428 hollow fibre membranes, BSCF5582 membranes and the modified surface LSCF6428 membrane. The design of the membrane reactor used in this study enables us to analyse the all the inlets and outlets of the reactor. The inlet gas was fed with a 30G hypodermic tubes into the middle of the membrane. The length of the membrane used in the reactor need to be at least 100mm long to be used for the experiments. This is to ensure that there will be enough length for the membrane to be sealed using high temperature silicone sealant (which can only withstand up to a temperature of 130^{o}C) at the cold-end of the membrane reactor. The furnace used in this study is a tube furnace by Vecstar (UK) equipped with Eurotherm® controller.

3.2.3 Membrane Reactor and Furnace

The first membrane reactor used in this study was adapted from the reactor design described by Franca[151]. Figure 3.5 shows the previous membrane reactor setup.

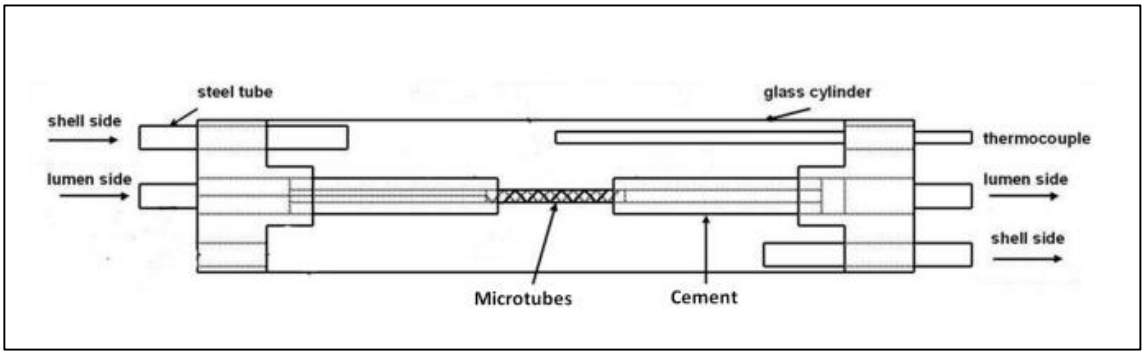

Figure 3.5: Previous design of membrane reactor [151].

In the thesis, it is stated that the stability of the membrane needed to be improved in order to withstand the temperature difference of the furnace. As reported in the thesis by Franca [151] a membrane having 300mm in length tends to bend when the reactor was heated up to 900^{o}C (the operating temperature). The bending was remarkable and causes membrane breakage. This is due to the thermal expansion of the membrane. Further explanations can be found in the thesis stated.

Based on the disadvantages and problems faced with the old reactor, we decided to make some changes to minimise the effects of thermal expansion on the membrane while the reactor is heated up. A new possible solution to this problem is through sealing one-end of the membrane. The membrane was then sealed on one end with a ceramic sealant (P24, Taogosai, Japan). The sealed membrane was calcined up to 700^{o}C with a heating rate of 2^{o}C min^{-1} prior to an experimental run. Figure 3.6

shows the schematic diagram of the membrane reactor setup used in this study. No leakage was found around the sealed part of the membrane.

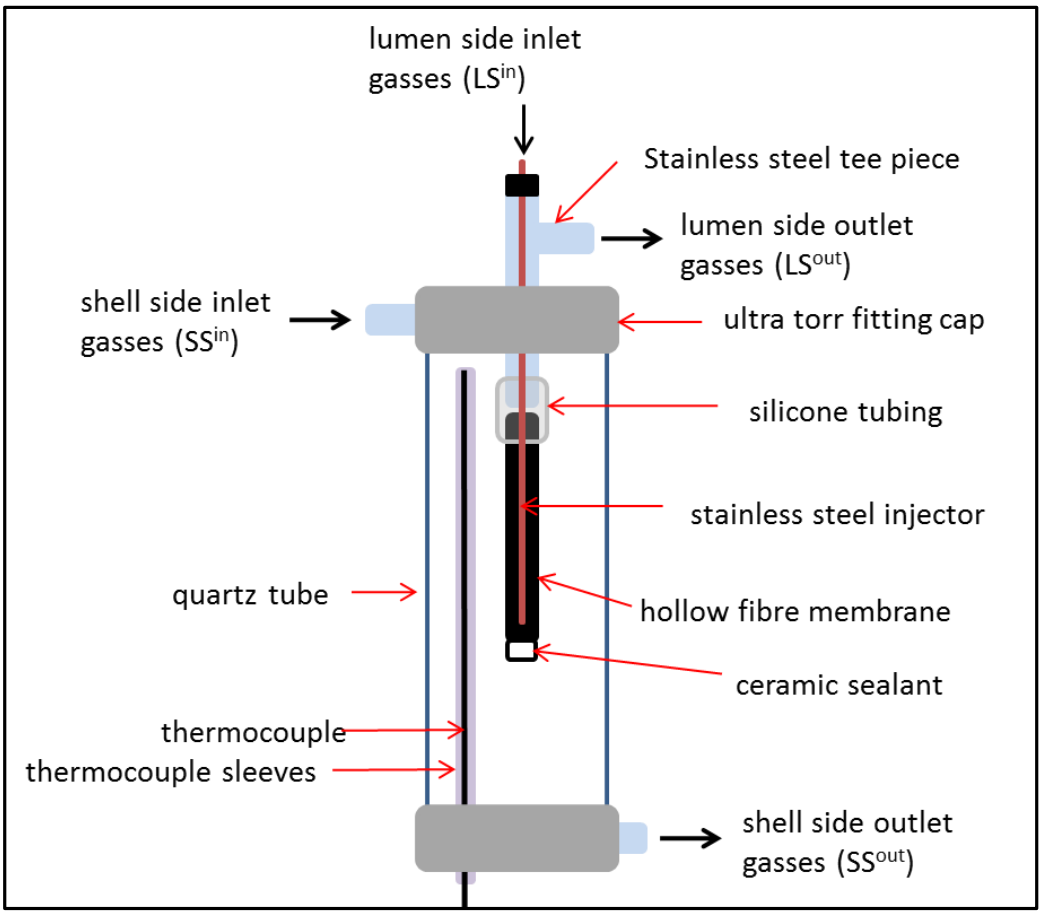

Figure 3.6: Membrane reactor setup for oxygen permeation studies

Since the inlet and outlet gases to and from the lumen are needed for material balance calculation purposes, newly designed inlet and outlet streams into and from the lumen side are needed. The inlet gas into the lumen side of the membrane was injected using a 30G hypodermic stainless steel tube. The opening of the tube was fitted with a vespel/graphite ferrule with the size of (1/16) inch x 0.6mm ID was used to secure and tightened the 30G hypodermic tube to the (1/16) inch swagelok female nut that further connects to a 70mm long (1/16)inch stainless steel tube. In order to avoid gas leakages between the (1/16) inch and the 30G hypodermic

needle, the connections were sealed with silicone sealant (Silicone Rubber Compound purchased from RS®). The sealant was left to dry for 20hours after assembling.

The furnace used in this experiment is an exclusive tube furnace (Vecstar, UK). The tube furnace dimension is 38mmID x 50mm OD x 150mm L, fitted with Eurotherm® three term programmer and solid state switching and type 'K' thermocouple.

The 30G hypodermic stainless steel injector was inserted into the lumen up to the isothermal region of the furnace. This is to reduce the possibility of other side reactions along the lower temperature region in the reactor. Figure 3.7 shows the temperature profile and the length of lumen inlet where the inlet gas was introduced into the membrane. The red region highlighted in the graph is showing the isothermal region and the first point of contact of the gas in the inlet in the reactor will be made within the isothermal region of the furnace.

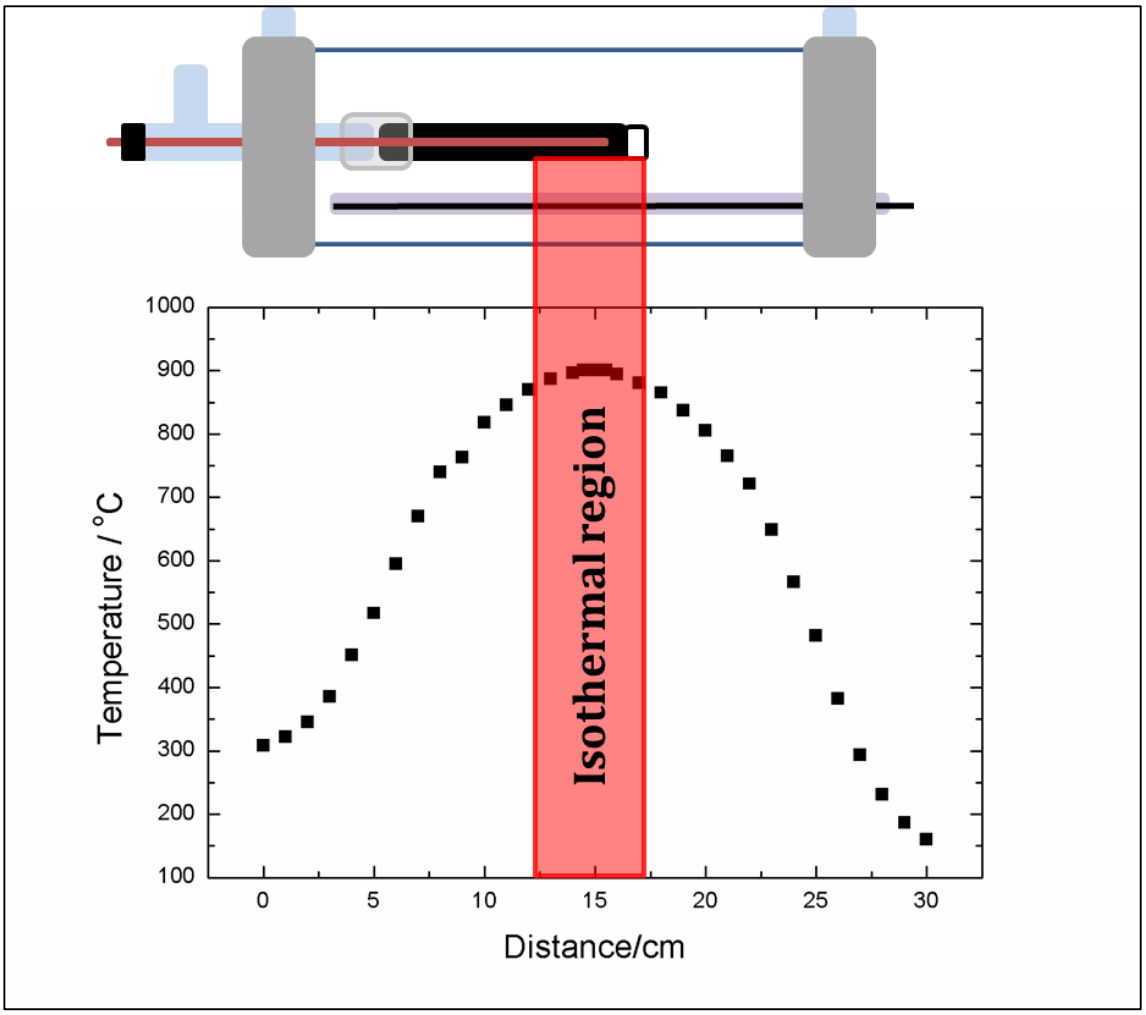

Figure 3.7: The temperature profile of the furnace showing isothermal region and how the membrane reactor is positioned in the furnace according to the temperature profile.

In order to monitor the operating temperature of the membrane reactor, a k-type thermocouple is inserted along the length of the reactor. All of the experiments reported in this thesis were conducted at 900°C and in atmospheric pressure.

3.2.4 Gas analyses

Gas chromatography

The gas analyses instruments used in this study are Gas Chromatographs (GC). The two GCs used in this study were Varian 3800 GCs one with a mole-sieve 5A packing

(Thames Restek, UK) for the analysis of hydrogen, oxygen, nitrogen and methane and carbon monoxide to be called GC-A.

The other outlet stream was installed with shincarbon packing (Thames Restek, UK) for the analysis of hydrogen, oxygen, nitrogen, carbon monoxide methane and carbon dioxide will be identified as GC-B in this thesis from now on. Shincarbon packing is not able to detect water. In the case of wet-gases transferred into the packing, water can be evaporated by operating the column at 400^{o}C.

Both GC-A and GC-B were equipped with the Thermal Conductive Detector (TCD). Argon is used as the carrier gas in both of the GCs although the common carrier gas for GCs is helium. This is because for low concentration of hydrogen in helium, the mixture displays a much lower thermal conductivity than that of pure helium [152, 153]. In this case, the used of helium as the carrier gas will results in a no-show of the peak in chromatograms hence giving a false-negative result reading on the hydrogen production level from the experiments.

The data is collected and saved using the software provided by Varian, UK named STAR. For the calibration, GC-A is calibrated with 1% of hydrogen, 2% of oxygen, 2% of nitrogen and 2% methane. GC-B is calibrated with 2% hydrogen, 2% oxygen 2% nitrogen, 2% carbon monoxide, 2% carbon dioxide and 5% methane. All the standard gases were purchased through ST Gas (UK) Ltd. Since material balance and oxygen permeations values calculated in this thesis were totally dependent on the readings obtained from these GCs a simple experiment was done to determine the largest deviation of the readings as to determine the percentage of error that need to be addressed in future calculations involving the data collected by the GCs. Figure 3.8 shows the reading of the deviation on calibrated values for both GCs.

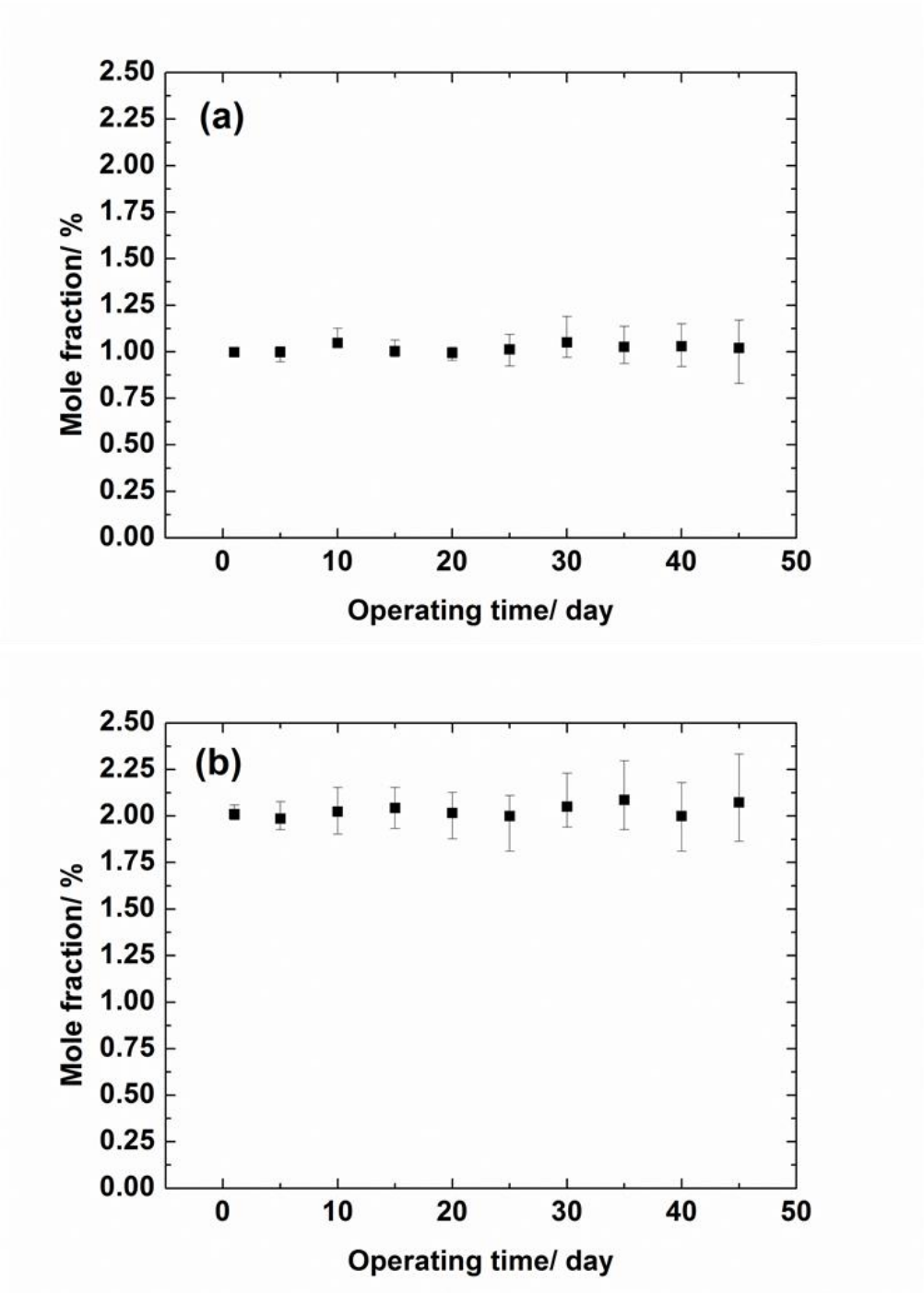

Figure 3.8: GCs deviation readings for oxygen signals upon feed slow of standards containing 1% mole fraction of oxygen and 2% mole fraction of oxygen respectively. (a) GCA- Mole sieve 5A packing (b) GCB-shincarbon packing.

The calibrations for both of the GCs were done once in two weeks to make sure that the deviations were kept not more than ±10%. The error percentage associated

with the reading of signals given by the GC Varian software was calculated using Equation 3.1 below;

$$\%\text{error} = \frac{|C_v - C_{v_o}|}{C_{v_o}} \times 100\% \qquad \text{Equation 3.1}$$

The highest error percentage obtained for GC-A is 6.76 % and 8.96% for GC-B. The deviation in both GCs were at the highest starting from hour 700 and this shows that a new re-calibration step needs to be done to avoid large deviations over the period of experiments. For sampling in experiment purposes, gas injections were made every 30 minutes making the total sampling for each sampling cycle is 30 minutes.

Normally GC-A will be used to analyse the outlet gases on the lumen side and GC-B will be used to analyse the outlet gases on the shell side. In the occasion of more than two outlets to be analysed, one of the GCs will be used alternately to minimise error.

Hygrometer

The water concentration from the outlet of the shell side was detected and measured by a dew point transmitter, DMT345 manufactured by Vaisala, Finland. DMT345 is a dew point transmitter that uses a dielectric material made of high polymer membrane, DRYCAP ® as a sensor. Figure 3.9 shows the built of an intelligent polymer used in the DMT345 dew point transmitter. Operation of the sensor depends upon the adsorption of water vapour into a porous non-conducting "sandwich" between two conductive layers built on top of a base ceramic substrate. In a water containing environment the polymer sensor will absorb water having the weight that is proportional to the relative humidity. The water occupies the free

space between the polymeric molecules, changing the dielectric constant of the polymer. This change is related to the amount of water absorbed and thus giving the new value for the amount of water in the system [154].

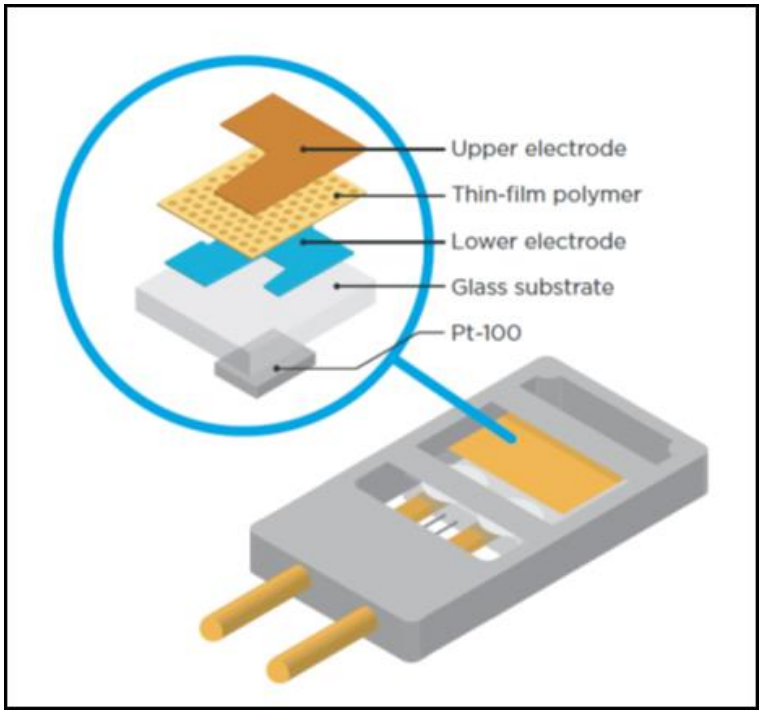

Figure 3.9: Schematic diagram of the polymer sensor incorporated in the hygrometer.

The water content in the outlet stream of the shell side was monitored by the hygrometer. The hygrometer is self-calibrated by the software that accompanies the hardware. To make sure that the hygrometer calibration is precise, a simple calibration was done to compare the reading of the hygrometer and the theoretical reading of water vapour at different temperature. Figure 3.10 shows the results of the reading of hygrometer versus the theoretical value of the water vapour we should be getting at each specific temperature.

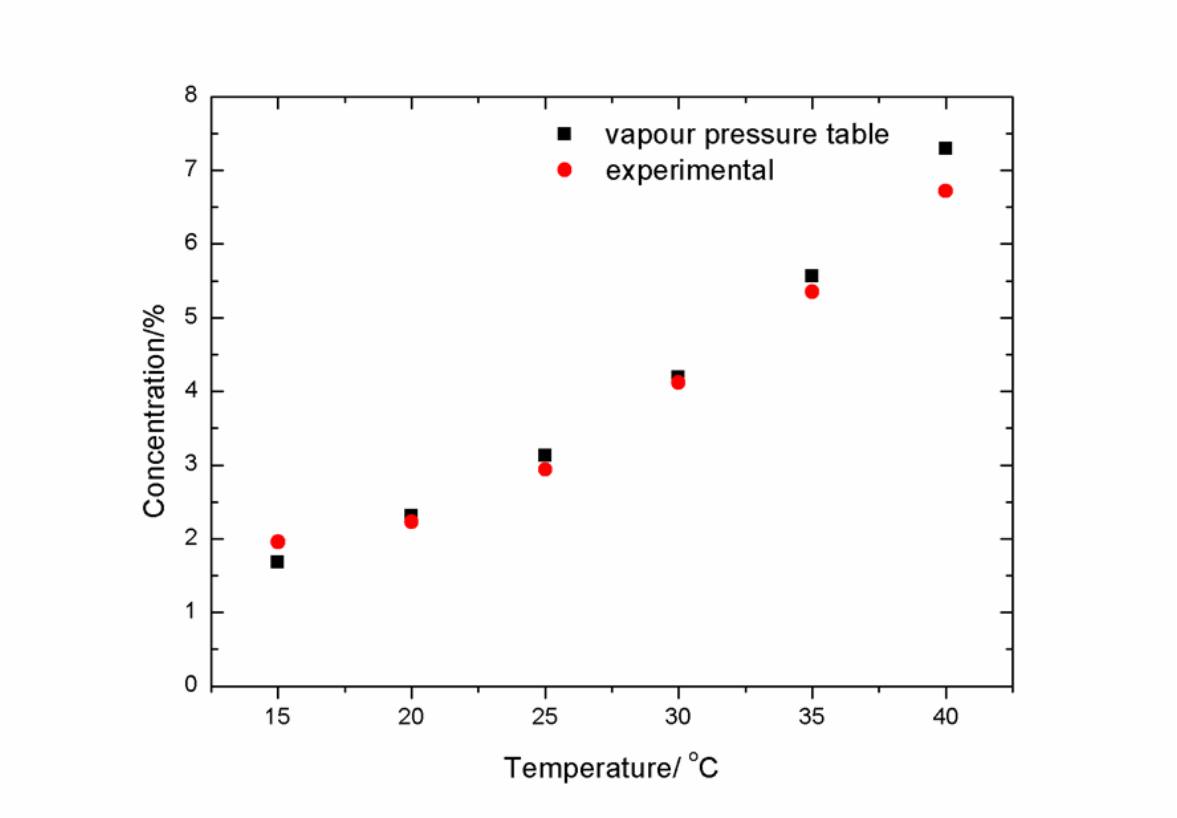

Figure 3.10: Calibration curve for the hygrometer.

As can be seen from the figure, the largest deviation for the concentration reading is at the temperature of 40°C. This may be due to the fast cooling of the stainless steel piping used to transport the water feed flow to the hygrometer inlet. To avoid error in the readings, we decided to fix the water concentration at 4% (30°C) at which the temperature and concentration readings of the system do not show much deviation.

3.2.5 Leak tests

In this study leak tests were conducted at different stages. The first leak test was done on the membranes upon arriving from the supplier. In this step the membrane is positioned vertically into a large measuring cylinder filled with water. One end of the membrane was fed to a 5bar of pressurised air (laboratory supplied air for cleaning). Any bubble detected from the surface of the membrane in the water

indicates that the membrane has small cracks. Membranes with detected cracks will be discarded.

The second stage of leak testing is done after the membrane was sealed, sintered and built-on to the piping system ready to be put into the quartz housing. Leak testing was performed by feeding the inlet of the membrane with 30mlmin^{-1} of argon measured by the digital flowmeter. The outlet flowrate of the membrane is then measured by the same digital flowmeter. A well-sealed membrane will give the same outlet flowrate as the inlet. In the case of different results (decreased flowrate detected in the outlet of the membrane) a leak detector was used to detect the point of leaks. If the leaks were from non-tight Swagelok fittings, tightening the screws can always solve the problem. Often the leaks were from imperfect sealing activity. For the shell side the whole reactor needs to be sealed with the ultra-torr fittings before any leak test can be performed. For the shell side, the leak testing was performed by feeding 30mlmin^{-1} of argon measured by the digital flowmeter at the inlet of the shell side chamber. The outlet flowrate is measured by the same digital flowmeter used to measure the flowrate at the inlet. A well-sealed shell side chamber will give the same inlet and outlet flowrate readings.

To ensure the membrane reactor is gas tight and the gas analysis by the GCs are reliable for further investigation in the study, we leak tested all of the membrane reactors before and after heating procedures. The membrane reactor took a minimum of two days for it setup. This is because the 30G stainless steel injector was sealed using liquid silicone sealant and need to be left to dry for 24 hours prior to heating. After the silicone sealant has dried, the membrane reactor needs to be leak tested.

The last leak test takes place before the experiment started is when the reactor temperature is at 900^{o}C. Leak tests were conducted by supplying both sides of the membranes with 30mlmin^{-1} of zero grade argon. Experiments will only be conducted when the readings for oxygen and nitrogen mole fraction signals were less than 0.05%. In such cases where leaks were detected in the last leak tests, the whole membrane reactor will be cooled down and the membrane will be replaced.

As for the calculation of oxygen permeation with leaks detected and observed, oxygen flux that is associated with leaks will be deducted from the total oxygen permeation flux calculation. In the case of using air as the inlet for the oxygen permeation experiment, the amount of oxygen caused by leaks can be calculated by its relationship to the percentage of nitrogen detected in the permeate side. Further details on the calculations of fluxes and error propagation will be discussed in the section 3.2.7.

3.2.6 System setup

Three types of experiments were used and are discussed in this chapter. The first experiment is the oxygen permeation study with non-reducing gas fed on the shell side. In this experiment the total oxygen permeation into the shell side from air on the lumen side can directly be calculated from the oxygen concentration obtained from the reading of the gas chromatography (GC). Figure 3.11 shows the schematic diagram of the experimental setup for the experiment. In this system the inlet gases were transported from the feed system into the shell side of the membrane reactor using 1/8'' Swagelok® PFA flexible tubing. The outlet gases from the lumen side of the reactor were transported to GC A and the outlet gases from the shell side were transported to GC B.

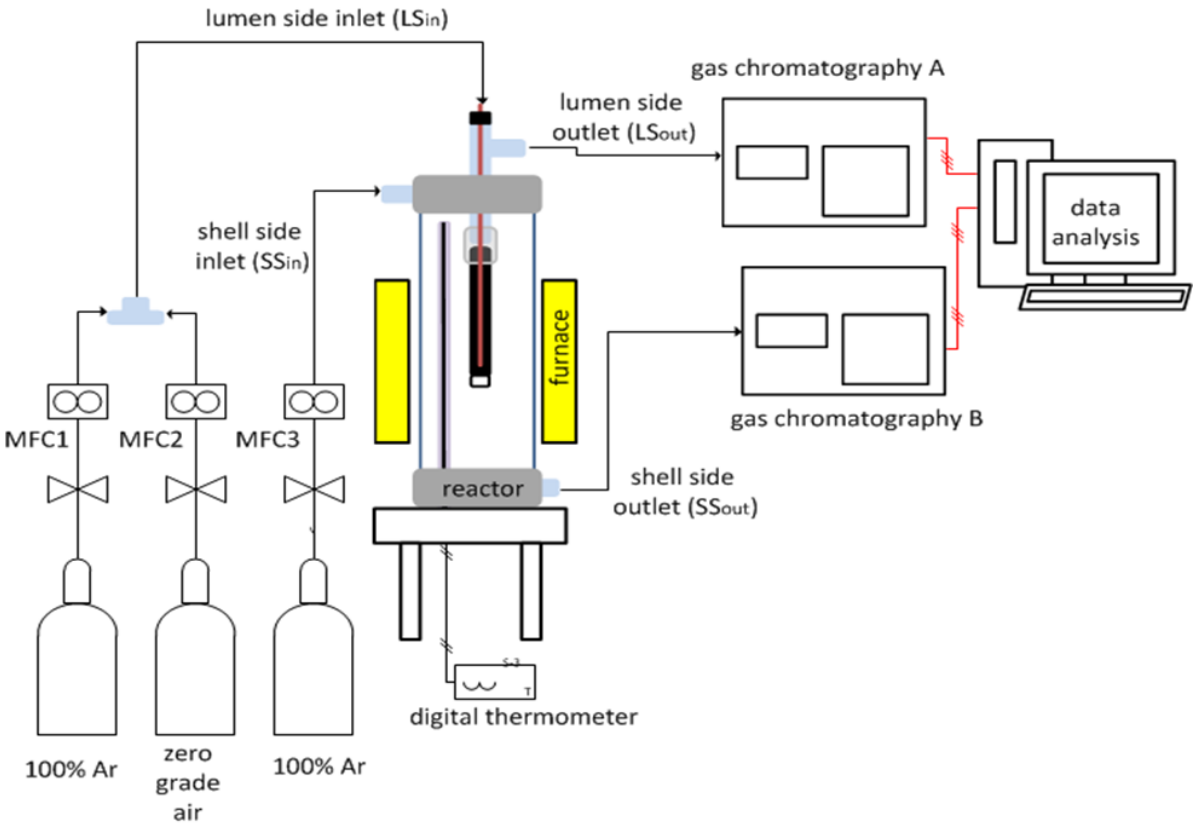

Figure 3.11: Experimental setup for studies on oxygen permeation without reducing gas.

The second experiment is the oxygen permeation study with reducing gas fed in the shell side of the membrane. Figure 3.12 shows the experimental setup for the experiment. In this experiment, methane will react with the permeated oxygen from the lumen side at the shell side. The main reactions that will take place on the shell side is the full combustion of methane and partial oxidation of methane of which will produce hydrogen, carbon monoxide, carbon dioxide and water. Streams containing water will be piped through the hygrometer for water content analysis and then pass through the GC for further quantification of the product gas concentrations.

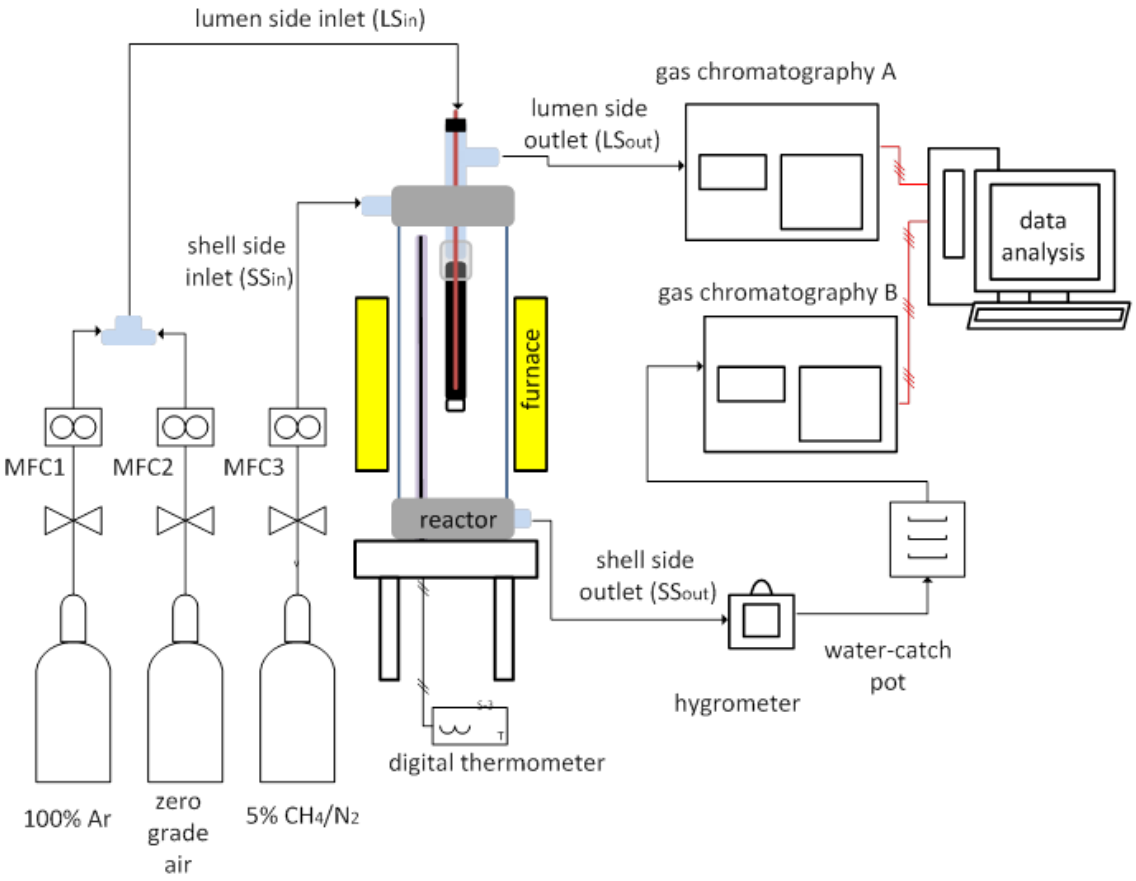

Figure 3.12: Schematic diagram for the experimental setup for oxygen permeation experiment with reducing gas fed into the shell side of the reactor

The third experiment involves the water splitting process on the lumen side and methane reforming process on the shell side. Figure 3.13 shows the experimental setup for the water splitting experiments. In this setup the lumen inlet gas was supplied through the water saturator where saturated water will be transported as the inlet of the membrane lumen.

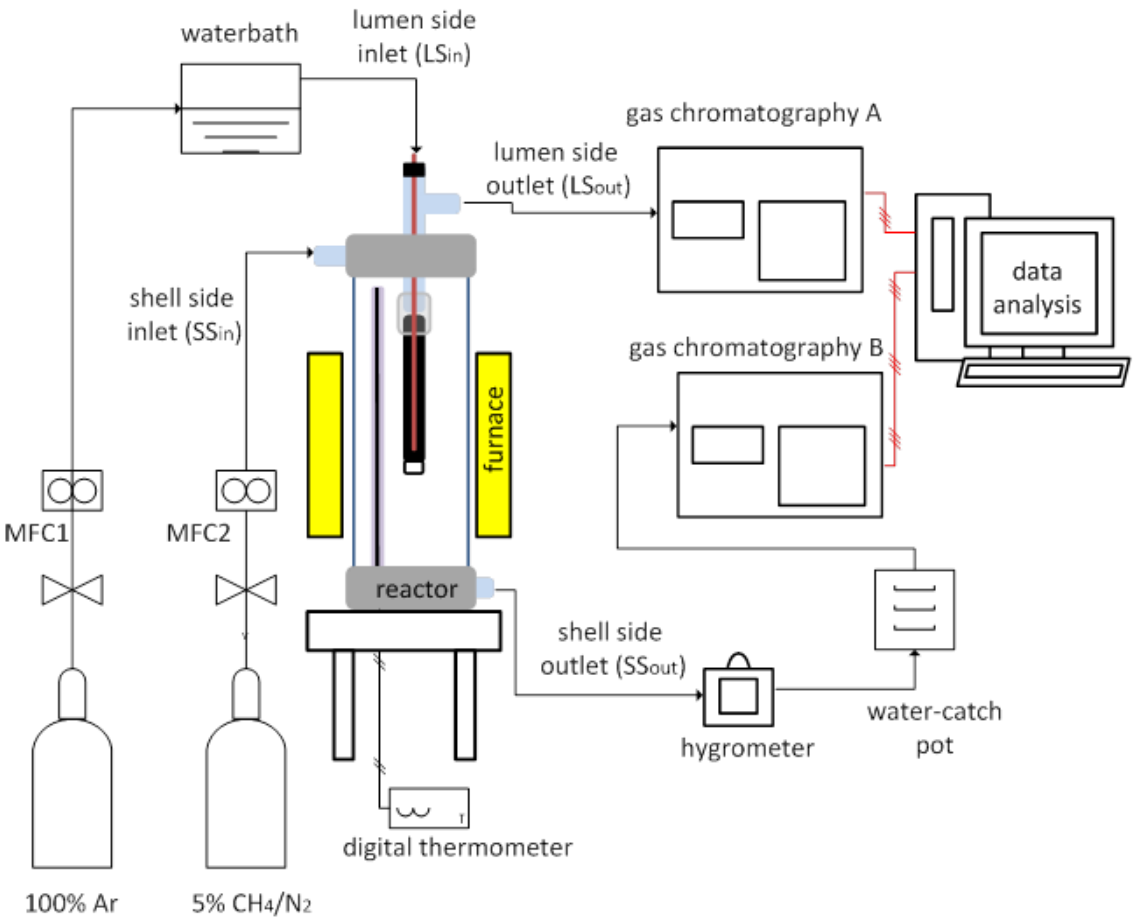

Figure 3.13: Experimental setup for the water splitting process with methane feed on the shell side and water feed on the lumen side

3.2.7 Notations, Material Balance and Error Propagation Calculations

All of the gas analysis values are obtained from the GCs' reading. The GCs were programmed to give values in terms of mole fraction of each gas. For the oxygen permeation experiments involving only air inlet into the lumen side and argon fed into the shell side, the oxygen mole fractions obtained from the GCs reading can be converted into molar flowrate, J_{O_2} ($\mu molO.s^{-1}$). Assuming ideal gas behaviour the oxygen permeation flux can be calculated using Equation 3.2

$$J_{O_2} = [O_2]_{out} F \frac{1}{V_m} \frac{1}{60} \times 10^6$$ Equation 3.2

Where

F is the inlet flowrate into the shell side (STP) ($mlmin^{-1}$)

V_m is the molar volume of ideal gas at 25°C (24 465 $mlmol^{-1}$)

$[O_2]_{out}$ (%) is mole fraction of the oxygen gas,

where

$[O_2]_{out} = y_{O_2} - \left(\frac{0.21}{0.79}\right) \times y_{N_2}$ with y_{O_2} is the GC reading for oxygen mole fraction and y_{N_2} is the GC reading for nitrogen mole fraction. In this case y_{N_2} denotes the amount of air leaks into the other chamber. Hence this amount was used to calculate the amount of oxygen leaks *i.e*; not permeated into the system by the membrane.

As for the reactive experiments, the oxygen permeation rates calculation involves the use of the inlet and outlet mole fractions obtained from both of the GCs used for product analyses. To simplify and make the further discussion about the oxygen permeation, material balances and error propagation calculations clearer, we individually identify each of the mole fractions of the inlets and outlets gases with specific notations. Figure 3.14 shows the notations that will be used throughout the chapter. All of the gases used in the shell side will be identified with a superscript SS1. Likewise the gases associated with the lumen side will be identified through the 'L1' superscript. To classify the direction of the gas flow, a subscript of either '(in)' or '(out)' will be used. '(in)' denotes the inlet into the SS or L1 and '(out)' represents the outlet from SS or L1. The total flowrate of the inlet to the lumen side

will be identified with the symbol n_T^{L1} while the inlet total flowrate to the shell side will be identified as n_T^{SS} .

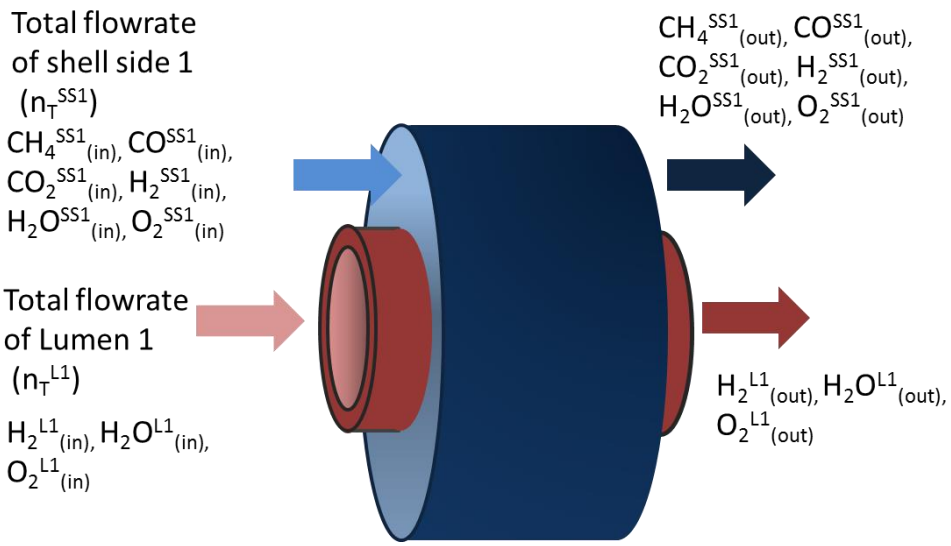

Figure 3.14: Notation used in the equations for oxygen permeation, material balance and error propagation calculations.

For the membrane system having methane as the feed to the shell side which may be coupled with lumen(s) fed with air and/or water; the oxygen permeation in the shell side, OP_{SS} can be calculated using Equation 3.3.

$$OP_{SS} = \left[2(O_{2(out)}) + \left(CO_{(out)}^{SS1} - CO_{(in)}^{SS1}\right) + 2\left(CO_{2(out)}^{SS1} - CO_{2(in)}^{SS1}\right) + \left(H_2O_{(out)}^{SS1} - H_2O_{(in)}^{SS1}\right)\right] n_T^{SS1} \qquad \text{Equation 3.3}$$

For the oxygen balance calculation, the OP_{SS} need to be compared with the amount of oxygen permeated from the lumen side, OP_{LS}. This value can be calculated by deducting the amount of oxygen supplied in the oxygen feed into lumen 1 with the detected amount of oxygen in the lumen outlet stream.

For the system having methane reforming on the shell side and water splitting on the lumen side, the amount of oxygen permeation on the shell side needs to be the same as the oxygen transported across the membrane; in this can the oxygen permeation from the lumen side.

$$OP_{SS} = OP_{LS} \qquad \text{Equation 3.4}$$

where

$$OP_{LS} = \left(H_{2(out)}^{L1} - H_{2(in)}^{L1}\right)]n_T^{L1} \qquad \text{Equation 3.5}$$

The maximum and minimum values of the GC readings will be based on the previous experiment reported earlier in section 3.2.4. The errors associated with GC deviation readings were proved to be less than 10%. In order to standardise on the error percentage, the error associated with the direct reading of the GC will be reported to have a maximum and minimum error of 10% from the real reading. This error limits were chosen to make sure that all of the error values calculated and presented in this thesis cover the maximum error the system would have achieved. Error propagations were calculated using these minimum and maximum errors and the largest deviation values from the later calculations will be used as the new error limit for the permeation rates value. Referring to the calculation of the OP_{SS} given earlier by Equation 3.3, the equation used to determine the error propagation associated with the OP_{SS} values is given by Equation 3.6 and Equation 3.7. The

largest deviation value from the main OPss results calculated using Equation 3.3 will be chosen to be the new maximum and minimum error limits to be reported in this thesis.

$$
\begin{aligned}
OP_{SS_{min}} = [\, & 2(O_{2(out)} - \Delta O_{2(out)}) \\
& + \left((CO^{SS1}_{(out)} - \Delta CO^{SS1}_{(out)}) - (CO^{SS1}_{(in)} - \Delta CO^{SS1}_{(in)})\right) \\
& + 2\left((CO^{SS1}_{2(out)} - \Delta CO^{SS1}_{2(out)})\right. \\
& \left. - (CO^{SS1}_{2(in)} - \Delta CO^{SS1}_{2(in)})\right) \\
& + \left((H_2O^{SS1}_{(out)} - \Delta H_2O^{SS1}_{(out)})\right. \\
& \left. - (H_2O^{SS1}_{(in)} - \Delta H_2O^{SS1}_{(in)})\right)](\, n_T^{SS1} - \Delta\, n_T^{SS1})
\end{aligned}
\qquad \text{Equation 3.6}
$$

$$
\begin{aligned}
OP_{SS_{max}} = [\, & 2(O_{2(out)} + \Delta O_{2(out)}) \\
& + \left((CO^{SS1}_{(out)} + \Delta CO^{SS1}_{(out)}) - (CO^{SS1}_{(in)} + \Delta CO^{SS1}_{(in)})\right) \\
& + 2\left((CO^{SS1}_{2(out)} + \Delta CO^{SS1}_{2(out)})\right. \\
& \left. - (CO^{SS1}_{2(in)} + \Delta CO^{SS1}_{2(in)})\right) \\
& + \left((H_2O^{SS1}_{(out)} + \Delta H_2O^{SS1}_{(out)})\right. \\
& \left. - (H_2O^{SS1}_{(in)} + \Delta H_2O^{SS1}_{(in)})\right)](\, n_T^{SS1} + \Delta\, n_T^{SS1})
\end{aligned}
\qquad \text{Equation 3.7}
$$

Detailed examples for the error propagation calculations for OP_{SS} reading (using real values) can be found in Appendix A1.

3.2.8 Post Experimental Analysis

Pre and post experimental analysis on the membrane surfaces was made using Scanning Electron Microscopy (SEM) and Energy Dispersive X-Ray Analysis (EDX), using a Hitachi TM3030, Japan. The scanning was made on both fresh and used samples under high vacuum condition, at 15kV without pre-treatment of the samples. Elemental analyses were conducted using the x-ray microanalysis (EDX) system assisted by Quantax 70 software. The SEM micrographs and EDX detailed

analyses however will only be shown and discussed in this thesis when there are major differences detected.

3.3 Results and Discussion

This section discusses the results on oxygen permeation done on two different hollow fibre membranes; (i) LSCF6428 and (ii) BSCF5582

3.3.1 Oxygen permeation without methane reforming

The first experiment on the oxygen permeation involves one lumen inlet (L1) with oxygen feed with another lumen inlet (L2) was fed with an inert gas (considered not active). This is to make sure that the permeation of oxygen was totally based on the material ability to transport oxygen from one side of the membrane to the other.

The oxygen permeation study involves the use of 30ml (STP)min^{-1} feed having 10% of oxygen and 40% nitrogen in argon fed into the lumen of the LSCF6428 membrane and 30$mlmin^{-1}$ of zero grade argon was fed into the shell side of the membrane. The experiment was conducted for more than 300 hours to evaluate the oxygen permeation ability of the LSCF6428 membrane. A similar oxygen permeation study procedure was also done for the BSCF5582 hollow fibre membrane. Figure 3.15 shows the overall oxygen permeation calculated in molar flowrate of oxygen versus time in hours. The oxygen permeation rates can be determined by calculating the number of moles of oxygen that has been transferred into the shell side. The calculation methods were thoroughly described in section 3.2.7.

The oxygen permeation rate from the lumen side into the shell side started to show stable rates after 30 hours of operation. There is an acceptable leak of nitrogen; an

average of 0.02 % mole fraction of nitrogen into the shell side at the beginning of the operation however the leak signals stabilised after three hours of operation. In this experiment the average oxygen permeation rates for the LSCF6428 membrane is at 0.24µmolO.s^{-1}. This result shows a similar trend to that obtained earlier in the study done by Franca *et al* [11] but with a slightly lower rate.

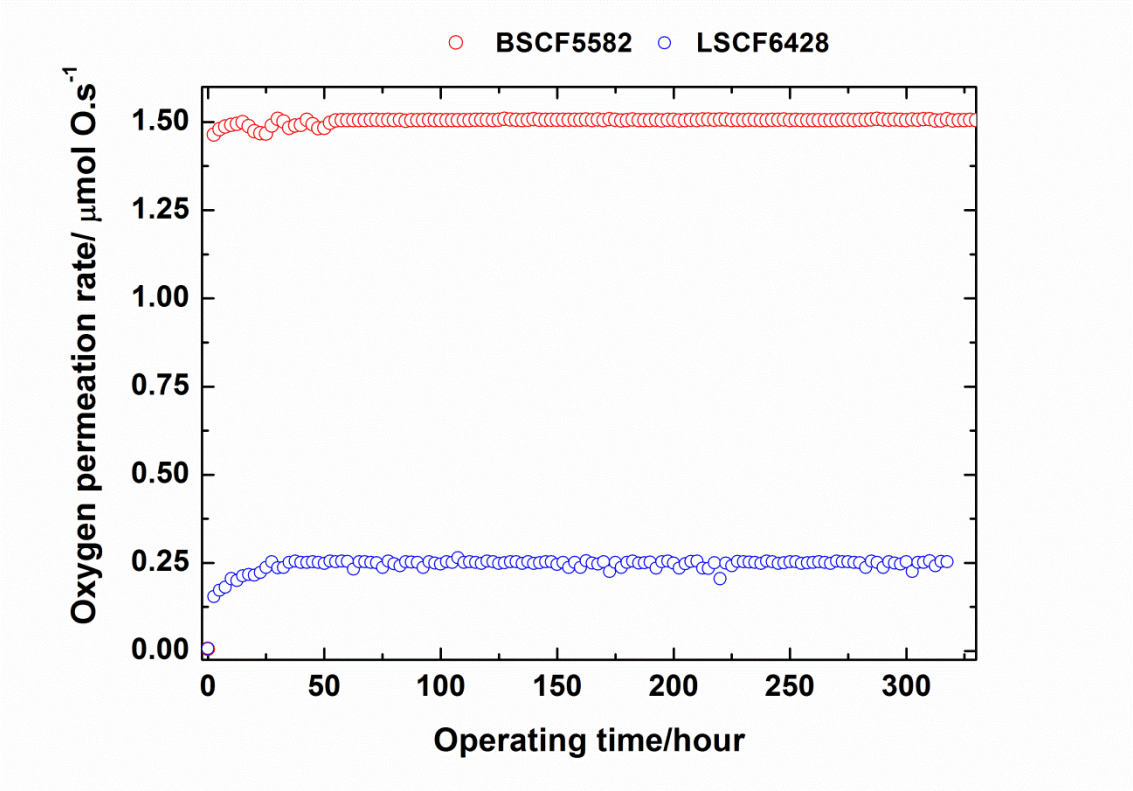

Figure 3.15: Oxygen permeation of (i) LSCF6428 hollow fibre membrane (ii) BSCF5582 hollow fibre membrane

The BSCF5582 membrane however shows a higher oxygen permeation rate than that of LSCF6428. The BSCF5582 membrane took more than 60 hours to give a stable oxygen permeation rate. As the membrane used in this permeation is the fresh as supplied membrane, the longer time to display stable results was probably caused by the act of oxygen filling the vacancies that are available in the material. The total oxygen permeation calculated for the BSCF5582 membrane is 1.50µmol.s-

[1], six times higher than the oxygen permeation in LSCF6428 in the same environment.

Both membranes demonstrate good stability in performing oxygen permeation for over 300hours of operation. The leaks however increased from 0.02% to 0.06% after 10 hours of operation and remained the same throughout the rest of the operating time. Leaks in the BSCF5582 membrane reactor were near negligible, 0.04% and do not increase upon start-up.

Based on the results obtained in these experiments we can conclude that both membranes show good chemical stability. Leaks were at minimum level which is considered insignificant for material balance calculations. The newly designed reactor helps to minimised the thermal degradation of the membrane thus prolonging the oxygen permeation operating time to more than 300 hours.

3.3.2 Oxygen Permeation with Methane Reforming

This section discusses the performance of LSCF6428 and BSCF5582 membranes in permeating oxygen under reducing conditions on one side of the membrane. In this experiment the shell side of the membrane reactors were fed with 30mlmin^{-1} of 5% methane in nitrogen while the lumen side were fed with 30mlmin^{-1} of 10% oxygen and 40% nitrogen in argon. Figure 3.16 shows the oxygen permeation rates for both of the membranes plotted against operating time and Table 3.3 lists the average mole fractions of the product compositions in the shell side of the membrane reactor. It is expected that by having this type of inlet configuration the permeated oxygen from the lumen side will react with the methane to perform (i) partial oxidation of methane to produce hydrogen and carbon monoxide, (ii) full

combustion of methane to produce carbon dioxide and water. The overall oxygen permeation rates were calculated using the equations presented in section 3.2.7.

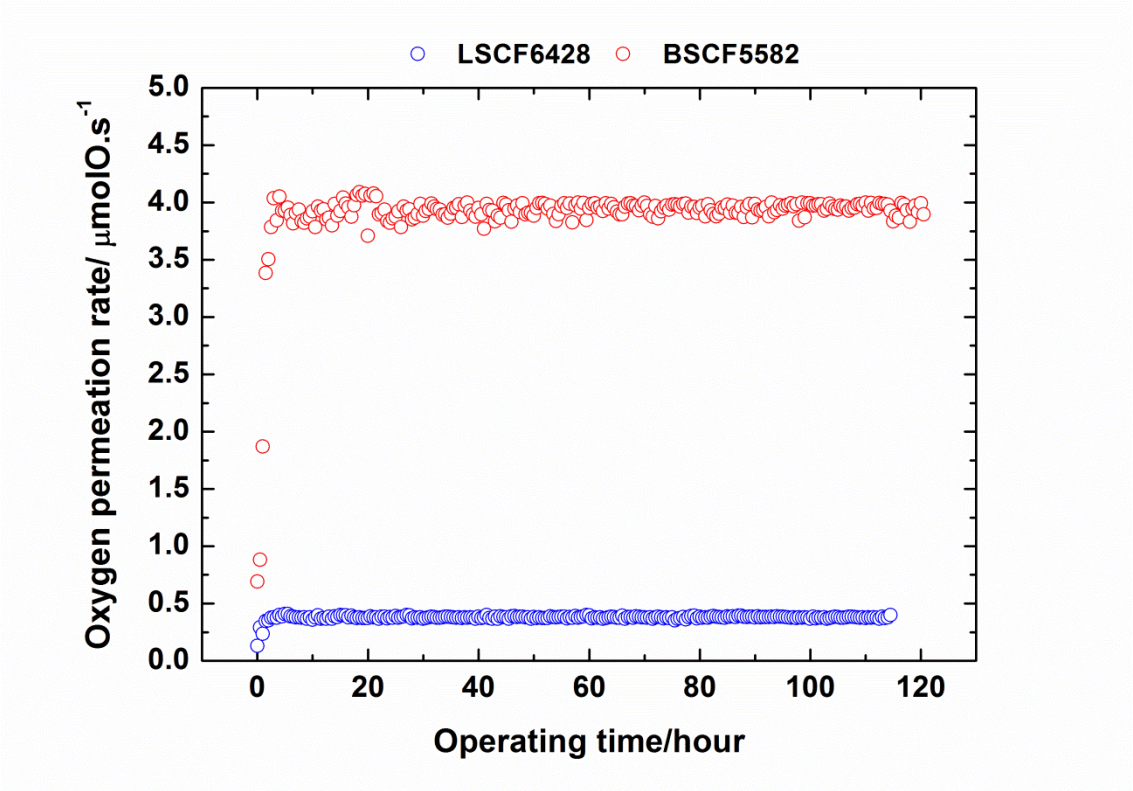

Figure 3.16: Oxygen permeation rate for membranes fed with 30mlmin^{-1}, 10% oxygen and 40% nitrogen in argon on the lumen side and 30mlmin^{-1}, 5% methane in nitrogen on the shell side.

The average oxygen permeation rate on the shell side of the LSCF6428 membrane is 0.38±0.05μmolO.s^{-1}, showing a slight increase from the average oxygen permeation rates obtained from the previous inlet configuration. The average oxygen permeation rate on the lumen side is at 0.39±0.02μmolO.s^{-1}. These values show that the oxygen balance for this system closes. The ratio of carbon monoxide to carbon dioxide is 0.11 showing a low concentration of carbon monoxide.

Table 3.3: The average mole fraction of the product compositions in the shell side for the membrane reactor fed by 30mlmin^{-1} of 5% methane in nitrogen on the shell side and 10% of oxygen, 40% nitrogen in argon.

	Lumen side/ Mole fraction (%)	**Shell side/ mole fraction (%)**					
	O_2	H_2	O_2	CO	CH_4	CO_2	H_2O
Inlet (LSCF6428)	10.0± 1.00	-		-	5.00± 0.50	-	-
Outlet (LSCF6428)	9.04± 0.90	0.16± 0.02		0.08± 0.01	4.00± 0.40	0.71± 0.07	0.36± 0.04
Inlet (BSCF5582)	10.00± 1.00				5.00± 0.50		
Outlet (BSCF5582)	0.54± 0.05	-	2.41± 0.24	-	1.02± 0.10	3.81± 0.38	6.53± 0.65

The BSCF5582 membrane however, shows nearly 100% permeation of oxygen from the lumen into the shell side. The results obtained from the analysis of the shell side gas outlet reveals that the permeated oxygen only results in the total combustion of methane. This shows that the oxygen permeated from the shell side is too high, making the methane to be the limiting reactant thus increasing the selectivity towards the production of carbon dioxide to 100%. This eliminates the potential of hydrogen production from the POM reaction to happen on the shell side of the

reactor. Overall oxygen permeation rate calculations show that the oxygen balance closes giving OP_{SS} rates at 3.88 ±0.39μmolO.s^{-1} and OP_{LS} at 3.87± 0.04μmolO.s^{-1}.

Post operation characterisations were conducted on both LSCF6428 and BSCF5582 membranes using SEM/EDX technique. No major changes were found on the surface of LSCF6428 membrane. As of for the BSCF5582 surface analysis, we detected a remarkable carbon deposition on the surface of the membrane. Figure 3.17 shows the SEM micrograph of the BSCF5582 membrane surface after the oxygen permeation coupled methane reforming experiment. The area shown in yellow oval mark depicts the impurities on the surface of the membrane. Further EDX elemental analysis revealed that the impurities detected on the surface are identified as carbon deposition.

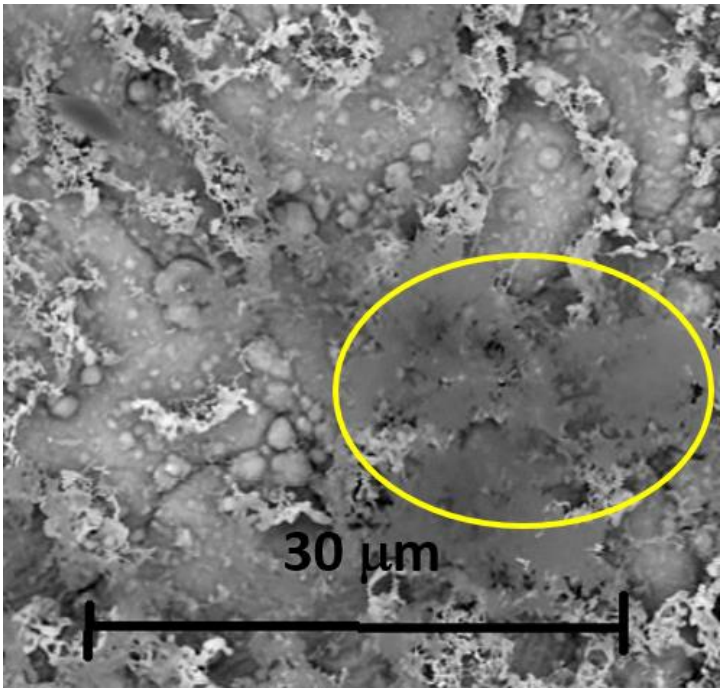

Figure 3.17: SEM micrograph of the BSCF5582 membrane surface upon exposure to 30mlmin^{-1} of 5% methane in nitrogen.

3.3.3 Water splitting coupled methane reforming

In this section the membranes were tested for their water splitting ability where 4% of water sweep in zero grade argon is fed into the lumen side of the membrane. The shell side of the membranes were fed with 30mlmin^{-1} continuous flow of 5% methane in nitrogen. This environment creates a highly oxidising environment on the lumen side and highly reducing environment on the shell side. Figure 3.18 shows the mole fraction of hydrogen productions in the lumen side of both membranes (a) LSCF6428 and (b) BSCF5582.

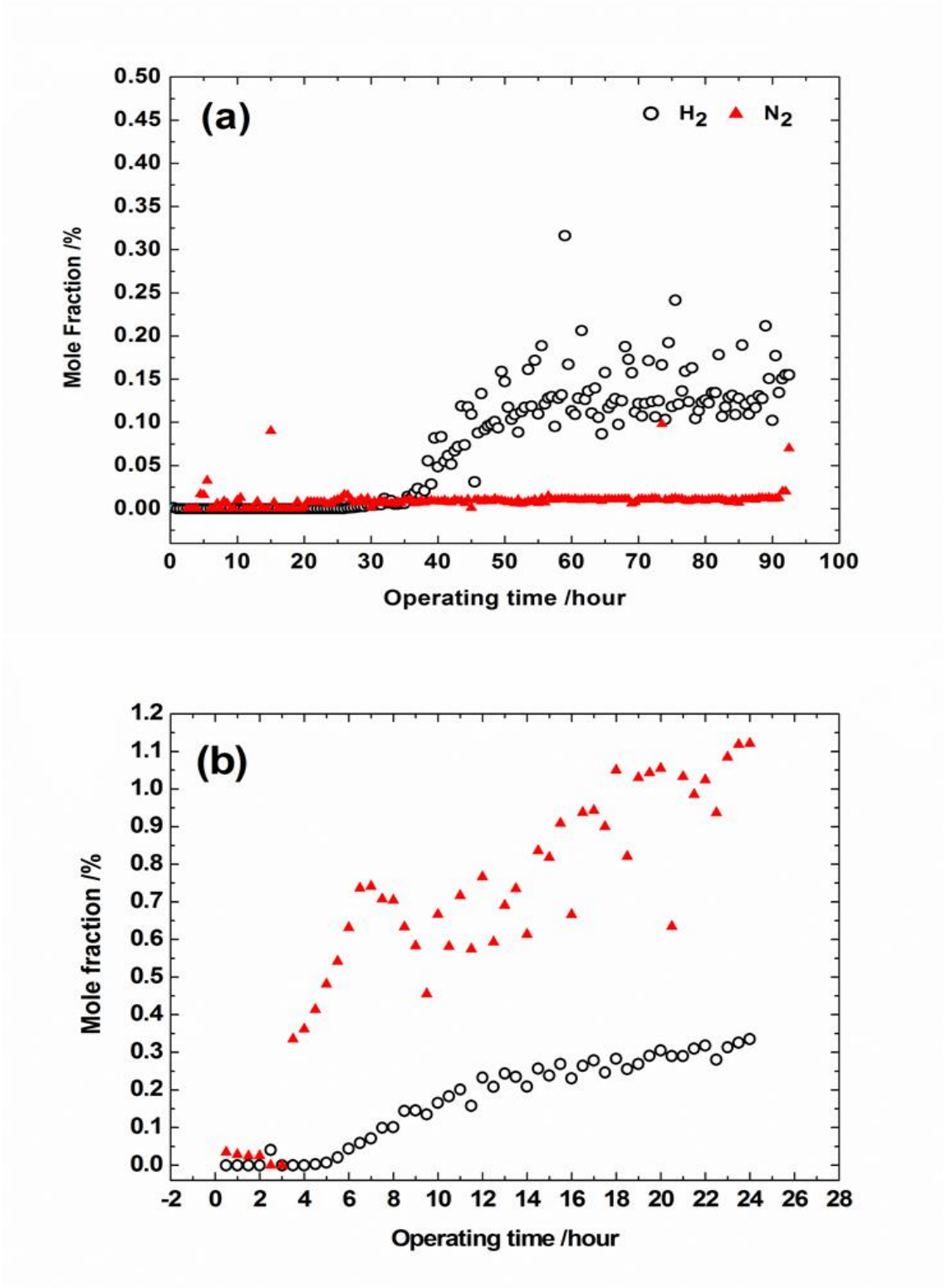

Figure 3.18: Hydrogen production in the lumen side (from water splitting reaction) for (a) LSCF6428 and (b) BSCF5582 membrane when the lumen inlet were fed with 30mlmin^{-1} of 4% of water in argon and shell side inlet were fed with 30mlmin^{-1} of 5% methane in nitrogen. Experiments were conducted individually for each membrane. Nitrogen signal showed in the graphs act as the tracer for leakages.

The LSCF6428 membrane shows stable hydrogen production with minimum leaks for over 90 hours of operation. The LSCF6428 membrane demonstrates an induction period of nearly 40 hours upon start-up before showing hydrogen production in the lumen side and oxidation products in the shell side.

BSCF5582 however shows an early sign of hydrogen production but gradually showing the sign of leakage with the increasing nitrogen signal detected in the outlet stream of the membrane lumen. This result shows similar trend reported by Leo *at al* [155] where the oxygen permeation from steam feed shows significant amount of hydrogen production after 20 hours of operation. Table 3.4 lists the average product compositions obtained from the inlet and outlet streams from the LSCF6428 membrane reactor.

Table 3.4: Average mole fraction (%) of products from the water-methane inlet experiment for the LSCF membrane. The lumen was fed with 30mlmin^{-1} of 4% of water and shell side inlet was fed with 30mlmin^{-1} of 5% methane in nitrogen.

	Lumen side/ Mole fraction (%)	Shell side/ mole fraction (%)				
	H_2	H_2	CO	CH_4	CO_2	H_2O
Inlet	-	-	-	5.00± 0.50	-	-
Outlet	0.16± 0.02	0.42± 0.04	0.16± 0.02	4.71± 0.47	0.02± 0.002	-

(-) not detected

Note that because the BSCF5582 membrane showed leakages too early after the permeation experiment started, the results on the hydrogen production in the

lumen might be from the water gas shift process thus making it not convincing to say that the products analysed from the shell side are produced with the permeated oxygen from the water splitting process on the lumen side. Furthermore when nitrogen signals was detected in the lumen side; there would probably be a methane leak in the lumen causing steam reforming hence producing hydrogen. There was no water in the outlet stream of the shell side. This may be because the main reaction occurred on the shell side in the POM. This is evidently shown in the small percentage of the average mole fraction of carbon dioxide (the other product generated from full combustion of methane).

Based on the calculation method presented in section 3.2.7, the average oxygen permeation rate from water splitting obtained on the lumen side of the LSCF6428 is $0.03\pm0.01\mu molO.s^{-1}$ whereas the oxygen permeation in the shell side is $0.04\pm0.01\mu molO.s^{-1}$. This shows a close oxygen balance between the oxygen transported from lumen and the oxygen reacted on the shell side.

The carbon monoxide to carbon dioxide ratio, CO/CO_2 is 8.53. This shows that there is a very limited supply of oxygen on the shell side of the membrane making oxygen the limiting reactant thus pushing the selectivity towards partial oxidation of methane hence producing more carbon monoxide and hydrogen.

The average rate of oxygen permeation into the shell side of LSCF6428 membrane obtained here is lower than that of reported in section 3.3.2. This is because extra heat of reaction is required in splitting water whereas the permeation of oxygen from an oxygen containing gas is only driven by the gradient in oxygen partial pressure between the two sides of the membrane.

Post operation characterisations were made on both LSCF6428 and BSCF5582 membranes to observe any remarkable difference on the surface of the membrane before and after operation. Figure 3.19 shows the SEM micrographs for the LSCF6428 membrane before and after the exposure of methane.

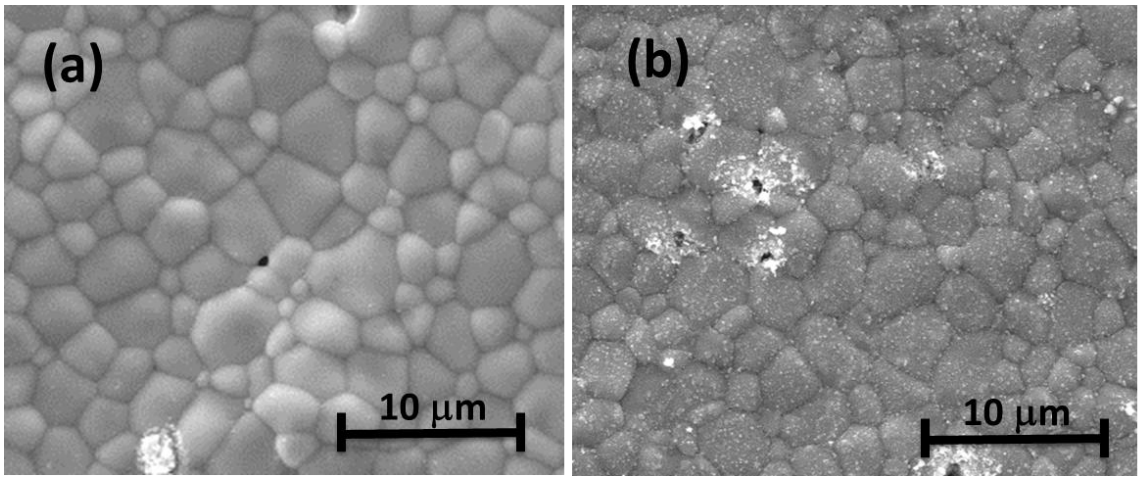

Figure 3.19: SEM micrographs for (a) fresh sample LSCF6428 membrane on the shell side surface (b) the same LSCF6428 membrane surface after being exposed to methane for *ca* 330hours.

After ca 330hours of operation with continuous supply of methane the surface shows fine crystals formation in the post characterisation imaging. Further analysis with a point elemental analysis however does not show any difference from the fresh membrane sample before reaction.

Figure 3.20 shows the micrograph of the LSCF6428 membrane lumen surface after methane-water splitting experiment where the lumen is previously exposed to 4% of water in argon.

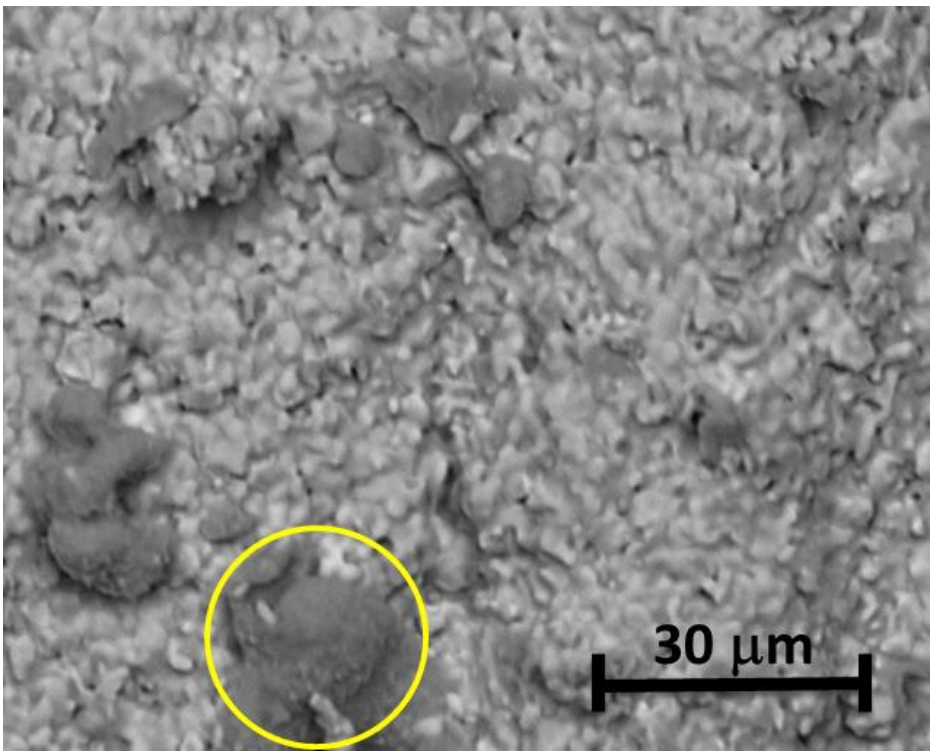

Figure 3.20: SEM micrograph on the lumen of LSCF6428 membrane after the membrane was exposed to 4% of water for more than 90 hours.

As we are not able to analyse the point-element analysis of the same lumen before the experiment (analysis can only be done after the membrane breaks because lumen is the inner surface of the membrane), we use the point-elemental analysis of a fresh lumen (from the same batch) for comparison purposes. Table 3.5 lists the approximate atomic concentration of elements on the area shown by the yellow circle in Figure 3.20 and the fresh as-supplied LSCF6428 lumen surface.

Table 3.5: Post experimental point-elemental analysis for the lumen side surface of LSCF6428 membrane exposed to 4% water.

Material	*Approximate atomic concentration (%)*				
	La	Sr	Co	Fe	C
Used LSCF6428 membrane (lumen side)	8.3	34.3	5.15	2.0	50.5
Unused LSCF6428 (lumen side)	25.9	19.4	6.2	40.2	-

Comparison of the results obtained from the EDX point-elemental analysis between a fresh as-supplied lumen side surface and the used lumen surface confirms that there is carbon deposition on the used lumen surface. There are also a big difference in the values of strontium as a result of strontium segregation on the post-experiment lumen side surface. This is expected for the water splitting side as strontium is needed to provide higher oxygen vacancies and give better oxygen permeation. Water might change the microstructures as of to improve the diffusion mechanism of the membrane [156, 157].

Elemental segregation was also observed on the surface of BSCF5582 that was exposed to 5% methane in nitrogen. Figure 3.21 shows the surface characterisation on BSCF5582 surfaces through SEM and EDX elemental mapping. The mapping results indicated that there were strontium segregation and carbon deposition bordering the segregated strontium atom. This might suggest the formation of $SrCO_3$ as an effect of the reaction between water, carbon dioxide and the membrane surface [155].

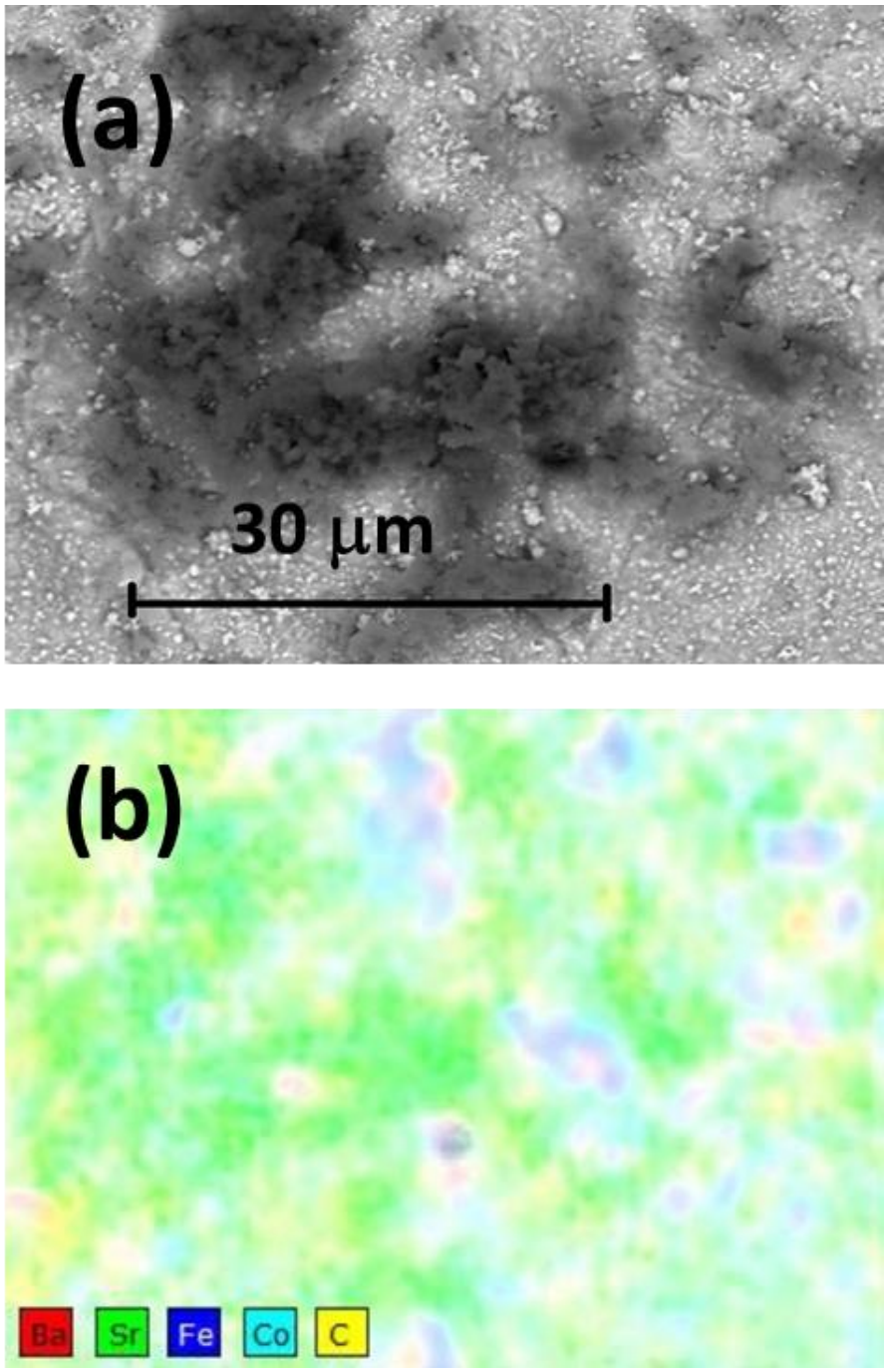

Figure 3.21: (a) SEM micrographs and (b) EDX mapping on the same spot for the reacted surface of BSCF5582 membrane after the exposure to 30mlmin^{-1} of 5% methane in nitrogen and lumen was fed with 10% of oxygen, 40% nitrogen in argon.

3.4 Summary

The experiments conducted and reported in this chapter demonstrated the ability of both the LSCF6428 and BSCF5582 hollow fibre membranes to permeate oxygen with different inlets into the shell and lumen sides.

The LSCF6428 has lower capability to permeate oxygen compared to BSCF5582 when inert gas was used as the sweep gas on the shell side of the membrane. The total oxygen permeation rate by the LSCF6428 membrane was in the same range as reported by Franca [151] for LSCF6428 used in similar environment. BSCF5582 however shows better permeation ability having higher average oxygen permeation rates at 3.88 ±0.39μmol$O.s^{-1}$.

For the oxygen permeation involving the use of a reducing gas methane on the shell side of the membrane, reaction on the shell side of the membrane reactor with LSCF6428 membrane produces hydrogen, carbon monoxide, carbon dioxide and water whereas BSCF5582 showed a total conversion of methane into carbon dioxide and water.

These two membranes were also tested for their performances in permeating oxygen with water and methane fed on different sides of the membrane. In contrast to the results obtained in the two earlier experiments, LSCF6428 shows better stability in permeating oxygen and thus produces hydrogen via water splitting process. The BSCF5582 membrane however demonstrates a large amount of leakages after a minimum of three hours exposure to both feeds. Further analysis on the surface of LSCF6428 after the water/methane-based hydrogen production

experiment through SEM/EDX confirms that there is strontium segregation on the surface of the LSCF6428 lumen.

As the aim for this thesis is to demonstrate simultaneous oxidation of methane and water splitting processes in one membrane reactor, the best membrane to be used to perform all the processes is the LSCF6428 membrane. In the next chapter this membrane will be used to demonstrate simultaneous methane oxidation and water splitting in a multiple-membrane reactor.

Chapter 4 Simultaneous Methane Oxidations and Water Splitting in One Membrane Reactor

4.1 Introduction

In this chapter we tried to combine two LSCF6428 membranes to evaluate their ability to simultaneously allow oxidation of methane and water splitting processes. LSCF6428 membranes were selected to be studied in this chapter because of their ability to produce hydrogen from both oxidation of methane and water splitting processes. The details on the individual membrane on the reactions were thoroughly discussed in Chapter 3.

The aim for this study is to simultaneously conduct methane oxidations and water splitting processes in the same reactor. Methane oxidations in this case consist of the full methane combustion (Equation 4.1) and partial oxidation of methane (Equation 4.2) processes. Both are exothermic in nature;

$CH_4 + 2O_2 \leftrightarrow CO_2 + 2H_2O$ $\Delta \boldsymbol{H_{900}}$ =-801.38 kJmol^{-1} Equation 4.1

$CH_4 + \frac{1}{2}O_2 \leftrightarrow CO + 2H_2$ $\Delta \boldsymbol{H_{900}}$ =-20.80 kJmol^{-1} Equation 4.2

The main reaction in this system is the full combustion of methane. The total heat of reaction at 900°C is forty times lower than that of from the partial oxidation of methane. Having a higher selectivity towards the production of hydrogen (through POM) will increase the total heat of reaction of the whole system. The partial oxidation of methane however has a lower Gibbs free energy thus making it thermodynamically less favourable in the environment where there were excessive amount of reactants i.e; methane and oxygen. The water splitting process on the other hand is an endothermic reaction;

$$H_2O \leftrightarrow \frac{1}{2}O_2 + H_2 \qquad \Delta \boldsymbol{H_{900}} = +249.45 \text{ kJmol}^{-1} \qquad \text{Equation 4.3}$$

Having proved that the LSCF6428 hollow fibre membranes are stable enough to undergo all these reactions individually, we now would like to investigate on the possibility to combine these three reactions so that they can be conducted in one membrane.

The idea behind combining and investigating on these three reactions is that if these three reactions can be made to occur in the same reactor, we will be able to produce hydrogen on both sides of the membrane. Synergising all the exothermic reactions and the endothermic reaction that run in this system will then enable us to produce hydrogen in a less energy intensive environment, the same concept applied in the idea of starting an ATR process.

The sections following will discuss the methodology and results of the study. An optimisation process in order to improve the findings of the study will also be included towards the end of the chapter.

4.2 Methodology

The overall membrane system used for the experiment for this chapter is as described in section 3.2.1. In order to minimise redundancies descriptions will only be made on systems that have never been explained before in the previous chapter. Thus in some part of this write-up, readers will be guide to refer to the specific section describing the related matter.

4.2.1 Feed system

The same feed system used and described in section 3.2.1 was used in this experiment.

4.2.2 Membrane Material and Characterisation

The experiment conducted for this chapter uses LSCF6428 hollow fibre membranes. The membranes are of the same batch obtained from Prof Li of Imperial College London. The average dimension, elemental distributions and pictorial surface analysis were as described for LSCF6428 membrane in section 3.2.2.

In the optimisation section, we made surface modifications on the as supplied membrane by coating a thin layer of LSCF6428 powder supplied by Praxair Ltd, USA.

In preparing the coating material, 5mg of LSCF6428 powder having an average particle diameter, d_{50} of 0.6μm was diluted in 90% methanol and applied over the length of 20cm of the membrane. The coated membranes were left to dry prior to a sintering process. The membranes were sintered for three hours at 700^{o}C following a heating rate of 2^{o}Cmin^{-1}. The sintered membrane were then cooled to room temperature with a rate of 2^{o}Cmin^{-1}.

A point elemental spectrum using EDX was made on the surface of the modified membrane to make sure that the powder was well distributed and sintered on the surface of the then as supplied membrane. Table 4.1 lists the detailed elemental analysis results on the surface-modified LSCF6428 membrane.

Table 4.1: Elemental analysis for the surface-modified LSCF6428 membrane

Material	*Approximate atomic concentration (%)*			
	La	Sr	Co	Fe
Modified surface LSCF6428	30.6	18.4	8.0	43.0
as-supplied LSCF6428	28.0	20.8	8.9	42.4

The point elemental analysis showed higher amount of La and Fe from the results obtained earlier on the as supplied LSCF6428 membrane reported in section 3.2.2.

4.2.3 Membrane Reactor and Furnaces

The experimental setup used in this chapter has the same setup as the previously used in chapter 3. Only this time the membrane reactor was slightly changed to be

able to house two or more hollow fibre membranes. Figure 4.1 shows the schematic diagram of the membrane reactor used in the experiment conducted in this chapter.

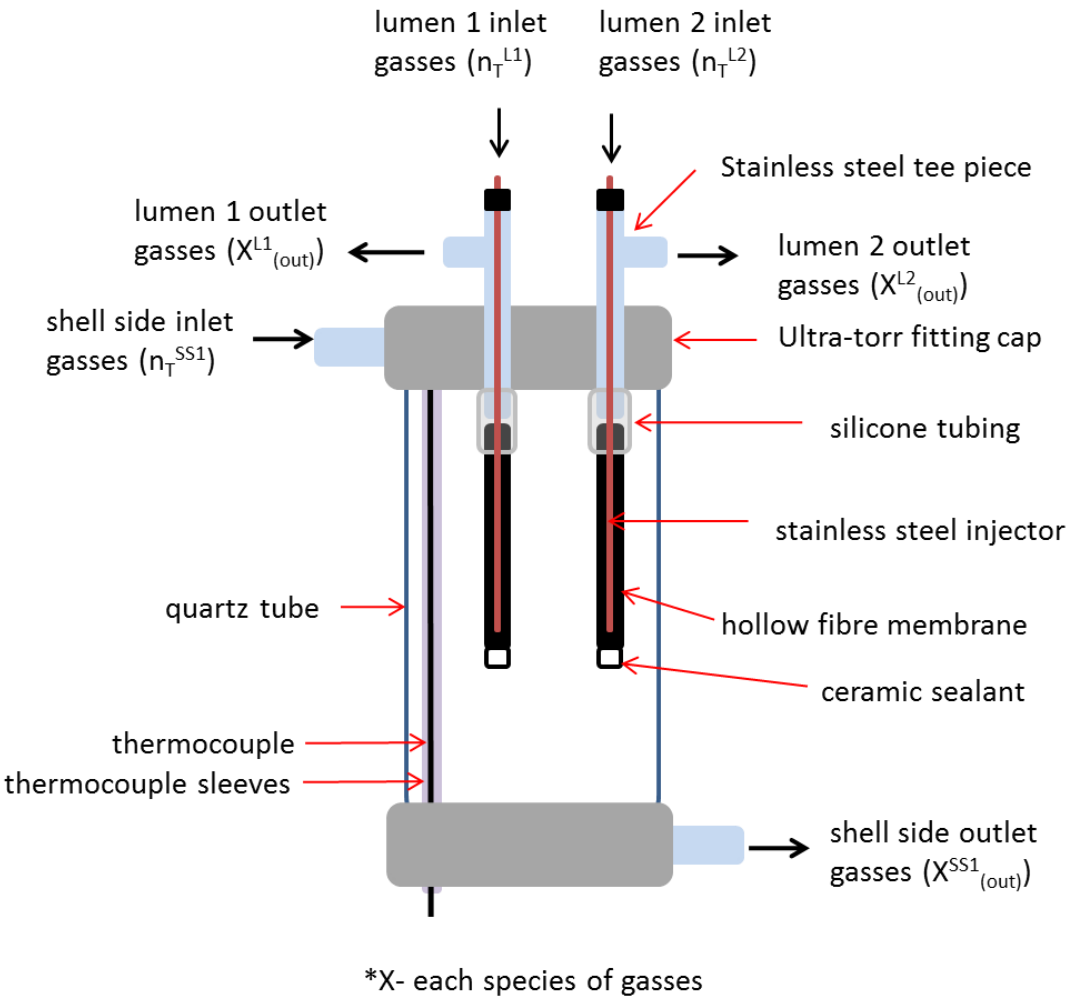

Figure 4.1: Multiple membrane reactor used for the experiment in this chapter

The same furnace described in section 3.2.3 was used in this experiment. The same reactor positioning approach was adopted following the temperature profile of the furnace. Figure 4.2 shows the overall setup for the experiment.

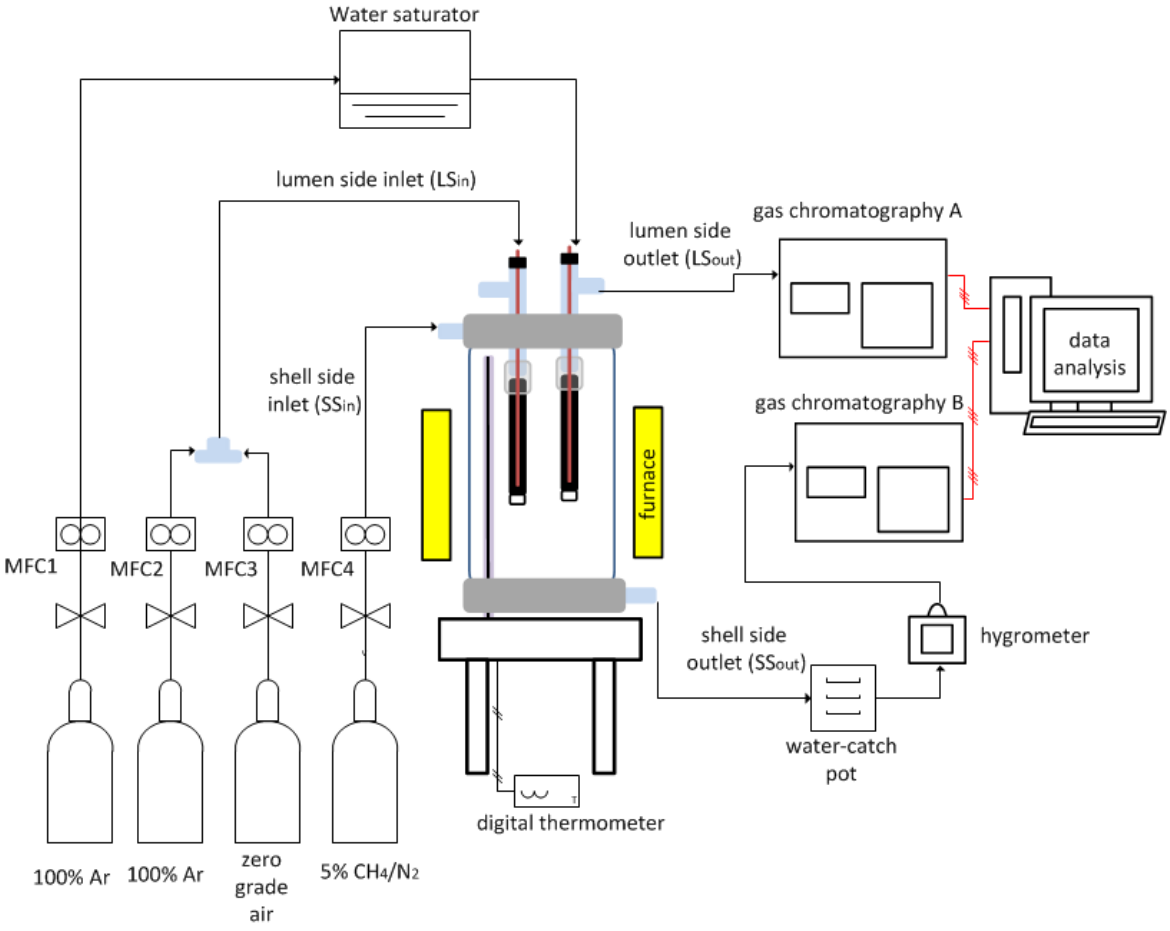

Figure 4.2: Experimental system setup for the simultaneous oxidations of methane and water splitting processes

4.2.4 Notations and Material Balance Equations

The fluxes obtained in this experiment can be calculated using Equation 3.2. The signals were provided by the GCs readings. Further calculations of the oxygen permeation on the shell side and the lumen side will be based on the oxygen containing products from the results of oxygen permeation in the multiple membrane reactor used in this study. Figure 4.3 illustrates the notations used for the material balance calculations. The gas inlets, outlets and total flowrate from lumen 1 and lumen 2 sides were identified by the superscript L1 and L2 respectively.

The subscript in the parenthesis at the end of each symbols differentiate between inlet and outlet streams. '(in)' refers to inlet while '(out)' refers to outlet.

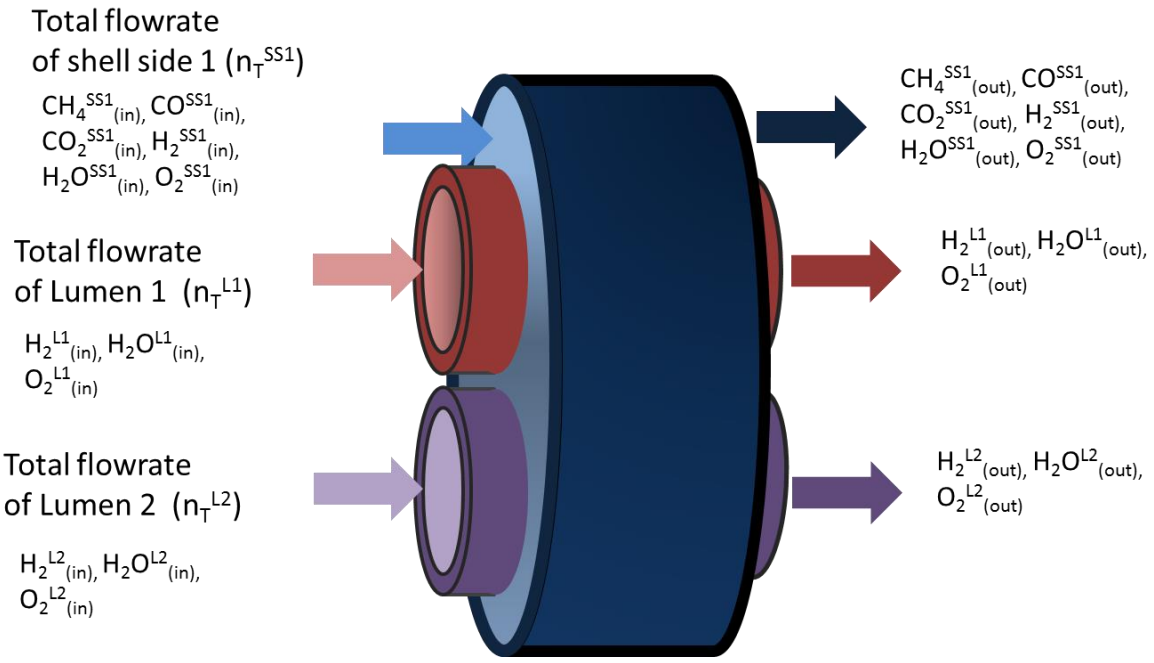

Figure 4.3: the notations used for the material balance calculations. Lumens are LSCF6428 membranes with different inlets and have individual outlets. Shell side is normally fed with 30mlmin^{-1} of 5% methane in nitrogen or 30mlmin^{-1} zero grade argon.

For the total oxygen permeation in the shell side OPss i.e; the total oxygen permeation rates from the two working lumens L1 and L2 can be calculated as below:

$$OP_{SS} = OP_{L1} + OP_{L2} \qquad \text{Equation 4.4}$$

Where

$$\mathrm{OP_{L1}} = [\,2(O_{2(out)}^{SS1} - O_{2(in)}^{SS1}) + (CO_{(out)}^{SS1} - CO_{(in)}^{SS1}) + 2(CO_{2(out)}^{SS1} - CO_{2(in)}^{SS1}) + (H_2O_{(out)}^{SS1} - H_2O_{(in)}^{SS1})]n_T^{SS1} \quad \text{Equation 4.5}$$

$$\mathrm{OP_{L2}} = \left(H_{2(out)}^{L2} - H_{2(in)}^{L2}\right) + 2(O_{2(out)}^{L2} - O_{2(in)}^{L2})]n_T^{L2} \quad \text{Equation 4.6}$$

The error propagation in the calculation of the rates of oxygen permeation and the material balance of each substance are the same as what have been discussed in section 3.2.7.

In the results and discussions section, the simple notations will be used to identify the membrane sides. SS refers to the shell side normally fed with either 30mlmin^{-1} of 5% methane in nitrogen or with 30mlmin^{-1} zero grade argon. The lumens will be identified with different number. L1 refers to lumen 1 and L2 refers to lumen 2.

4.3 Results and Discussion

In this chapter different sets of inlet configurations were run throughout the operation of the membranes in one reactor. The membrane performance will be discussed based on the dynamic responses obtained through the changes in the product compositions of SS, L1 and L2.

In order to be able to make a complete material balance for the system, all of the inlets and outlets gas readings need to be monitored and quantified. In certain cases

where there were more than two outlets to be monitored, the outlet streams need to be alternately changed for sampling purposes. Although some of the average rates were calculated at different operating time, we make sure that the minimum sampling time for an average to be taken and fit to be in discussion is at least 5 hours of operation.

For a better reference, the inlet configurations will be named according to the order of Shell-Lumen 1- Lumen 2 feed. The abbreviation will be based on the combination of the first letter of each inlet gas. As an example the first inlet configuration for this experiment is methane-argon-oxygen, giving the abbreviation to be used in the discussion of the results for this feed configuration is M-A-O.

Table 4.2 lists the different inlet combinations, the total molar flow rates for each inlet and operating time for each experiment.

Table 4.2: Experimental table

Inlets feed notation	**Temperature /^{o}C**	**Shell side sweep (n_T^S) rate(s) / µmols^{-1}**	**Lumen 1 side sweep (n_T^{L1}) rate(s) / µmols^{-1}**	**Lumen 2 side sweep (n_T^{L2}) rate(s)/µmols^{-1}**	**Duration / hours**
		atmospheric air	atmospheric air	atmospheric air	11
M-A-O	900	5% methane 13.63 ±1.36	argon 13.63 ±1.36	oxygen 20.45±2.05	6
M-W-O	900	5% methane 13.63 ±1.36	water 13.63 ±1.36	oxygen 20.45 ±2.05	24
A-W-O	900	argon 13.630 ±1.360	water 13.630 ±1.360	oxygen 20.45 ±2.05	64
M-W-O	900	methane 13.630 ±1.360	water 13.630 ±1.360	oxygen 20.445 ±2.045	52

Inlets feed notation	Temperature /^{o}C	Shell side sweep (n_T^S) rate(s) / µmols^{-1}	Lumen 1 side sweep (n_T^{L1}) rate(s) / µmols^{-1}	Lumen 2 side sweep (n_T^{L2}) rate(s)/µmols^{-1}	Duration / hours
M-W-A	900	methane 13.630 ±1.360	water 13.630 ±1.360	argon 13.630 ±1.360	29
A-W-A	900	argon 13.63 ±1.36	water 13.630 ±1.360	argon 13.630 ±1.360	13
M-W-A	900	methane 13.63 ±1.36	water 13.630 ±1.360	argon 13.630 ±1.360	60
900-25		atmospheric air	atmospheric air	atmospheric air	11

4.3.1 Methane-argon-oxygen (M-A-O)

The first experiment conducted in the membrane reactor after the temperature reaches 900^{o}C is the M-A-O experiment. The experiment was held running continuously up to seven hours. Figure 4.4 shows the GC measurements for the (a) SS product concentrations and (b) excess reactant concentrations in L2. The products in SS were hydrogen, carbon monoxide, carbon dioxide and water. Figure 4.4 does not show the mole fractions of the products in L1 because no other product/ gas was detected other than argon (feed).

Figure 4.4 shows that partial oxidation and full combustion took place in the shell side. The shell side product mole fractions took two hours to stabilise and this is possibly because the oxygen permeation from the L2 is just taking place and filling the oxygen vacancies in the material.

The mole fraction of oxygen detected in the oxygen fed lumen side, L2 was very low in the first four hours of operation. The dynamic response of oxygen mole fraction in the L2 indicates that the oxygen vacancies mobility is active in the membrane materials. The products mole fraction detected in the outlet of the shell side also showed dynamic responses in the first 2 hours of the experiment. SS products however started to stabilise after two hours of operation.

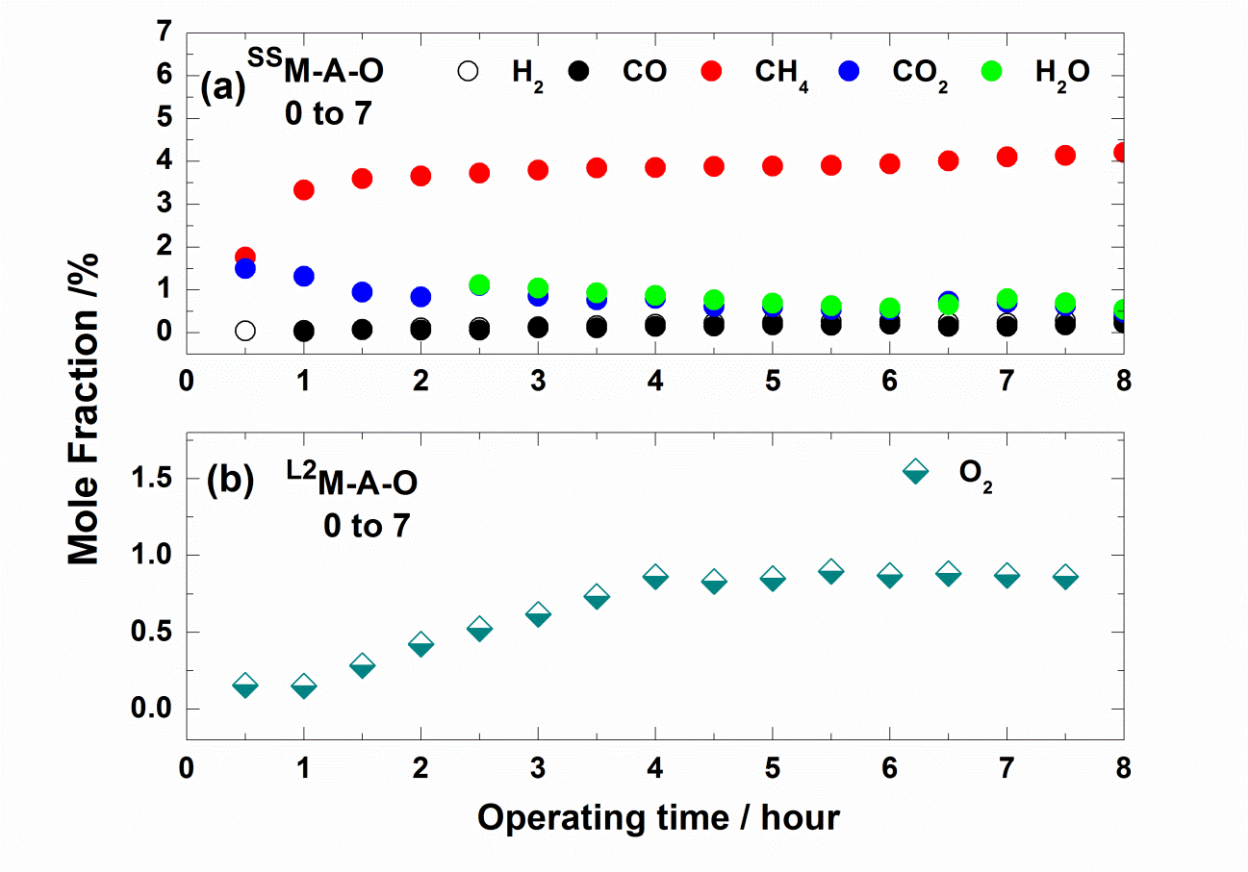

Figure 4.4: Graphs showing the outlet mole fractions as detected using the GCs on both sides of membrane reactor; (a) shows the products detected in the outlet of the shell side (b) shows the products detected in the outlet of the lumen 2 (L2). The membrane reactor was fed with 30mlmin^{-1} of 5% methane in nitrogen, lumen 1 (L1) was fed with 30mlmin^{-1} of zero-grade argon and L2 was fed with 20mlmin^{-1} of 2% oxygen, 8% nitrogen in argon.

It is expected that the products in the SS would satisfy the product ratios following Equation 4.1 and Equation 4.2. In a normal behaviour following these two listed

equations the amount of hydrogen should double the amount of carbon monoxide and the same ratio should be seen here. A simple calculation from the average mole ratio starting from hour 0 to 7 discloses that the ratio of carbon dioxide to water in this experiment is 1.05 and the ratio of carbon monoxide to hydrogen is 0.75.

The total oxygen permeation in the SS of the reactor is 0.37±0.04μmolO.s^{-1}. This is consistent with the results obtained earlier fed with same inlet configuration using the individual membrane reactor setup reported in section 3.3.2. The membranes in this reactor however took less time to show stable results. This is most likely because there is more surface area available for the surface exchange of oxygen to occur from another unused membrane available in the reactor. That membrane lumen was fed with 30mlmin^{-1} argon. Although the membrane was not fed with reacting gases, the membrane increases the surface area for surface reaction between methane and the perovskite.

Further analysis on the total oxygen permeation on L2 gives OP_{L2} rate at 0.29±0.05μmolO.s^{-1}. This value makes the oxygen balance closed following this inlet configuration. Further calculation on the selectivity of carbon dioxide to carbon monoxide shows that the ratio is at 0.87±0.19. The experiment is then continued with another inlet configuration using both of the membranes in the reactor. The discussion for that inlet configuration is in the next section.

4.3.2 Simultaneous Methane Oxidations and Water Splitting (M-W-O)

This experiment utilises on the three inlets where; (i) SS was fed with 30mlmin^{-1} of 5% methane in nitrogen (ii) L1 was fed with 4% water in argon and (iii) L2 was fed

with 2% oxygen, 8% of nitrogen in argon. This experiment was aimed to perform the simultaneous methane oxidations and water splitting reactions in the same reactor. Figure 4.5 shows the outlet concentrations in (a) SS (b) L1 and (c) L2 in response to the M-W-O inlet configuration.

The system was already fed with methane on the SS in the previous configuration. The introduction of water into L1 however causes dynamic responses in almost every product concentration of the SS from the start-up to five hours of the experiment time. These responses however, gradually stabilised after eight to 13 hours of operation. The unreacted methane average mole fraction increases after the responses stabilised. This shows that the methane conversion rates are lower in this inlet configuration as to compare with the previous inlet configuration.

It is also observed that there is an amount of un-reacted oxygen in the SS. It could be the reason to explain the very small amount of hydrogen production in L1. This is because when there is un-reacted oxygen in SS, it increases the partial pressure of oxygen in the SS and suppresses any more oxygen permeation into the shell. This inhibited the water splitting process.

The oxygen concentration in the outlet stream from L2 shows similar results with the individual membrane performance reported in section 3.3.2. Oxygen balance calculations revealed that the total oxygen permeation into SS by both L1 and L2 matches the amount of oxygen concentration in all the products found in the SS. The product ratio analyses also showed similar trend with what had been observed in the M-A-O experiment. The ratio of CO_2 to H_2O is 3.47 and the ratio of CO to H_2 is 0.62

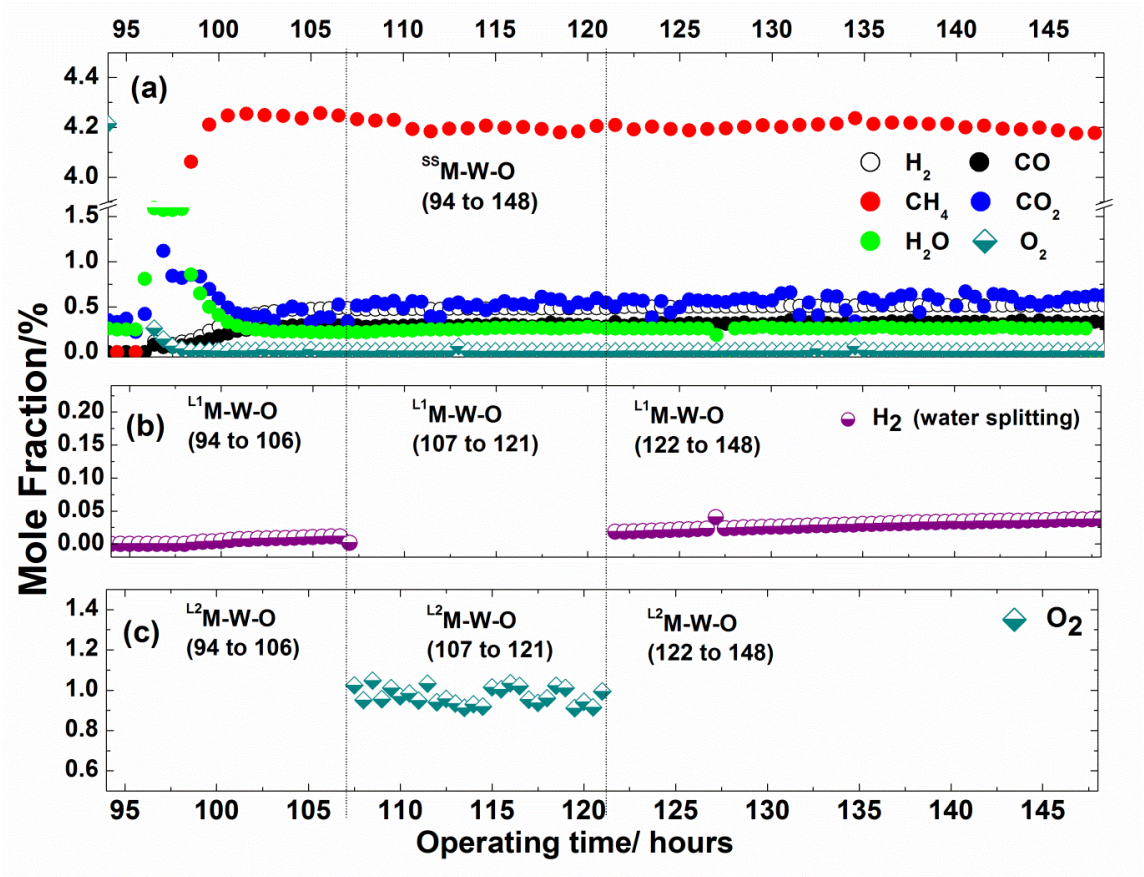

Figure 4.5: Graphs showing the mole fractions as detected using the GCs for the three outlets from the membrane reactor; (a) shows the products detected in the shell side, (b) shows the products detected in the lumen 1 (L1) and (c) shows the products detected in the lumen 2 (L2). The shell side of the membrane was fed with 30mlmin^{-1} of 5% methane in nitrogen, L1 was fed with 30mlmin^{-1} of 4% water in argon and L2 was fed with 20mlmin^{-1} of 2% oxygen, 8% nitrogen in argon.

Oxygen balance analyses were calculated for SS, L1 and L2 and the OP_{SS} rate is at 0.20±0.02µmolO.s^{-1}. This is slightly lower than what was achieved earlier in the M-A-O experiment. The OP_{L1} and OP_{L2} are $0.003 \pm 0.001\mu molO.s^{-1}$ and $0.42 \pm 0.12\mu molO.s^{-1}$ respectively. The oxygen permeation rate in L2 for this experiment doubled the amount of oxygen permeation from the same lumen obtained in the M-A-O experiment.

4.3.3 Methane-Water-Argon (M-W-A)

In the previous inlet configuration results, we claimed that the water splitting process in L1 was halted because there was unreacted oxygen in the SS. This is however not certain because that was the first time for L1 to be used in the inlet configuration.

In this section, we will be discussing on two M-W-A experiments. The first M-W-A was conducted at 148 to 177 hours as the continuation from M-W-O experiment and the second M-W-A started at hour 190 to 251. Figure 4.6(a) shows the product compositions identified and measured in the SS and L1 for the overall 103 hours of operation with M-W-A, A-W-A and M-W-A inlets configurations.

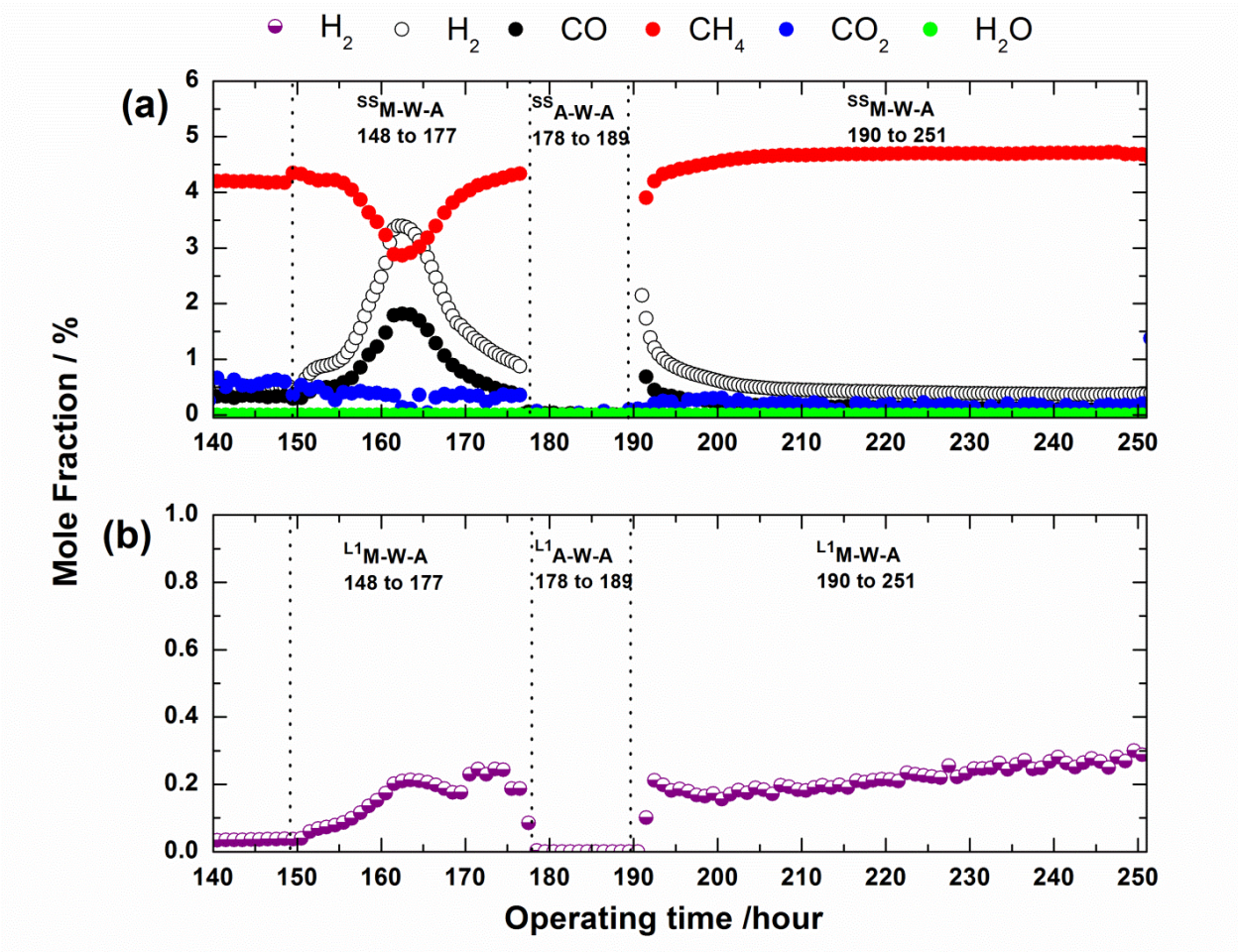

Figure 4.6: Graphs showing the mole fractions as detected using the GCs for the two outlets from the membrane reactor; (a) shows the products detected in the shell side, (b) shows the products detected in the lumen 1 (L1). The shell side of the membrane was fed with 30mlmin^{-1} of 5% methane in nitrogen from hour 148 to 177, 30mlmin^{-1} of zero grade argon from hour 178 to 189 and 30mlmmin^{-1} of 5% methane in nitrogen at hour 190 to 251. L1 was fed with 30mlmin^{-1} of 4% water in argon and L2 was fed with 30mlmin^{-1} of zero grade argon.

In the first M-W-A experiment; hour 148 to 177, inlet gas configurations were changed from M-W-O to M-W-A by switching the oxygen in L2 to argon. A sharp increase in syngas production was observed two hours after the switching making a peak at hour 162. The syngas production then started to decrease to the concentration as in the M-W-O configurations. An increase in hydrogen production was also detected in the L1 lumen side (Figure 4.6(b)) instantaneously after the switching. This does not show a similar trend with the water splitting process done

previously, as reported in section 3.3.3. In the previous experiment with the same inlet configuration, the membrane started to produce hydrogen after 30 hours from start-up time. This is possibly because the system was having abundant oxygen in the shell from the oxygen permeation in L1 earlier on. Once the inlet gases in L2 were changed from oxygen to argon, the oxygen content decreased abruptly resulting in the drop of partial pressure of oxygen in the SS thus increasing the potential for the water splitting to occur in L1. This is also might be because the oxygen vacancies in the material were already being occupied with oxygen molecule from the oxygen inlet earlier. This makes it easier to start permeation and split water when water is fed replacing oxygen. Note that splitting of water needs more chemical potential than the oxygen permeation from oxygen containing inlet. This explains the change in activity level and lower permeation results in this set where the inlet for the lumen is water instead of oxygen. The overall permeation in the SS was totally associated with the oxygen permeation from the water splitting process. Calculation on the oxygen permeation from the water splitting lumen L1 gives a rate of $0.03\pm0.01 \mu molO.s^{-1}$.

It is also observed from Figure 4.6(b) that the concentration of hydrogen in L1 started to increase steadily at the same time as the formation of the syngas. The hydrogen production in the L1 however started to stabilise and does not show similar trend as in the SS. An oxygen balance was made on the both sides of the membranes to verify if the oxygen usage in the SS is at the same amount as the oxygen loss in the L1. The concentration of hydrogen in L1 went to the same level as was measured earlier in the first M-W-A experiment but the product concentrations in the SS differed. OP_{ss} calculated for this inlet configuration is at $0.07\pm0.01 \mu molO.s^{-1}$.

The results obtained from this inlet configuration confirmed that the LSCF6428 membrane used in L1 is active and is capable of conducting the water splitting process. This also suggests that the low hydrogen production from water splitting reaction in L1 reported in section 4.3.2 is not related to the chemical inactivity of the membrane but very much dependent on the high partial pressure of the oxygen in the SS.

In order to increase the production of hydrogen production in the L1, some solutions need to be made to either increase the retention time of methane in the SS so that more permeated oxygen that is available in the SS get to react.

4.4 Characterisation

Figure 4.7 shows the SEM characterisation for the surface of one of the LSCF6428 membranes used in the experiment.

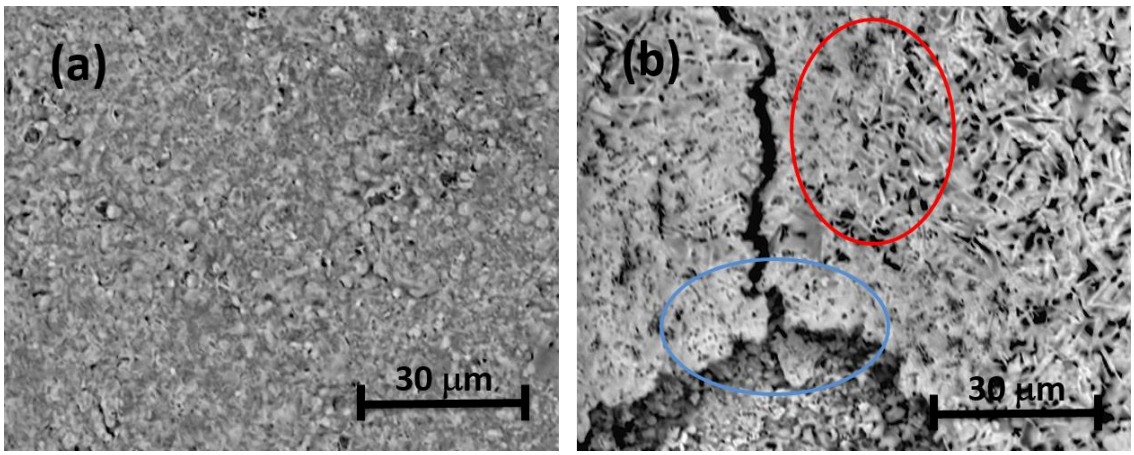

Figure 4.7: LSCF6428 shell side (a) before experiment (b) after experiment

Figure 4.7(a) is the micrographs of the same membrane before the experiment and Figure 4.7(b) shows the micrographs after the experiment at the length within the

isothermal region. The membrane was exposed to reducing gas such as carbon monoxide, hydrogen and methane which causes peeling of the surface of the membrane. The peeling shown in the figure (red oval mark) reveals a second layer of a finger-like structure and causes leakage in the overall performance of the membrane. This is might be due to the material segregation on the surface of the membrane, when the surface was exposed to carbon dioxide, methane, hydrogen and water. Further point-base elemental analysis conducted using EDX shows that there was carbon deposition all over the surface. As can be seen in Figure 4.7(b), the peeling further develops a crack in the inner layer of the membrane (shown in blue oval mark). This phenomenon also shows that the membrane surface is not chemically stable when it is exposed to reducing gases.

4.5 Optimisation

The results discussed in section 4.3.2 show that the oxygen permeation in the first membrane was very high, producing unreacted and/or lower reactivity oxygen on the shell side. Moreover the results for the simultaneous reactions in the multi-membrane reactor showed that there were limited hydrogen production in the water inlet lumen (L1) making it hard to conclude if the hydrogen signal obtained is from the water splitting process of just a random error reading. It is also believed that the oxygen permeation in the water inlet lumen was slower because the shell side of the membrane was not reducing enough for the oxygen to be transported across the membrane. This halted the water splitting process in the second membrane. Another reason can also be that the SS is having other products that would act as a buffer and hinders the water splitting in the L1. In order to improve

the performance of the membrane in performing simultaneous reforming and water splitting processes, several optimisation trials have been conducted. Amongst them is the use of modified surface LSCF6428 membranes.

As the water splitting process is one of the main reactions in this study, some modifications need to be made in order to lower the partial pressure of the oxygen in the shell side thus increasing the possibility of water splitting to occur in the lumen side. A study done by Tan et al. [158] showed that the a surface modified membrane coated with similar material (in this case LSCF6428) showed an increase in the oxygen permeation rate by 1.67-9.31 times than that is obtained by the unmodified surface of the LSCF6428 membrane itself. Based on this study a surface modification of the LSCF6428 membrane was made by coating another layer of porous LSCF6429 powder onto the outer surface of the membrane. The membranes were then sintered at high temperature prior to experimental usage.

As this optimisation study was conducted mainly to help increase the rates of the water splitting process, an individual membrane reactor experiment was conducted to observe the performance of the modified surface LSCF6428 membrane for the water splitting process. The reactor setup and experimental rig were discussed in section 3.2.3 and 3.2.6 respectively. The inlet configuration used in this experiment mimics the inlet configuration used in the water splitting coupled methane reforming experiment discussed in section 3.3.3. This is to make comparison of the performance of the aforementioned modified surface membrane ability in performing oxygen permeation for the water splitting process. Table 4.3 shows the average compositions of the shell side. These data were used to calculate the oxygen balance in the reactor. For the oxygen balance calculation, the average oxygen permeation rate in the shell side is $0.05\pm0.01\mu molO.s^{-1}$ whereas the oxygen

permeation rate in the lumen side is 0.04±0.01μmolO.s^{-1}. The results on the oxygen permeation with methane fed in the shell side and water fed in the lumen side shows that the average oxygen permeation rates were increased by a factor of 1.1 from what have been obtained earlier; refer section 3.3.3. This confirms the findings presented by Tan et al. [158].

Table 4.3: Average mole fraction of products obtained from the oxygen permeation with methane fed in the shell side and water fed in lumen side. Average values were taken from hour 60 to hour 80.

	Lumen side/ μmols^{-1}	Shell side/ μmols^{-1}				
	H_2	H_2	CO	CH_4	CO_2	H_2O
Inlet	-	-	-	5.00± 0.50	-	-
Outlet	0.20± 0.02	0.43± 0.04	0.19± 0.02	4.68± 0.47	0.02± 0.00	-

This can also be seen from the hydrogen production detected in the lumen side as the results of water splitting process. Figure 4.8 shows the overall mole fraction of hydrogen production in the shell side of the membrane reactor.

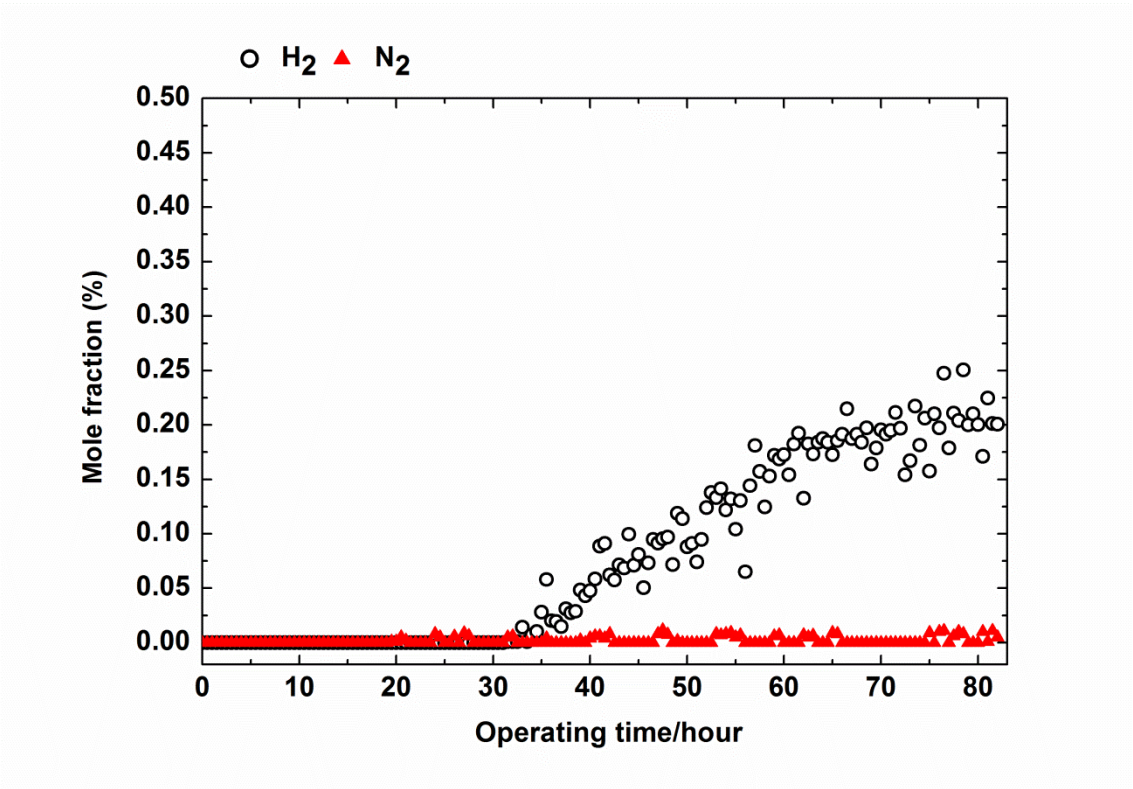

Figure 4.8: Hydrogen production in the lumen side of the modified surface LSCF6428 membrane when the lumen was fed with 30mlmin^{-1} of 4% of water and shell side inlet were fed with 30mlmin^{-1} of 5% methane in nitrogen.

The results also show that the modified surface membrane took more than 30 hours of induction time before showing the signs of hydrogen production. This trend is similar to what has been obtained earlier in section 3.3.3. The hydrogen production rate however took 30 hours to stabilise and show a good stability with water inlet on the lumen side, showing similar performance as the unmodified surface LSCF6428 membrane. Post operation characterisation was made to compare the surface structure changes using SEM. Figure 4.9 shows the SEM micrographs of the (a) post-sintered surface of the modified-surface of LSCF6428 membrane and (b) post-experimental surface of the same membrane.

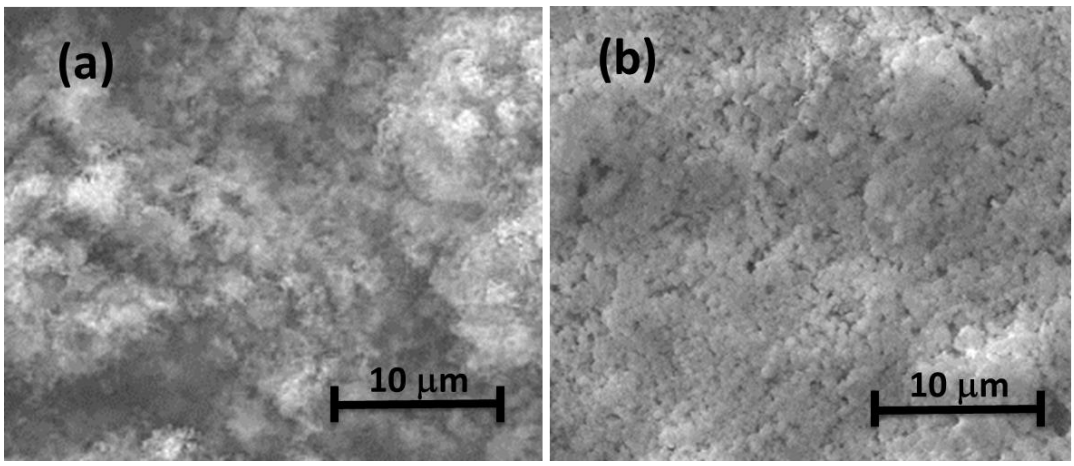

Figure 4.9: SEM micrographs of the modified surface LSCF6428 membrane (a) before water splitting process and (b) after water splitting process

The post operation membrane surface shows a dense layer of LSCF6428 powder compared with the pre-operation membrane surface. EDX analyses does not show any significant different in elements before and after the experiment.

The reported results show that the modified-surface LSCF6428 is a good candidate to be used as an alternative membrane to replace the as-supplied LSCF6428 membrane for the water splitting process. Further experiments were conducted following the same approach as reported in section 4.3.2 to investigate the potential of these membranes in conducting simultaneous methane oxidations and water splitting processes in one membrane. The results, however shows negative response since the membrane designated for the water splitting process was showing large leaks and found broken after two hours of operation. This may be caused by the large surface area in both of the membrane surfaces used in the membrane reactor. With large surface areas, surface exchange is more likely to occur and this causes the methane to be converted into either syngas or carbon dioxide. Higher amounts of carbon monoxide and hydrogen will create a reducing environment in the shell

side and increase the possibility of breaks in the membrane that was fed with water in the lumen side.

Other trials conducted in the optimisation process included running the as-supplied LSCF6428 membrane for the water splitting process with CO/CO_2 mixture fed in the shell side of the membrane and water in the lumen side of the membrane. At a higher ratio of CO/CO_2, the membrane suffers breakage after very short working hours. This shows that the membrane is not chemically stable when being exposed to a highly reducing and highly oxidising gas (water in argon on the lumen side of the membrane) at the same time. At a lower ratio of CO/CO_2 mixture on the shell side, traces of hydrogen were detected in the lumen side but since the hydrogen mole fraction was so small, it does not give a conclusive proof that the water splitting process is really occurring in the lumen side. Moreover no significant changes were observed in the readings of carbon monoxide and carbon dioxide mole fractions at the outlet of the reactor making it difficult to conclude that the experiment was working.

Another optimisation trial used the membrane painted with a thin layer of platinum film. Platinum was chosen over other catalysts because it is well studied and there were claims that platinum can increase the methane conversion as well as the selectivity towards syngas production [159, 160]. In the trial experiment, the membrane surface was painted with platinum paste and sintered up to 900^oC prior to use. The membrane however developed cracks and breaks after a few hours of operation. This shows that the catalytic activity was too high resulting in a highly reducing environment in the shell side thus breaking the membrane. Therefore this particular modified membrane surface is not suitable to be used here.

4.6 Summary

In this chapter, LSCF6428 membranes were used to simultaneously perform methane oxidations/reforming and the water splitting process. A different reactor and experimental setup was used to house two membranes in one shell side. These membranes however have individual inlets and outlets. This is to make sure that all of the gases going in and out of the system can be monitored, detected and analysed individually for material balance purposes.

The first experiment only utilises one membrane although the two membranes are available in the reactor. The average oxygen permeation rate in the shell side is consistent with the oxygen permeation rate obtained earlier, reported in section 3.3.2. Simultaneous methane oxidations and water splitting processes were conducted afterward show that hydrogen production occurs in both SS and L1. The mole fraction of hydrogen obtained in L1 however is inconsistent with the results of the water splitting coupled reforming experiment discussed earlier in 3.3.3. This is due to the presence of unreacted oxygen on shell side of the membrane reactor. The final experiment confirms the claim that L1 shows good permeation and hydrogen production rate via water splitting and is consistent with the individual membrane discussed in section 3.3.3. Oxygen balances in the system for the three different inlet configurations were closed.

A few optimisation trials were conducted in an effort to increase the production of hydrogen in the water splitting process. The modified surface of the LSCF6428 membrane shows promising results in increasing the hydrogen production through the water splitting process in an individual membrane experiment run. Other

optimisation trial runs show insignificant results thus will not be considered for further studies.

Chapter 5 Catalyst Assisted Simultaneous Methane Oxidations and Water Splitting

5.1 Introduction

This chapter discusses on the improvement of simultaneous methane oxidations and water splitting processes in one membrane reactor with the use of a catalyst and a modified membrane for water splitting process. As mentioned earlier in section 0, a few trials were conducted in the effort to increase hydrogen production via the water splitting process. The only working membrane with improved performance after modifications was the modified surface LSCF6428 membrane. In this chapter, the simultaneous methane reforming and water splitting processes will be conducted in a system consisting three reactors in series. The first reactor will be dedicated to the oxygen permeation from the methane reforming process, second reactor will be the catalytic chamber and the last reactor will work on the water splitting coupled methane reforming processes.

5.2 Experimental setup

5.2.1 Gases

Firstly is the feed system. The feed system consists of four mass flow controllers (MFC) supplied by Brooks, UK. The gas cylinders were connected to a regulator and a safety valve before entering the MFC inlets. Table 5.1 lists the type of gases and the provider company used with each MFC.

Table 5.1: List of gases, composition and their provider company.

MFC number	Gas	Composition	Provider company
MFC1	Argon	100% (Zero Grade)	BOC, UK
MFC2	Air	100% (Zero Grade)	BOC, UK
MFC3	Methane/Nitrogen	5% (99.5 % certification)	BOC, UK
MFC4	Air	100% (Zero Grade)	BOC, UK

The type of pipes used to transport the gases into the second part of the system are of PFA tubing size 1/8" obtained from Swagelok, UK.

5.2.2 Membrane Material and Characterisation

The membrane material used in this for Reactor 1 (R1) is the LSCF6428 hollow fibre and modified surface LSCF6428 hollow fibre for Reactor 3 (R3). The SEM micrographs and EDX analysis of the LSCF6428 hollow fibre are provided in section 3.2.2 and the SEM micrographs and EDX analysis of the modified surface LSCF6428 hollow fibre are provided in section 4.2.1. The additional material used individually in the second reactor is the 1% Pt/Al_2O_3 catalyst. This type of catalyst is widely reported to help increase the selectivity of the partial oxidation of methane [161].

5.2.3 Reactor design and setup

The system setup for use in this experiment utilises three different reactors. These three reactors were arranged in series. The first reactor, Reactor 1 (R1) is a membrane reactor used for the oxygen permeation process. The design of R1 is similar to the individual membrane reactor shown and described previously in section 3.2.3. The second rector is Reactor 2 (R2). This reactor is the catalyst reactor. The point of including this reactor in the system is to increase the oxygen consumption in the membrane system. As discussed before in Chapter 4, when two membranes; one for oxygen permeation and another one for water splitting process were put together in one membrane, it was found out that there were unreacted oxygen available on the shell side. This causes an increase in the partial pressure of the oxygen and halted the water splitting that occurs in one of the lumens meant for the water splitting process.

Figure 5.1 shows the configuration of R2. R2 housed the 1% platinum/Al_2O_3 in an 99% alumina tube having a dimension of 10mm (ID)x 12mm (OD) x 320 (L). The

catalyst is weighed as required and positioned in the centre of the reactor. Quartz wool was used to secure the position of the packed catalyst in place. Both sides of the alumina openings were closed and tightened using two pairs of modified ultra-torr fittings supplied by Swagelok (UK).

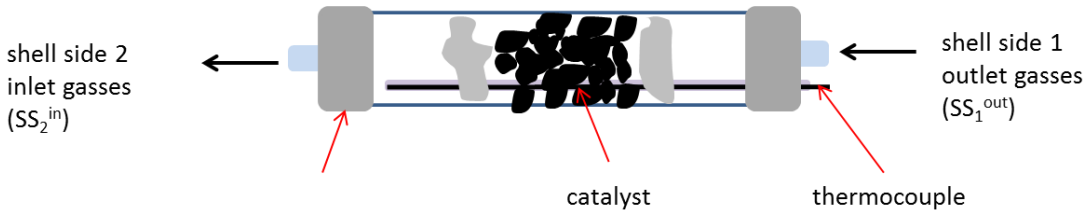

Figure 5.1: Catalyst reactor (R2)

The catalyst used in this study was the as supplied 1% Pt supported on alumina beads obtained from Sigma-Aldrich. Prior to any experimental usage the Pt catalyst needs to be reduced with a continuous flow of 30mlmin^{-1} of 10% hydrogen in helium while the reactor was heated up from room temperature to 600^{o}C. This is to ensure all the oxides were removed and the catalyst is fully activated before performing any experiments. To avoid re-oxidation to the catalyst R2 was fed with a continuous supply of argon with a flowrate of 30mlmin^{-1} and heated up to the operating temperature, 900^{o}C.

The last reactor in the series is Reactor 3 (R3). R3 is a membrane reactor having a similar setup as R1. This membrane reactor is to perform the water splitting process with the shell outlet consisting of the product gases from the catalytic partial oxidation of methane that have occurred in R1 and R2. The inlet to the shell side of this membrane reactor (SS2) is the outlet of R2.

Figure 4.2 shows the schematic diagram the three reactor experimental setup used in the experiment discussed in this chapter. Note that the basic on the setup is still the same from the one used in previous chapters but the one presented here has an extension of two other reactor arranged in series to the first reactor.

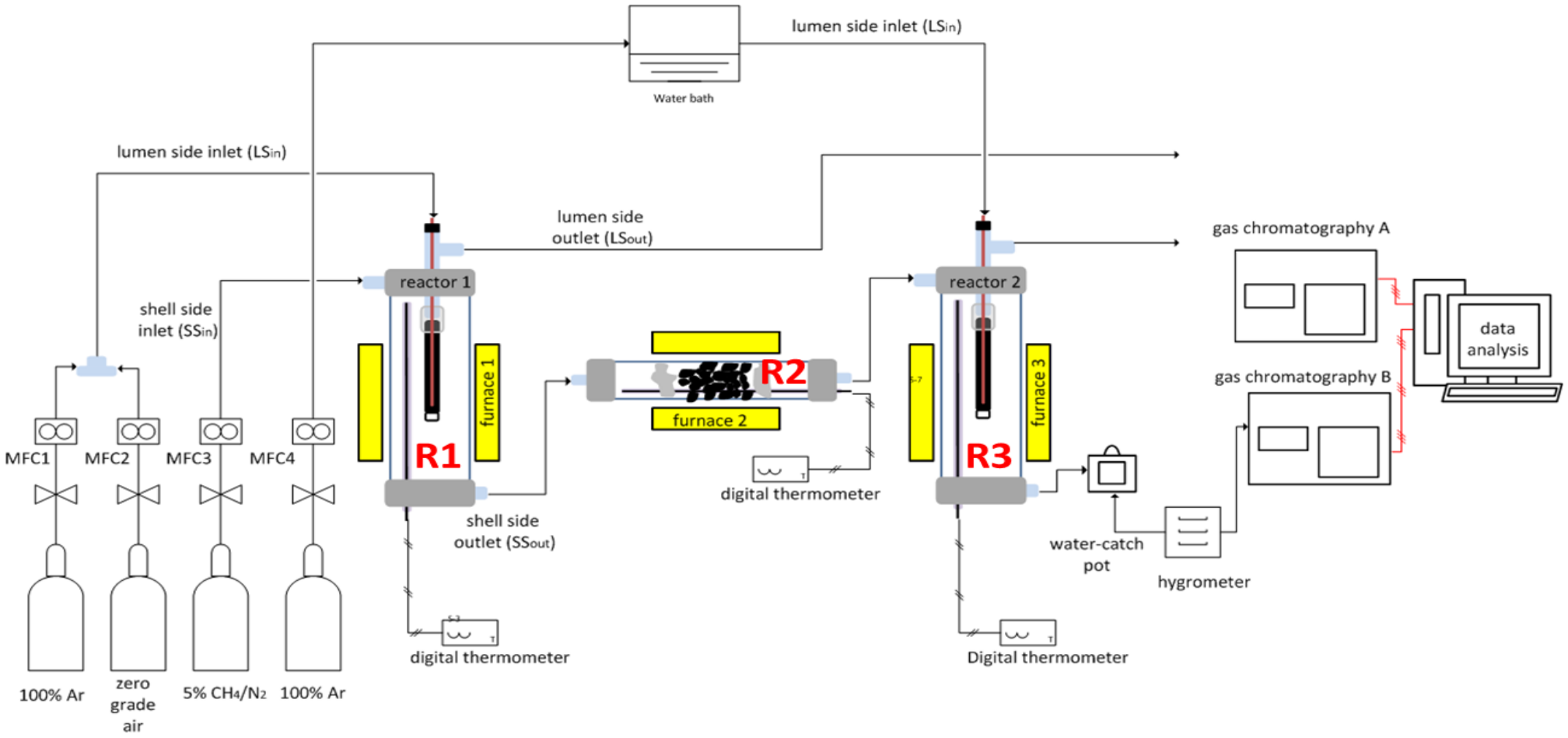

Figure 5.2: Experimental system setup for the catalyst assisted simultaneous methane oxidation and water splitting

5.2.4 Gas Analysis

The gas analyses used in this chapter are similar to those reported earlier in section 3.2.4. In the case when there are more than two streams to be analysed at the same time, we would alternately change the sampling streams after long time intervals to make sure that the average calculation for the results can be used to represent the overall behaviour of the system.

5.2.5 Notations and material balance calculations method

The readings of the inlet and outlet gases were obtained in terms of mole fractions. As mentioned and discussed earlier in chapter 3, we decided to maintain the minimum and maximum error for the mole fraction readings at 10%. Figure 5.3 shows the notations used in the material balance calculations. In the experiment conducted for this chapter, the outlet of the shell side of R1 will be the inlet to the catalyst containing reactor R2. In this case the notation used for the inlet or outlet gases of the shell side of the membrane reactor will be identified by the subscript of either 'in' referring to inlet and 'out' referring to outlet. The superscript denotes the sides of the membrane and reactor number. For example, $H_2{}^{LSR1}{}_{(out)}$ means the mole fraction of hydrogen from the outlet of the lumen side membrane in R1.

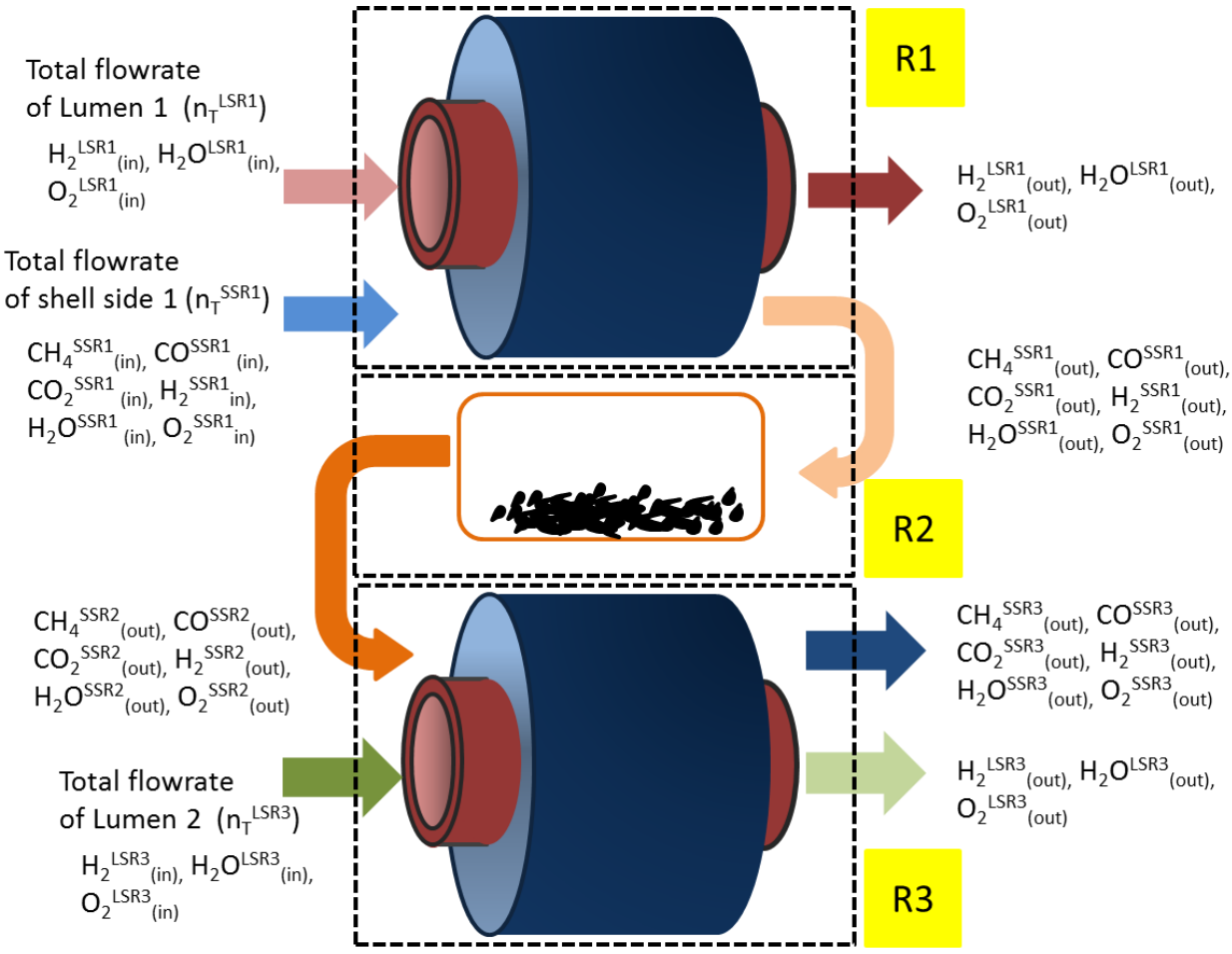

Figure 5.3: The notations used in the material balance equations.

To avoid confusion, all equations derived for the use of material balance purposes further discussed next will be using the notations shown in Figure 5.3.

The oxygen permeation rate in the shell side of R1 can be calculated using Equation 5.1 and the oxygen permeation from the lumen side of R1 can be calculated using Equation 5.2.

$$\mathrm{OP_{SSR1}} = [\,2(O_{2(out)}^{\mathrm{SSR1}} - O_{2(in)}^{\mathrm{SSR1}}) + (CO_{(out)}^{SSR1} - CO_{(in)}^{SSR1}) + 2(CO_{2(out)}^{SSR1} - CO_{2(in)}^{SSR1}) + (H_2O_{(\mathrm{out})}^{\mathrm{SSR1}} - H_2O_{(\mathrm{in})}^{\mathrm{SSR1}})]n_T^{SSR1} \qquad \text{Equation 5.1}$$

$$\mathrm{OP_{LSR1}} = 2(O_{2(in)}^{LSR1} - O_{2(out)}^{LSR1})n_T^{LSR1} \qquad \text{Equation 5.2}$$

As the products from the reaction that occurred in R1 were transferred into R2, the oxygen permeation from the lumen side of R1, LSR1 was assumed to be the same throughout the experiment. Since the aim of using 1% Pt/Al_2O_3 catalyst was to increase the production of hydrogen in the product composition of R1 and extend the contact time between methane in the SS1 with the unreacted permeated oxygen in R1, the overall oxygen permeation in the R2 needs to be calculated and observed. Overall oxygen permeation rate in R2, $\mathrm{OP_{SSR2}}$ can be calculated using Equation 5.3.

$$\begin{aligned}\mathrm{OP_{SSR2}} = [\, & 2(O_{2(out)}^{\mathrm{SSR2}} - O_{2(in)}^{\mathrm{SSR1}}) + (CO_{(out)}^{SSR2} - CO_{(in)}^{SSR1}) \\ & + 2(CO_{2(out)}^{SSR2} - CO_{2(in)}^{SSR1}) \\ & + (H_2O_{(\mathrm{out})}^{\mathrm{SSR2}} - H_2O_{(\mathrm{in})}^{\mathrm{SSR1}})]n_T^{SSR1}\end{aligned} \qquad \text{Equation 5.3}$$

Further experiment will then use all the three reactors for simultaneous methane reforming and water splitting process. For this experiment, the total oxygen balance for the whole system can be defined as following (refer Equation 5.4).

$$\mathrm{OP_{SSR3}} = \mathrm{OP_{LSR1}} + \mathrm{OP_{LSR3}} \qquad \text{Equation 5.4}$$

$\mathrm{OP_{SSR3}}$ is the overall oxygen permeation rate from the shell side outlet of R3 which can be calculated using Equation 5.5, $\mathrm{OP_{LSR1}}$ is the oxygen permeation rate in the

lumen side membrane in R1 (refer Equation 5.2) and OP_{LSR2} is the oxygen permeation rate in the lumen side membrane in R2, that can be calculated using Equation 5.6.

$$OP_{SSR3} = \left[2\left(O_{2(out)}^{SSR3} - O_{2(in)}^{SSR1}\right) + \left(CO_{(out)}^{SSR3} - CO_{(in)}^{SSR1}\right) + 2\left(CO_{2(out)}^{SSR3} - CO_{2(in)}^{SSR1}\right) + \left(H_2O_{(out)}^{SSR3} - H_2O_{(in)}^{SSR1}\right)\right] n_T^{SSR1} \quad \text{Equation 5.5}$$

$$OP_{LSR3} = \left[H_{2(out)}^{LSR3} - H_{2(in)}^{LSR3}\right] n_T^{LSR3} \quad \text{Equation 5.6}$$

The calculations on error propagation were done based on the same technique described in section 3.2.7.

5.3 Results and Discussion

This section discusses the ability of both as-supplied and modified LSCF6428 membranes in performing hydrogen production with the help of the 1%/Al_2O_3 catalyst. In this experiment, there were seven sets of inlet configuration conducted in series. Table 5.2 lists the inlet configurations for the system throughout the whole experiments.

Table 5.2: List of inlet configurations used in the series of experiment reported in this chapter.

operating time/hours	Inlet configuration notations	Reactor 1 (R1) total molar feed flowrate(s) /µmols^{-1}		Reactor 2 (R2) total molar feed flowrate / µmols^{-1}	Reactor 3 (R3) total molar feed flowrate(s) / µmols^{-1}	
		$n_T^{SSR1}{}_{(in)}$	$n_T^{LSR1}{}_{(in)}$			$n_T^{LSR3}{}_{(in)}$
Figure 5.4	$(M\text{-}O\text{-}A)_{R1}$	methane 20.44±2.04	oxygen 20.44±2.04			
Figure 5.4	$(A\text{-}O\text{-}A)_{R1}$	zero grade Ar 20.44±2.04	oxygen 20.44±2.044			
Figure 5.4	$(M\text{-}O\text{-}A)_{R1}$	methane 20.44±2.04	oxygen 20.44±2.04			
Figure 5.5	$(M\text{-}O\text{-}A)_{R2}$	methane 20.44±2.04	oxygen 20.44±2.04	SSR1(out)		
Figure 5.6	$(M\text{-}O\text{-}W)_{R3}$	methane 20.44±2.04	oxygen 20.44±2.04	SSR1(out)	SSR2(out)	water 20.44±2.04
Figure 5.6	$(M\text{-}O\text{-}A)_{R3}$	methane 20.44±2.04	oxygen 20.44±2.044	SSR1(out)	SSR2(out)	zero grade Ar 20.44±2.04
Figure 5.6	$(M\text{-}O\text{-}W)_{R3}$	methane 20.44±2.04	oxygen 20.44±2.04	SSR1(out)	SSR2(out)	water 20.44±2.04

** blank shaded region represent no inlet/ chamber was not in use for the particular inlet configuration*

The first column indicates the figures relate to the experiment that will be shown and discussed later in this section. The columns were separated according to the inlets in each reactor. For easy reference, the inlet configurations were named according to first alphabet of the gas inlet introduced to the system following the

(Shell side inlet-Lumen 1 inlet- Lumen 2 inlet)$_{reactor}$ arrangement. The 'reactor' in subscript print denotes the reactor name where the data were collected from.

Primarily, the first inlet configuration only utilises one reactor, R1. The purpose of running R1 individually is to monitor the outlet gas composition and to observe on any sign of unreacted oxygen in the outlet of R1, SSR1. This step will also provide useful data for the calculation of oxygen permeation rate in the lumen side of R1. This also to make sure that the analysed results were enough to perform material balances calculations for the whole system. Figure 3.6 shows the product composition of SSR1 and LSR1 over 45 hours of operation. LSR1 was fed with 30(STP) mlmin^{-1} of 10% oxygen, 41% of nitrogen in argon.

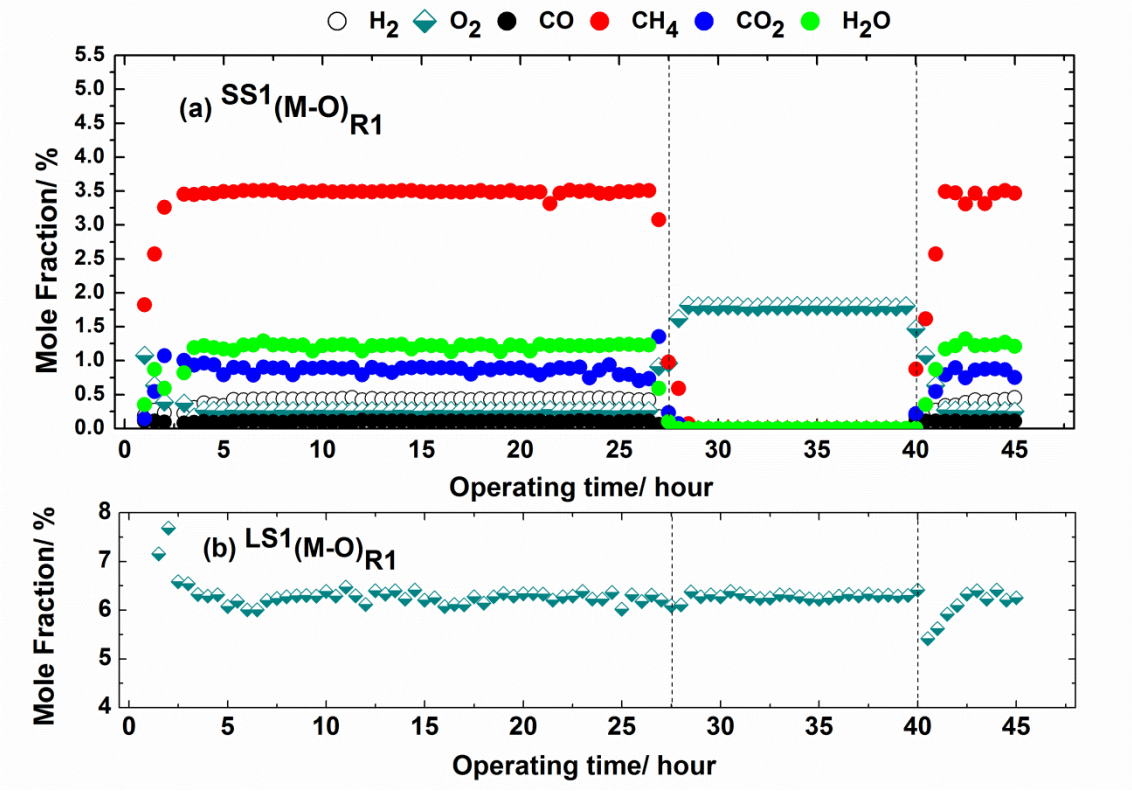

Figure 5.4: The outlet gas composition of (a) SSR1(out) previously fed with 30mlmin^{-1} with 5% methane in nitrogen and (b) LSR1(out), fed with 30mlmin^{-1} of 10% oxygen and 40% nitrogen in argon.

Table 5.3 shows the average mole fractions of all the reactant and product gases both on the shell side and the lumen side of the reactor used in the experiment. These values were used in the material balance calculations.

Table 5.3: Average mole fraction of reactants and products in the shell side (S1) and the lumen side (L1) for R1

Average mole fraction of reactant(s) and product(s) in the shell side of R1; SSR1(out)						
gases/A	H_2	O_2	CO	CH_4	CO_2	H_2O
$(A)^{S1}{}_{(in)}$ (%)	n/a	n/a	n/a	(5.05 ±0.51)	n/a	n/a
$(A)^{S1}{}_{(out)}$ (%)	(0.42 ±0.04)	(0.27 ±0.03)	(0.11 ±0.001)	(3.49 ±0.35)	(0.87 ±0.09)	(1.21 ±0.12)
Average mole fraction of reactant(s) and product(s) in the lumen side of R1 (L1)						
gases/A	O_2		N_2			
$(A)^{L1}{}_{(in)}$ (%)	(10.64±1.06)		(41.78±4.18)			
$(A)^{L1}{}_{(out)}$ (%)	(6. 28±0.63)		(41.90±4.19)			

Results show that the oxygen mole fraction in the lumen side of L1 detected at the first hour of operation was at *ca* 10%. The oxygen mole fraction however started to drop to *ca* 6% once the syngas was detected. This system shows a steady production of hydrogen and carbon dioxide in the shell side after 3 hours of

operation. The gas inlet of SSR1(in) was changed from 30mlmin^{-1} of 5% methane in argon to 30mlmin^{-1} of zero grade argon at hour 27 of operation time. This is to ensure and confirm that the results obtained earlier on were caused by the effects of oxygen permeation through the oxygen vacancies of perovskites and not caused by the effects of membrane leaks. The results of the change of the SSR1 inlet feed can be seen in the same figure. The mole fractions of all the combined oxidation products in the shell side declined abruptly after the changing of the feed gases.

A simple oxygen balance calculation shows that the amount of oxygen existing on the shell side was the same as what is consumed in the lumen side, L1 and that the oxygen balances were closed. Oxygen permeation rates were also calculated for both sides of the membrane. The average oxygen permeation rate, OP_{SSR1} is at 0.73±0.15μmolO.s^{-1} and the OP_{LSR1} is at 0.76±0.26 μmolO.s^{-1}. The average CO/CO_2 ratio is 0.12. This shows that the full oxidation of methane was the more desired reaction in this system because of the high oxygen concentration in the SSR1. There are also small amounts of unreacted oxygen found in the product composition of SSR1. The detected unreacted oxygen mole fraction was up to 0.3%. This will increase the oxygen partial pressure in the SSRI and lower down the chance of further oxygen permeation from the lumen side if the same gas composition from this outlet was to be used as the inlet of another individual membrane reactor specifically for oxygen permeation via the water splitting process.

In order to increase the consumption of unreacted oxygen in the SSR1 product, the SSR1 outlet was connected to a catalyst containing reactor, R2 containing 1%Pt/Al_2O_3. Pt catalyst was chosen in this experiment based on the claims that it can improve the conversion of hydrocarbons and lower the possibility of carbon deposition [160, 162]. The next inlet configuration setup utilises the catalyst

containing reactor R2. In this experiment, SSR1(out) will be used as the inlet to R2. Figure 5.5 shows the mole fraction of products obtained from the outlet of R2, SSR2(out).

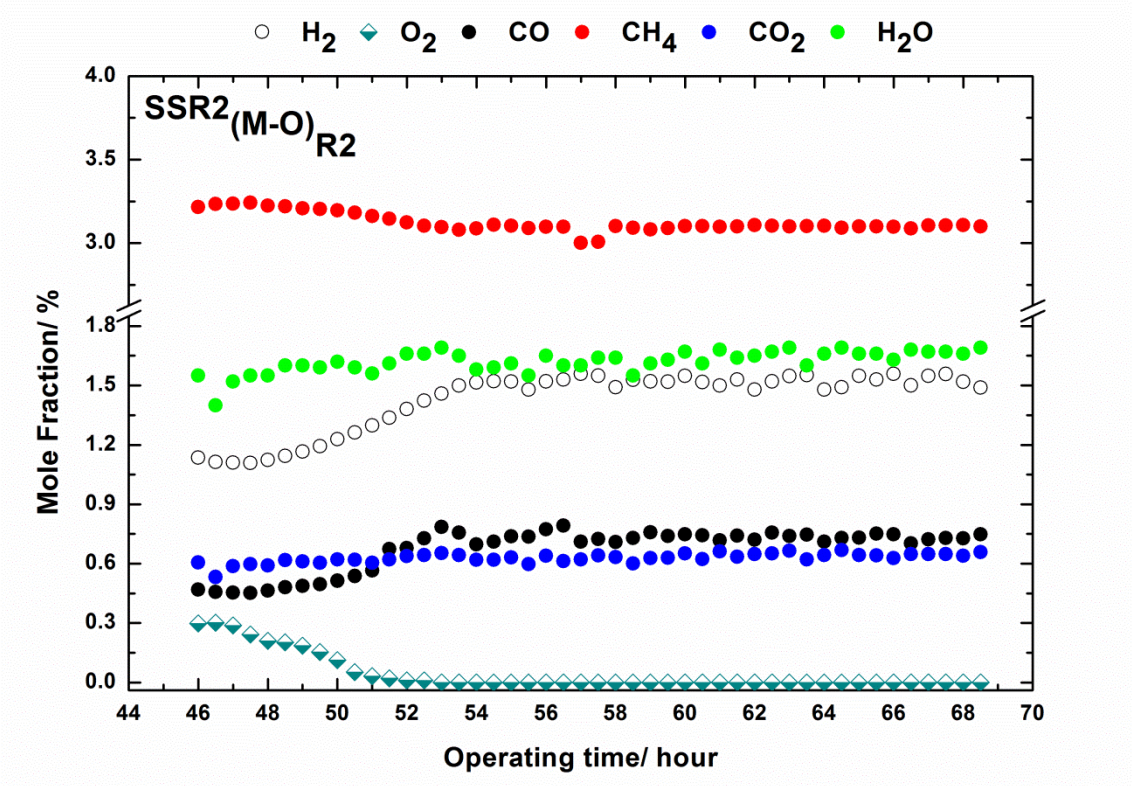

Figure 5.5: The mole fractions of gases obtained from SSR2(out). The inlet to R2 comprising of the products of methane reforming gases produced in SSR1. SSR1 was earlier fed with 30mlmin^{-1} of 5% methane in argon while LSR1 was fed with 30%mlmin^{-1} of 10% of oxygen, 40% of nitrogen in argon.

Dynamic responses were observed in the mole fraction obtained from the outlet of the SSR2(out) right after the inlet introduction was made to R2. The CO/CO_2 ratio increases from 0.12 to 1. This can be seen with the increasing values of the carbon monoxide and hydrogen mole fraction along the time of operation. The changes however stabilised after 8 hours of operation. This is mainly because there was higher concentration of oxygen in the inlet accumulated from the previous experiment prior to the introduction of inlet into R2. As can be seen in the figure,

the initial mole fraction of oxygen was at 0.3% but decreased as the reading of the mole fraction of the products in the SSR2 reading stabilised at hour 54. The platinum catalyst helps to increase the conversion of methane and shifts the selectivity towards the partial oxidation of methane. In this case there were limited reforming processes because there were no significant changes in the mole fraction of water and carbon dioxide. Table 5.4 lists the average mole fraction values of reactant and product taken at hour 53 to hour 69. These data will be used in the material balance and oxygen permeation rates calculations.

Table 5.4: Average mole fraction of reactants and products for the feed configuration (M-O) starting from hour 53 to hour 69.

Average mole fraction of reactant(s) and product(s) from the inlet and outlet of R2 and the outlet of L1						
gases/A	H_2	O_2	CO	CH_4	CO_2	H_2O
$(A)^{SS1}{}_{(in)}$ (%)	n/a	n/a	n/a	5.05 ±0.51	n/a	n/a
$(A)^{SS1}{}_{(out)}$ (%)	1.43 ±0.14	0.00	0.68 ±0.07	3.12 ±0.03	0.63 ±0.07	1.62 ±0.16
Average mole fraction of reactant(s) and product(s) in the lumen side of R1 (L1)						
gases/A	O_2		N_2			
$(A)^{L1}{}_{(in)}$ (%)	10.64±1.06		41.78±4.18			
$(A)^{L1}{}_{(out)}$ (%)	6. 30±0.63		41.35±4.14			

The oxygen permeation rate for the shell side, OP_{SSR1} calculated is at 0.73±0.15µmol $O.s^{-1}$ and the oxygen permeated through the membrane from the lumen, OP_{LSR1} is at 0.76±0.26 µmol $O.s^{-1}$. Oxygen balance calculations on both sides of the membrane were closed. The rate of hydrogen production is at the highest compared to the other results obtained from oxygen permeation with methane reforming experiments such as in the one reported earlier in section 3.3.2. This shows that the use of catalyst was able to increase the selectivity towards hydrogen productions.

The use of the catalyst reactor, R2 has utilised almost all of the unreacted oxygen in the shell side inlet gas composition. This provides an oxygen deficit environment in the SSR2(out). It is expected that by connecting this stream into the last reactor, R3, we can increase the oxygen permeation rate of the lumen side in R3 hence increasing the hydrogen production via water splitting.

The next inlet configuration set tested using this system is the (M-O-W)-(M-O-A)-(M-O-W) experiment. This experiment mimics the inlet configuration set used for the simultaneous methane reforming and water splitting conducted and discussed in section 4.3.2 and 4.3.3. In this experiment, the oxygen permeation from LSR1 into R1 is maintained by continuously feeding the inlet with 30$mlmin^{-1}$ of 10% of oxygen, 41% of nitrogen in argon. The SSR1 was continuously fed with 30$mlmin^{-1}$ of 5% methane balance in argon. Figure 5.6 shows the product composition in mole fraction percentage obtained from the outlets of (a) lumen side of membrane 2 (LSR3) (b) shell side of membrane reactor 2 (SSR2) and (c) lumen side of the first membrane in R1 (LSR1). The water splitting process started to show nearly three hours subsequent to the inlet introduction into the shell side of R3.

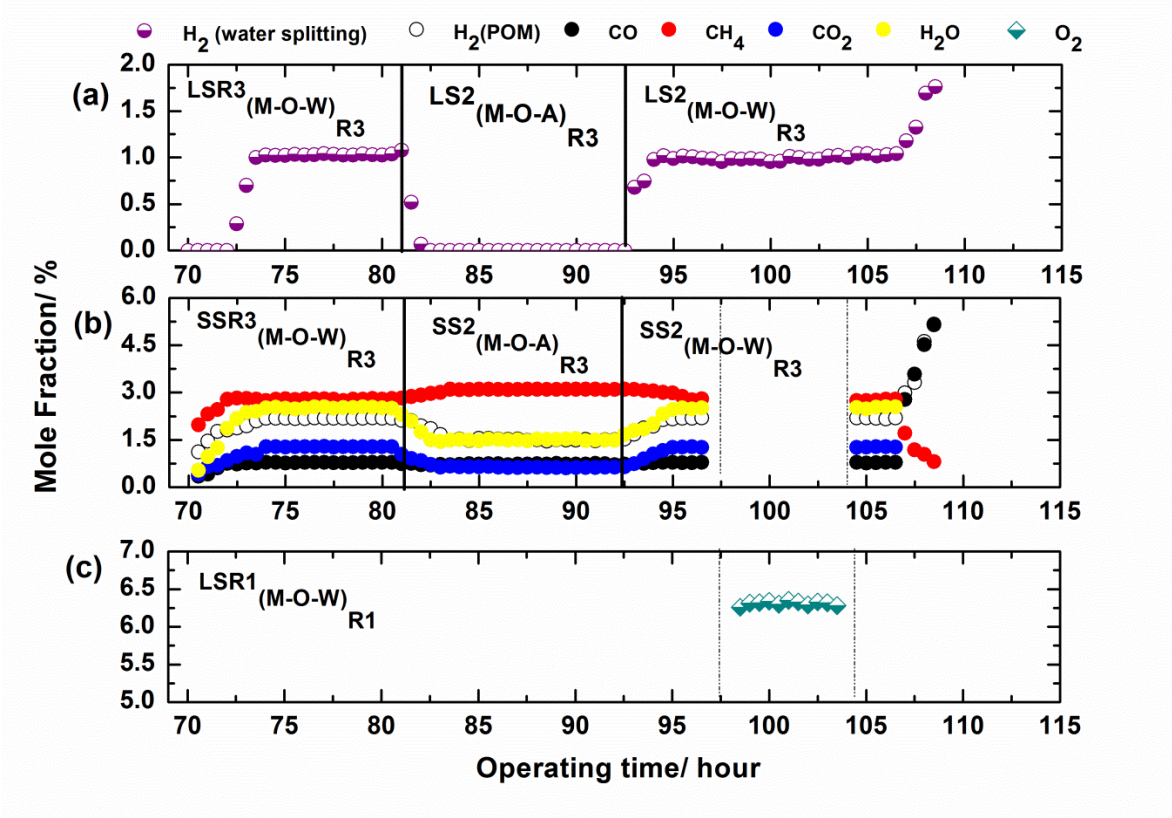

Figure 5.6: The gas composition obtained from the simultaneous methane reforming and water splitting reactions from three different outlets. ; (a) LSR3 outlet gas composition earlier fed with 30mlmin^{-1} of 4% water in argon (b) SSR3 outlet gas composition fed with the outlet of R1originates from the outlet of SSR1 earlier fed with 30mlmin^{-1} of 5% methane in nitrogen and (c) LSR1 outlet gas composition earlier fed with 30mlmin^{-1} of 10% oxygen and 40% of nitrogen in argon. Inlet configuration changed from (M-O-W) at hour 70 to 81 to (M-O-A) at hour 82 to93 and to (M-O-W) at hour 93 to 109 respectively.

Through this feed configuration it is observed that the hydrogen and water in the SSR3 (out) increased by a factor of 1.5 from the previous reading obtained from the SSR2(out) outlet. This suggests that there is extra hydrogen production occurring in R3. It is also observed that the methane conversion in R3 increased from 18% (as from the previous $(M\text{-}O)_{R2}$ experiment)to 44.2%. The inlet composition in SSR2 has a 1:1 ratio of hydrogen to water. This might act as the buffer for the water splitting on the shell side. Hydrogen production from the water splitting process in L2 shows

consistent results with the previous run of the water splitting process using the same batch of modified LSCF6428 membrane reported in section 0.

The LSR1 oxygen mole fraction signal however did not show any changes since the beginning of the experiment. Recalling from the results in section 0, hydrogen production was only observed after a 30 hour induction period. In contrast the present M-O-W inlet configuration experiment took a three hour induction period for hydrogen production. This may be caused by a more oxidising environment in SSR3 whereby there is a mixture of carbon monoxide and methane. Furthermore the higher surface area of the modified LSCF6428 membrane provides better contact between methane and the permeated oxygen in the LSR2 hence greatly shortening the induction period to 3 hours. To reconfirm the water splitting process in the LSR2, the inlet configuration was changed for, M-O-W to M-O-A at hour 70. A hydrogen mole fraction was not detected. This confirmed that the hydrogen production detected earlier was from the water splitting process in the LSR3 and not from inter-chamber leaks.

The inlet configuration was changed again to M-O-W at hour 93 to observe the stability of the membrane to withstand both oxidising and reducing environments, at the same time simultaneously producing hydrogen via methane reforming and the water splitting process. The hydrogen mole fraction in LSR3 was detected instantaneously after the changing of inlet configuration and lasted for 14 hours before showing signs of leakage and breaking afterwards. The results obtained by this newly introduced surface-modified membrane however shows better stability as of to compare to the one presented in section 4.3.2. Table 5.5 lists the average mole fractions for all the products in both inlets and outlets from the system.

Table 5.5: Average mole fractions (%) for the products found in the outlets of LSR3, SSR1 and LSR1 for M- O-W experiment

(a) Average mole fraction (%)of reactant(s) and product(s) in LSR3						
gases/(A)	H_2			O_2		
$(A)^{LSR3}_{(in)}$	n/a			n/a		
$(A)^{LSR3}_{(out)}$	1.03±0.01			n/a		
(b) Average mole fraction (%) of reactant(s) and product(s) in SSR3						
gases/(A)	H_2	O_2	CO	CH_4	CO_2	H_2O
$(A)^{SSR1}_{(in)}$	n/a	n/a	n/a	5.05 ±0.51	n/a	n/a
$(A)^{SSR3}_{(out)}$	2.19 ±0.02	n/a	0.78 ±0.08	2.79 ±0.03	1.24 ±0.01	2.49 ±0.03
(c) Average mole fraction (%)of reactant(s) and product(s) in LSR1						
gases/A	O_2			N_2		
$(A)^{LSR1}_{(in)}$	10.64±1.06			41.78±4.19		
$(A)^{LSR1}_{(out)}$	6. 31±0.63			40.55±4.06		

The oxygen permeation rate in the shell side of the R3 membrane reactor, OP_{SSR3} is 1.18±0.24 μmol $O.s^{-1}$. The summation of oxygen permeation rates from both of the lumen sides is at 1.72±0.36 μmol $O.s^{-1}$. This shows a closed oxygen balance on both sides of the membranes throughout the system.

5.4 Summary

The results obtained and discussed in this chapter confirm that the simultaneous methane reforming and water splitting can be conducted in membrane reactors. The use of a catalyst improved the selectivity towards the hydrogen production on the shell side. The hydrogen production via the water splitting reaction shows stable results and is able to produce hydrogen for more than 15 hours of operation.

Chapter 6 Conclusions and Suggested Future Work

6.1 Overall outcomes

The aim of this study is to assess the ability of perovskites MIEC ceramic hollow fibre membranes to allow simultaneous methane oxidations and water splitting processes. The main idea behind the aim was to study the ability of an autothermal hydrogen production by synergising the exothermic and endothermic processes involved in the membrane reactor. By proving this, the membrane reactor can be used to produce syngas at a lower energy demand.

Previous study on the water splitting process involving the use of hollow fibre membranes suffered from membrane disintegration and breakages. This study shows that the design of the reactor plays an important role in determining the long term performance and the stability of the membranes in the membrane reactor. Given that, major changes were made in the classical design of the membrane reactor previously used for hydrogen production via water splitting process. In this newly designed reactor, the membranes were sealed on one end allowing inlet gas into the lumen to be inserted using a hypodermic needle-like tube. As we believed that material balance on a working system is one of the important points to be

mentioned in the membrane system study, all of the conducted experiments were designed to generate information sufficient for material balance calculations purposes.

This study started with the evaluation of two famous and proven membrane materials that were being studied for oxygen permeation; LSCF6428 and BSCF5582. These membranes were tested for permeation activities under different conditions (i) oxygen permeation without reducing gas on the shell side with oxygen containing gas on the lumen side (ii) oxygen permeation with reducing gas fed into the shell side of the membrane reactor with oxygen containing gas on the lumen side (iii) oxygen permeation with methane fed on the shell side and water fed in the lumen side. The BSCF5582 membranes show high permeation rates in the first two conditions but could not survive the last condition. The highest average oxygen permeation rate obtained by this membrane is at 3.88 ± 0.39μmol$O.s^{-1}$. The LSCF6428 however demonstrated much lower oxygen permeation for both two earlier conditions but showed good stability and hydrogen production rate in the water splitting processes. The highest average oxygen permeation rate for the LSCF6428 membrane was obtained through condition (ii), amounting to 0.38±0.05 μmolOs^{-1}.

As the main aim of this thesis to study on the stability of simultaneous methane oxidations and water splitting, LSCF6428 was chosen to be studied upon in the multiple-membrane reactor system presented in Chapter 4. The experiment was conducted by changing the inlet-configurations where one of the inlet configurations used will lead to simultaneous methane oxidations and water splitting. Observations were mainly focused on the changes in the product compositions analysed at the output of the shell side and lumens of the membranes.

There are three sets of inlet configuration and a few of them were repeated alternately with other sets for confirmation of the results. The inlet configuration that leads to simultaneous methane oxidation and water splitting processes shows that these three reactions can be done in a membrane reactor simultaneously but with limitations. Consequently hydrogen was produced on both sides of the membrane; however the hydrogen produced from the water splitting side was at a lower concentration than that of what has been obtained earlier in an individual run. It is detected that the main problem of this system is that there is unreacted oxygen in the shell side of the membrane. This may results in an increase in the oxygen partial pressure of the shell side thus reducing the chance of oxygen permeation from the membrane designated for the water splitting process.

The LSCF6428 membranes used in the multiple-membrane reactor show a good sign of oxygen permeation with diluted air but halted the oxygen permeation with the lumen fed with water. This is because there was unreacted oxygen on the shell side. The presence of water, unreacted oxygen and carbon monoxide in the same chamber also shows a sign of the water gas shift reaction to occur on the shell side. Efforts have been made to increase the unreacted oxygen utilisation on the shell side but none of the optimisation experiments showed promising results. We however are able to increase the rate of hydrogen production by a factor of 1.1 via the water splitting process using a modified surface membrane. However catalytic assisted simultaneous methane reforming and water splitting processes show promising results with both shell side and lumen side producing hydrogen. The overall oxygen balances were close. This confirms that simultaneous methane reforming and water splitting processes can be conducted using a membrane reactor.

6.2 Suggested future works

As this is the first autothermal hydrogen production process to be tried on a membrane system, the aim is much more focussed on the ability of the membrane reactor to simultaneously perform methane oxidation and water splitting processes. Further improvements can be done by optimising the studied parameters reported in this study. Other parameters that was not looked at in this study

(i) Increase membrane chemical stability. There is evidence in the experiments conducted that the membrane surface peels and causing breakage occurs while the experiments were still running. These problems can be solved by increasing the thickness of the membrane.

(ii) Develop mathematical modelling to design better membrane inlet configurations in the reactor-one with suggestion to use two membranes for water splitting and one membrane for oxygen permeation from an oxygen containing gas feed.

(iii) To produce pure hydrogen on both sides of the membrane; another type of reactor design can be applied. One possibility is to use a housing meant for the catalyst and a second is by having a hydrogen separation membrane to separate the hydrogen from carbon monoxide, carbon dioxide and water.

(iv) Other more fundamental studies on the membrane material and fabrication can also be done for example by coating a membrane with an optimum amount of Pt paste in order to get the right CO/CO_2 ratio. This will result in a better production of hydrogen on the SS and enhancing the production of hydrogen through water splitting.

References

1. Nelson, A.E., *Fundamentals of Industrial Catalytic Processes, 2nd Edition. C. H. Bartholomew and Robert J. Farrauto John Wiley and Sons, Hoboken, NJ, 966 pp., 2006.* The Canadian Journal of Chemical Engineering, 2007. **85**(1): p. 127-128.
2. Balat, H. and E. Kırtay, *Hydrogen from biomass – Present scenario and future prospects.* International Journal of Hydrogen Energy, 2010. **35**(14): p. 7416-7426.
3. Crocker, M., *Thermochemical Conversion of Biomass to Liquid Fuels and Chemicals*. 2010, Royal Society of Chemistry.
4. Ni, M., et al., *Potential of renewable hydrogen production for energy supply in Hong Kong.* International Journal of Hydrogen Energy, 2006. **31**(10): p. 1401-1412.
5. Satyapal, S., et al., *The U.S. Department of Energy's National Hydrogen Storage Project: Progress towards meeting hydrogen-powered vehicle requirements.* Catalysis Today, 2007. **120**(3-4 SPEC. ISS.): p. 246-256.
6. C.E.G. Padro, V.P., *Survey of the Economics of Hydrogen Technologies*. 1999, National Renewable Energy Laboratory (NREL): Golden (Colorado, USA) (1999).
7. Gallucci, F., et al., *Recent advances on membranes and membrane reactors for hydrogen production.* Chemical Engineering Science, 2013. **92**(0): p. 40-66.
8. Sunarso, J., et al., *Mixed ionic–electronic conducting (MIEC) ceramic-based membranes for oxygen separation.* Journal of Membrane Science, 2008. **320**(1–2): p. 13-41.
9. Balachandran, U., et al., *Ceramic membrane reactor for converting methane to syngas.* Catalysis Today, 1997. **36**(3): p. 265-272.
10. Chen, C.-s., et al., *Conversion of Methane to Syngas by a Membrane-Based Oxidation–Reforming Process.* Angewandte Chemie International Edition, 2003. **42**(42): p. 5196-5198.
11. Franca, R.V., A. Thursfield, and I.S. Metcalfe, *La0.6Sr0.4Co0.2Fe0.8O3–δ microtubular membranes for hydrogen production from water splitting.* Journal of Membrane Science, 2012. **389**(0): p. 173-181.
12. Bang, Y., J.G. Seo, and I.K. Song, *Hydrogen production by steam reforming of liquefied natural gas (LNG) over mesoporous Ni–La–Al2O3 aerogel catalysts: Effect of La content.* International Journal of Hydrogen Energy, 2011. **36**(14): p. 8307-8315.
13. Cormos, C.-C., et al., *Innovative concepts for hydrogen production processes based on coal gasification with capture.* International Journal of Hydrogen Energy, 2008. **33**(4): p. 1286-1294.
14. Li, F. and L.-S. Fan, *Clean coal conversion processes - progress and challenges.* Energy & Environmental Science, 2008. **1**(2): p. 248-267.

15. Balat, M., *Potential importance of hydrogen as a future solution to environmental and transportation problems.* International Journal of Hydrogen Energy, 2008. **33**(15): p. 4013-4029.
16. Winter, C.-J., *Hydrogen energy — Abundant, efficient, clean: A debate over the energy-system-of-change.* International Journal of Hydrogen Energy, 2009. **34**(14, Supplement 1): p. S1-S52.
17. Montañez, M.K., R. Molina, and S. Moreno, *Nickel catalysts obtained from hydrotalcites by coprecipitation and urea hydrolysis for hydrogen production.* International Journal of Hydrogen Energy, 2014. **39**(16): p. 8225-8237.
18. Ursúa, A., L.M. Gandía, and P. Sanchis, *Hydrogen production from water electrolysis: Current status and future trends.* Proceedings of the IEEE, 2012. **100**(2): p. 410-426.
19. Koumi Ngoh, S. and D. Njomo, *An overview of hydrogen gas production from solar energy.* Renewable and Sustainable Energy Reviews, 2012. **16**(9): p. 6782-6792.
20. Miyake, J., et al., *Simulation of the daily sunlight illumination pattern for bacterial photo-hydrogen production.* Journal of Bioscience and Bioengineering, 1999. **88**(6): p. 659-663.
21. Luk, H.T., et al., *Techno-economic Analysis of Distributed Hydrogen Production from Natural Gas.* Chinese Journal of Chemical Engineering, 2012. **20**(3): p. 489-496.
22. Song, C., *Fuel processing for low-temperature and high-temperature fuel cells: Challenges, and opportunities for sustainable development in the 21st century.* Catalysis Today, 2002. **77**(1–2): p. 17-49.
23. Ryi, S.-K., et al., *Methane steam reforming with a novel catalytic nickel membrane for effective hydrogen production.* Journal of Membrane Science, 2009. **339**(1–2): p. 189-194.
24. Barelli, L., et al., *Hydrogen production through sorption-enhanced steam methane reforming and membrane technology: A review.* Energy, 2008. **33**(4): p. 554-570.
25. Voss, C., *Applications of Pressure Swing Adsorption Technology.* Adsorption, 2005. **11**(1): p. 527-529.
26. Simpson, A.P. and A.E. Lutz, *Exergy analysis of hydrogen production via steam methane reforming.* International Journal of Hydrogen Energy, 2007. **32**(18): p. 4811-4820.
27. Basini, L., *Issues in H2 and synthesis gas technologies for refinery, GTL and small and distributed industrial needs.* Catalysis Today, 2005. **106**(1–4): p. 34-40.
28. Aboosadi, Z.A., M.R. Rahimpour, and A. Jahanmiri, *A novel integrated thermally coupled configuration for methane-steam reforming and hydrogenation of nitrobenzene to aniline.* International Journal of Hydrogen Energy, 2011. **36**(4): p. 2960-2968.
29. Chen, W., et al., *Oxygen-selective membranes integrated with oxy-fuel combustion.* Journal of Membrane Science, 2014. **463**(0): p. 166-172.
30. Zhou, L., et al., *Self-activation and self-regenerative activity of trace Ru-doped plate-type anodic alumina supported nickel catalysts in steam reforming of methane.* Catalysis Communications, 2008. **10**(3): p. 325-329.
31. Chen, Y.-g., et al., *Promoting effect of Pt, Pd and Rh noble metals to the Ni0.03Mg0.97O solid solution catalysts for the reforming of CH4 with CO2.* Applied Catalysis A: General, 1997. **165**(1–2): p. 335-347.

32. Radfarnia, H.R. and M.C. Iliuta, *Development of Al-stabilized CaO–nickel hybrid sorbent–catalyst for sorption-enhanced steam methane reforming.* Chemical Engineering Science, 2014. **109**(0): p. 212-219.
33. Kim, Y.H., et al., *Effect of bed void volume on pressure vacuum swing adsorption for air separation.* Korean Journal of Chemical Engineering, 2014. **31**(1): p. 132-141.
34. Jee, J.G., et al., *Three-bed PVSA process for high-purity O2 generation from ambient air.* AIChE Journal, 2005. **51**(11): p. 2988-2999.
35. Lin, Y.S., *Microporous and dense inorganic membranes: current status and prospective.* Separation and Purification Technology, 2001. **25**(1–3): p. 39-55.
36. Sá, S., et al., *Hydrogen production by methanol steam reforming in a membrane reactor: Palladium vs carbon molecular sieve membranes.* Journal of Membrane Science, 2009. **339**(1–2): p. 160-170.
37. Flanagan, T.B. and W.A. Oates, *The Palladium-Hydrogen System.* Annual Review of Materials Science, 1991. **21**(1): p. 269-304.
38. Yun, S. and S. Ted Oyama, *Correlations in palladium membranes for hydrogen separation: A review.* Journal of Membrane Science, 2011. **375**(1–2): p. 28-45.
39. Lu, G.Q., et al., *Inorganic membranes for hydrogen production and purification: A critical review and perspective.* Journal of Colloid and Interface Science, 2007. **314**(2): p. 589-603.
40. Lutz, A.E., et al., *Thermodynamic analysis of hydrogen production by partial oxidation reforming.* International Journal of Hydrogen Energy, 2004. **29**(8): p. 809-816.
41. Choudhary, V.R., A.S. Mammon, and S.D. Sansare, *Selective Oxidation of Methane to CO and H2 over Ni/MgO at Low Temperatures.* Angewandte Chemie International Edition in English, 1992. **31**(9): p. 1189-1190.
42. Tsang, S.C., J.B. Claridge, and M.L.H. Green, *Recent advances in the conversion of methane to synthesis gas.* Catalysis Today, 1995. **23**(1): p. 3-15.
43. Christian Enger, B., R. Lødeng, and A. Holmen, *A review of catalytic partial oxidation of methane to synthesis gas with emphasis on reaction mechanisms over transition metal catalysts.* Applied Catalysis A: General, 2008. **346**(1–2): p. 1-27.
44. Choudhary, V.R., A.M. Rajput, and B. Prabhakar, *Nonequilibrium Oxidative Conversion of Methane to CO and H2 with High Selectivity and Productivity over Ni/Al2O3 at Low Temperatures.* Journal of Catalysis, 1993. **139**(1): p. 326-328.
45. Nakagawa, K., et al., *Partial oxidation of methane to synthesis gas over iridium–nickel bimetallic catalysts.* Applied Catalysis A: General, 1999. **180**(1–2): p. 183-193.
46. Mattos, L.V., et al., *Partial oxidation of methane on Pt/Ce–ZrO2 catalysts.* Catalysis Today, 2002. **77**(3): p. 245-256.
47. Zhu, J., et al., *Effect of surface composition of yttrium-stabilized zirconia on partial oxidation of methane to synthesis gas.* Journal of Catalysis, 2005. **230**(2): p. 291-300.
48. Tan, X. and K. Li, *Design of mixed conducting ceramic membranes/reactors for the partial oxidation of methane to syngas.* AIChE Journal, 2009. **55**(10): p. 2675-2685.
49. Liu, K., C. Song, and V. Subramani, *Hydrogen and Syngas Production and Purification Technologies*. 2009, Hoboken, NJ, USA: Wiley.

50. Bharadwaj, S.S. and L.D. Schmidt, *Catalytic partial oxidation of natural gas to syngas.* Fuel Processing Technology, 1995. **42**(2–3): p. 109-127.
51. Bakkerud, P.K., *Update on synthesis gas production for GTL.* Catalysis Today, 2005. **106**(1–4): p. 30-33.
52. Cassinelli, W.H., et al., *Study of the properties of supported Pd catalysts for steam and autothermal reforming of methane.* Applied Catalysis A: General, 2014. **475**(0): p. 256-269.
53. Yan, Y., J. Zhang, and L. Zhang, *Properties of thermodynamic equilibrium-based methane autothermal reforming to generate hydrogen.* International Journal of Hydrogen Energy, 2013. **38**(35): p. 15744-15750.
54. Molinari, R., T. Marino, and P. Argurio, *Photocatalytic membrane reactors for hydrogen production from water.* International Journal of Hydrogen Energy, 2014. **39**(14): p. 7247-7261.
55. Patil, C.S., M. van Sint Annaland, and J.A.M. Kuipers, *Design of a Novel Autothermal Membrane-Assisted Fluidized-Bed Reactor for the Production of Ultrapure Hydrogen from Methane.* Industrial & Engineering Chemistry Research, 2005. **44**(25): p. 9502-9512.
56. Gallucci, F., M. van Sint Annaland, and J.A.M. Kuipers, *Autothermal reforming of methane with integrated CO2 capture in novel fluidized bed membrane reactors.* Asia-Pacific Journal of Chemical Engineering, 2009. **4**(3): p. 334-344.
57. Gallucci, F., M. Sint Annaland, and J.A.M. Kuipers, *Autothermal Reforming of Methane with Integrated CO2 Capture in a Novel Fluidized Bed Membrane Reactor. Part 2 Comparison of Reactor Configurations.* Topics in Catalysis, 2008. **51**(1-4): p. 146-157.
58. Roses, L., et al., *Experimental study of steam methane reforming in a Pd-based fluidized bed membrane reactor.* Chemical Engineering Journal, 2013. **222**(0): p. 307-320.
59. Rosen, M.A., *Energy and exergy analyses of electrolytic hydrogen production.* International Journal of Hydrogen Energy, 1995. **20**(7): p. 547-553.
60. Ewan, B.C.R. and R.W.K. Allen, *A figure of merit assessment of the routes to hydrogen.* International Journal of Hydrogen Energy, 2005. **30**(8): p. 809-819.
61. Stojić, D.L., et al., *Hydrogen generation from water electrolysis—possibilities of energy saving.* Journal of Power Sources, 2003. **118**(1–2): p. 315-319.
62. Ghirardi, M.L., et al., *Microalgae: a green source of renewable H2.* Trends in Biotechnology, 2000. **18**(12): p. 506-511.
63. Melis, A., *Green alga hydrogen production: progress, challenges and prospects.* International Journal of Hydrogen Energy, 2002. **27**(11–12): p. 1217-1228.
64. Demirbas, A., *Hydrogen production from carbonaceous solid wastes by steam reforming.* Energy Sources, Part A: Recovery, Utilization and Environmental Effects, 2008. **30**(10): p. 924-931.
65. Nathao, C., U. Sirisukpoka, and N. Pisutpaisal, *Production of hydrogen and methane by one and two stage fermentation of food waste.* International Journal of Hydrogen Energy, 2013. **38**(35): p. 15764-15769.
66. Koc, R., N.K. Kazantzis, and Y. Hua Ma, *A process dynamic modeling and control framework for performance assessment of Pd/alloy-based membrane reactors used in hydrogen production.* International Journal of Hydrogen Energy, 2011. **36**(8): p. 4934-4951.
67. Koc, R., N.K. Kazantzis, and Y.H. Ma, *Membrane technology embedded into IGCC plants with CO2 capture: An economic performance evaluation under*

uncertainty. International Journal of Greenhouse Gas Control, 2014. **26**(0): p. 22-38.
68. Zhu, J. and J. Chen, *Perovskite-Type Oxides: Synthesis and Application in Catalysis*. Perovskites : Structure, Properties and Uses. 2010, Hauppauge, NY, USA: Nova.
69. Chroneos, A., et al., *Oxygen transport in perovskite and related oxides: A brief review.* Journal of Alloys and Compounds, 2010. **494**(1–2): p. 190-195.
70. Skinner, S.J. and J.A. Kilner, *Oxygen ion conductors.* Materials Today, 2003. **6**(3): p. 30-37.
71. Lobera, M.P., et al., *On the use of supported ceria membranes for oxyfuel process/syngas production.* Journal of Membrane Science, 2011. **385–386**(0): p. 154-161.
72. Hayashi, H., et al., *Structural consideration on the ionic conductivity of perovskite-type oxides.* Solid State Ionics, 1999. **122**(1–4): p. 1-15.
73. Lin, Y.-S., W. Wang, and J. Han, *Oxygen permeation through thin mixed-conducting solid oxide membranes.* AIChE Journal, 1994. **40**(5): p. 786-798.
74. Holc, J., et al., *Electrical and microstructural characterisation of (La0.8Sr0.2)(Fe1 − xAlx)O3 and (La0.8Sr0.2)(Mn1 − xAlx)O3 as possible SOFC cathode materials.* Solid State Ionics, 1997. **95**(3–4): p. 259-268.
75. Kuščer, D., et al., *Electrical and microstructural characteristics of materials in the LaMnO3±δ–LaAlO3–SrMnO3−δ system.* Journal of Power Sources, 1998. **71**(1–2): p. 195-198.
76. Wang, H., et al., *Perovskite hollow-fiber membranes for the production of oxygen-enriched air.* Angewandte Chemie - International Edition, 2005. **44**(42): p. 6906-6909.
77. Niehoff, P., et al., *Oxygen transport through supported Ba0.5Sr0.5Co0.8Fe0.2O3â˜Î´ membranes.* Separation and Purification Technology, 2014. **121**(0): p. 60-67.
78. Hashim, S.M., A.R. Mohamed, and S. Bhatia, *Current status of ceramic-based membranes for oxygen separation from air.* Advances in Colloid and Interface Science, 2010. **160**(1–2): p. 88-100.
79. Hashim, S.S., A.R. Mohamed, and S. Bhatia, *Oxygen separation from air using ceramic-based membrane technology for sustainable fuel production and power generation.* Renewable and Sustainable Energy Reviews, 2011. **15**(2): p. 1284-1293.
80. Miller, C.F., et al., *Advances in ion transport membrane technology for Syngas production.* Catalysis Today, 2014. **228**(0): p. 152-157.
81. Wei, Y., et al., *Dense ceramic oxygen permeable membranes and catalytic membrane reactors.* Chemical Engineering Journal, 2013. **220**(0): p. 185-203.
82. Saracco, G., G.F. Vesteeg, and W.P.M. van Swaaij, *Current hurdles to the success of high-temperature membrane reactors.* Journal of Membrane Science, 1994. **95**(2): p. 105-123.
83. Chen, T., et al., *Improved oxygen permeability of Ce0.8Sm0.2O2−δ–PrBaCo2O5+δ dual-phase membrane by surface-modifying porous layer.* International Journal of Hydrogen Energy, 2012. **37**(24): p. 19133-19137.
84. Luo, H., et al., *CO2-Stable and Cobalt-Free Dual-Phase Membrane for Oxygen Separation.* Angewandte Chemie International Edition, 2011. **50**(3): p. 759-763.
85. Pan, H., et al., *Improvement of oxygen permeation in perovskite hollow fibre membranes by the enhanced surface exchange kinetics.* Journal of Membrane Science, 2013. **428**(0): p. 198-204.

86. Teraoka, Y., et al., *Mixed ionic-electronic conductivity of La1−xSrxCo1−yFeyO3−δ perovskite-type oxides.* Materials Research Bulletin, 1988. **23**(1): p. 51-58.
87. Teraoka, Y., et al., *OXYGEN PERMEATION THROUGH PEROVSKITE-TYPE OXIDES.* Chemistry Letters, 1985. **14**(11): p. 1743-1746.
88. Nakamura, T., M. Misono, and Y. Yoneda, *Reduction-oxidation and catalytic properties of La1 − xSrxCoO3.* Journal of Catalysis, 1983. **83**(1): p. 151-159.
89. Arai, H., et al., *Catalytic combustion of methane over various perovskite-type oxides.* Applied Catalysis, 1986. **26**(0): p. 265-276.
90. Cao, G.Z., *Electrical conductivity and oxygen semipermeability of terbia and yttria stabilized zirconia.* Journal of Applied Electrochemistry, 1994. **24**(12): p. 1222-1227.
91. Martynczuk, J., et al., *Performance of zinc-doped perovskite-type membranes at intermediate temperatures for long-term oxygen permeation and under a carbon dioxide atmosphere.* Journal of Membrane Science, 2009. **344**(1–2): p. 62-70.
92. Martynczuk, J., M. Arnold, and A. Feldhoff, *Influence of grain size on the oxygen permeation performance of perovskite-type (Ba0.5Sr0.5)(Fe0.8Zn0.2)O3−δ membranes.* Journal of Membrane Science, 2008. **322**(2): p. 375-382.
93. Vente, J.F., et al., *Properties and performance of BaxSr1-xCo 0.8Fe0.2O3-δ materials for oxygen transport membranes.* Journal of Solid State Electrochemistry, 2006. **10**(8): p. 581-588.
94. Ishigaki, T., et al., *Diffusion of oxide ion vacancies in perovskite-type oxides.* Journal of Solid State Chemistry, 1988. **73**(1): p. 179-187.
95. Kuhn, M., et al., *Oxygen nonstoichiometry and thermo-chemical stability of perovskite-type La0.6Sr0.4Co1-yFeyO 3-δ (y = 0, 0.2, 0.4, 0.5, 0.6, 0.8, 1) materials.* Journal of the Electrochemical Society, 2013. **160**(1): p. F34-F42.
96. Ito, W., T. Nagai, and T. Sakon, *Oxygen separation from compressed air using a mixed conducting perovskite-type oxide membrane.* Solid State Ionics, 2007. **178**(11-12): p. 809-816.
97. Cheng, Y., et al., *Investigation of Ba fully occupied A-site BaCo0.7Fe0.3-xNbxO3-δ perovskite stabilized by low concentration of Nb for oxygen permeation membrane.* Journal of Membrane Science, 2008. **322**(2): p. 484-490.
98. Diethelm, S. and J. Van herle, *Oxygen transport through dense La0.6Sr0.4Fe0.8Co0.2O3-δ perovskite-type permeation membranes.* Journal of the European Ceramic Society, 2004. **24**(6): p. 1319-1323.
99. Song, S., et al., *Oxygen permeation and partial oxidation of methane reaction in Ba0.9Co0.7Fe0.2Nb0.1O3−δ oxygen permeation membrane.* Journal of Membrane Science, 2012. **415–416**(0): p. 654-662.
100. Song, J., et al., *BaCe0.85Tb0.05Co0.1O3−δ perovskite hollow fibre membranes for hydrogen/oxygen permeation.* International Journal of Hydrogen Energy, 2013. **38**(19): p. 7904-7912.
101. Park, J.H., K.Y. Kim, and S.D. Park, *Oxygen permeation and stability of La0.6Sr0.4TixFe1−xO3−δ (x = 0.2 and 0.3) membrane.* Desalination, 2009. **245**(1–3): p. 559-569.
102. Kim, J.P., et al., *Significant improvement of the oxygen permeation flux of tubular Ba0.5Sr0.5Co0.8Fe0.2O3 − δ membranes covered by a thin La0.6Sr0.4Ti0.3Fe0.7O3 − δ layer.* Materials Letters, 2011. **65**(14): p. 2168-2170.

103. Kim, J.-M., et al., *Properties of oxygen permeation and partial oxidation of methane in La0.6Sr0.4CoO3−δ (LSC)–La0.7Sr0.3Ga0.6Fe0.4O3−δ (LSGF) membrane.* Journal of Membrane Science, 2005. **250**(1–2): p. 11-16.
104. Tan, X., et al., *La0.7Sr0.3FeO3−α perovskite hollow fiber membranes for oxygen permeation and methane conversion.* Separation and Purification Technology, 2012. **96**(0): p. 89-97.
105. Yang, N.-T., Y. Kathiraser, and S. Kawi, *A new asymmetric SrCo0.8Fe0.1Ga0.1O3−δ perovskite hollow fiber membrane for stable oxygen permeability under reducing condition.* Journal of Membrane Science, 2013. **428**(0): p. 78-85.
106. Wang, Z., et al., *Ultra-high oxygen permeable BaBiCoNb hollow fiber membranes and their stability under pure CH4 atmosphere.* Journal of Membrane Science, 2014. **465**(0): p. 151-158.
107. Vivet, A., et al., *New route for high oxygen semi-permeation through surface-modified dense La1â˜xSrxFe1â˜yGayO3â˜Î´ perovskite membranes.* Journal of Membrane Science, 2014. **454**(0): p. 97-108.
108. Hayamizu, Y., M. Kato, and H. Takamura, *Effects of surface modification on the oxygen permeation of Ba0.5Sr0.5Co0.8Fe0.2O3â˜Î´ membrane.* Journal of Membrane Science, 2014. **462**(0): p. 147-152.
109. Jiang, Q., K.J. Nordheden, and S.M. Stagg-Williams, *Oxygen permeation study and improvement of Ba0.5Sr0.5Co0.8Fe0.2Ox perovskite ceramic membranes.* Journal of Membrane Science, 2011. **369**(1–2): p. 174-181.
110. Leo, A., S. Liu, and J.C.D.d. Costa, *Development of mixed conducting membranes for clean coal energy delivery.* International Journal of Greenhouse Gas Control, 2009. **3**(4): p. 357-367.
111. Shao, Z. and S.M. Halle, *A high-performance cathode for the next generation of solid-oxide fuel cells.* Nature, 2004. **431**(7005): p. 170-173.
112. Omata, K., et al., *Oxidative coupling of methane using a membrane reactor.* Applied Catalysis, 1989. **52**(1): p. L1-L4.
113. Lafarga, D., J. Santamaria, and M. Menéndez, *Methane oxidative coupling using porous ceramic membrane reactors—I. reactor development.* Chemical Engineering Science, 1994. **49**(12): p. 2005-2013.
114. Thursfield, A., et al., *Chemical looping and oxygen permeable ceramic membranes for hydrogen production - a review.* Energy & Environmental Science, 2012. **5**(6): p. 7421-7459.
115. Liu, J.-j., et al., *Partial oxidation of methane in a Zr0.84Y0.16O1.92–La0.8Sr0.2Cr0.5Fe0.5O3−δ hollow fiber membrane reactor targeting solid oxide fuel cell applications.* Journal of Power Sources, 2012. **217**(0): p. 287-290.
116. Shao, Z., et al., *Investigation of the permeation behavior and stability of a Ba0.5Sr0.5Co0.8Fe0.2O3−δ oxygen membrane.* Journal of Membrane Science, 2000. **172**(1–2): p. 177-188.
117. Shao, Z., et al., *Performance of a mixed-conducting ceramic membrane reactor with high oxygen permeability for methane conversion.* Journal of Membrane Science, 2001. **183**(2): p. 181-192.
118. Thursfield, A. and I.S. Metcalfe, *Methane oxidation in a mixed ionic–electronic conducting ceramic hollow fibre reactor module.* Journal of Solid State Electrochemistry, 2006. **10**(8): p. 604-616.
119. Balachandran, U., et al., *Dense ceramic membranes for partial oxidation of methane to syngas.* Applied Catalysis A: General, 1995. **133**(1): p. 19-29.

120. Kathiraser, Y. and S. Kawi, *La0.6Sr0.4Co0.8Ga0.2O3-δ (LSCG) hollow fiber membrane reactor: Partial oxidation of methane at medium temperature.* AIChE Journal, 2013. **59**(10): p. 3874-3885.
121. Kniep, J. and Y.S. Lin, *Partial oxidation of methane and oxygen permeation in SrCoFeOx membrane reactor with different catalysts.* Industrial and Engineering Chemistry Research, 2011. **50**(13): p. 7941-7948.
122. Tsai, C.-Y., et al., *Dense perovskite membrane reactors for partial oxidation of methane to syngas.* AIChE Journal, 1997. **43**(S11): p. 2741-2750.
123. Yang, N.-T., Y. Kathiraser, and S. Kawi, *La0.6Sr0.4Co0.8Ni0.2O3−δ hollow fiber membrane reactor: Integrated oxygen separation – CO2 reforming of methane reaction for hydrogen production.* International Journal of Hydrogen Energy, 2013. **38**(11): p. 4483-4491.
124. Slade, D.A., et al., *Mixed-conducting oxygen permeable ceramic membranes for the carbon dioxide reforming of methane.* Green Chemistry, 2007. **9**(6): p. 577-581.
125. San José-Alonso, D., M.J. Illán-Gómez, and M.C. Román-Martínez, *Low metal content Co and Ni alumina supported catalysts for the CO2 reforming of methane.* International Journal of Hydrogen Energy, 2013. **38**(5): p. 2230-2239.
126. Han, K.-S., et al., *Direct methane cracking using a mixed conducting ceramic membrane for production of hydrogen and carbon.* International Journal of Hydrogen Energy, 2013. **38**(36): p. 16133-16139.
127. Zhang, Y., et al., *A novel tubular oxygen-permeable membrane reactor for partial oxidation of CH4 in coke oven gas to syngas.* International Journal of Hydrogen Energy, 2013. **38**(21): p. 8783-8789.
128. Balachandran, U., et al., *Use of mixed conducting membranes to produce hydrogen by water dissociation.* International Journal of Hydrogen Energy, 2004. **29**(3): p. 291-296.
129. Balachandran, U., T.H. Lee, and S.E. Dorris, *Hydrogen production by water dissociation using mixed conducting dense ceramic membranes.* International Journal of Hydrogen Energy, 2007. **32**(4): p. 451-456.
130. Jiang, H., et al., *Improved water dissociation and nitrous oxide decomposition by in situ oxygen removal in perovskite catalytic membrane reactor.* Catalysis Today, 2010. **156**(3–4): p. 187-190.
131. Park, C.Y., et al., *Hydrogen production from fossil and renewable sources using an oxygen transport membrane.* International Journal of Hydrogen Energy, 2010. **35**(9): p. 4103-4110.
132. Cao, Z., et al., *Simultaneous overcome of the equilibrium limitations in BSCF oxygen-permeable membrane reactors: Water splitting and methane coupling.* Catalysis Today, 2012. **193**(1): p. 2-7.
133. Park, C.Y., et al., *A cobalt-free oxygen transport membrane, BaFe0.9Zr0.1O3−δ, and its application for producing hydrogen.* International Journal of Hydrogen Energy, 2013. **38**(15): p. 6450-6459.
134. Armor, J.N., *Applications of catalytic inorganic membrane reactors to refinery products.* Journal of Membrane Science, 1998. **147**(2): p. 217-233.
135. van Doorn, R.H.E., H.J.M. Bouwmeester, and A.J. Burggraaf, *Kinetic decomposition of La0.3Sr0.7CoO3−δ perovskite membranes during oxygen permeation.* Solid State Ionics, 1998. **111**(3–4): p. 263-272.
136. Wang, B., et al., *Stabilities of La0.6Sr0.4Co0.2Fe0.8O3−δ oxygen separation membranes—Effects of kinetic demixing/decomposition and impurity segregation.* Journal of Membrane Science, 2009. **344**(1–2): p. 101-106.

137. Wang, B., et al., *A further investigation of the kinetic demixing/decomposition of La0.6Sr0.4Co0.2Fe0.8O3−δ oxygen separation membranes.* Journal of Membrane Science, 2011. **369**(1–2): p. 526-535.
138. Iguchi, F., et al., *Oxygen permeation properties and the stability of La0.6Sr0.4Fe0.8Co0.2O3 studied by Raman spectroscopy.* Solid State Ionics, 2006. **177**(26–32): p. 2281-2284.
139. Dong, X. and W. Jin, *Mixed conducting ceramic membranes for high efficiency power generation with CO2 capture.* Current Opinion in Chemical Engineering, 2012. **1**(2): p. 163-170.
140. Lein, H.L., et al., *High-temperature creep behavior of mixed conducting la0.5Sr 0.5Fe1-xCoxO3-8 (0.5 ≤ x ≤ 1) materials.* Journal of the American Ceramic Society, 2006. **89**(9): p. 2895-2898.
141. Rutkowski, B., et al., *Creep behaviour of tubular Ba0.5Sr0.5Co0.8Fe0.2O3−δ gas separation membranes.* Journal of the European Ceramic Society, 2011. **31**(4): p. 493-499.
142. Huang, B.X. and J. Malzbender, *The effect of an oxygen partial pressure gradient on the mechanical behavior of perovskite membrane materials.* Journal of the European Ceramic Society, 2014. **34**(7): p. 1777-1782.
143. Pećanac, G., S. Baumann, and J. Malzbender, *Mechanical properties and lifetime predictions for Ba0.5Sr0.5Co0.8Fe0.2O3−δ membrane material.* Journal of Membrane Science, 2011. **385–386**(0): p. 263-268.
144. Sharma, K., et al., *A new formulation of barium–strontium silicate glasses and glass-ceramics for high-temperature sealant.* International Journal of Hydrogen Energy, 2012. **37**(15): p. 11360-11369.
145. Zhang, T. and Q. Zou, *Tuning the thermal properties of borosilicate glass ceramic seals for solid oxide fuel cells.* Journal of the European Ceramic Society, 2012. **32**(16): p. 4009-4013.
146. Vivet, A., et al., *Influence of glass and gold sealants materials on oxygen permeation performances in La0.8Sr0.2Fe0.7Ga0.3O3−δ perovskite membranes.* Journal of Membrane Science, 2011. **366**(1–2): p. 132-138.
147. Qi, X., F.T. Akin, and Y.S. Lin, *Ceramic–glass composite high temperature seals for dense ionic-conducting ceramic membranes.* Journal of Membrane Science, 2001. **193**(2): p. 185-193.
148. Liang, F., et al., *High-purity oxygen production by a dead-end Ba0.5Sr0.5Co0.8Fe0.2O3−δ tube membrane.* Catalysis Today, 2012. **193**(1): p. 95-100.
149. Tan, X., Y. Liu, and K. Li, *Preparation of LSCF Ceramic Hollow-Fiber Membranes for Oxygen Production by a Phase-Inversion/Sintering Technique.* Industrial & Engineering Chemistry Research, 2004. **44**(1): p. 61-66.
150. Buysse, C., et al., *Fabrication and oxygen permeability of gastight, macrovoid-free Ba0.5Sr0.5Co0.8Fe0.2O3−δ capillaries for high temperature gas separation.* Journal of Membrane Science, 2010. **359**(1–2): p. 86-92.
151. Franca, R.V., *Perovskite Microtubular Membranes for Pure Hydrogen Production from Water Splitting*, in *School of Chemical Engineering and Advanced Materials*. 2013, Newcastle University, UK: United Kingdpm.
152. Lindsay, A.L. and L.A. Bromley, *Thermal Conductivity of Gas Mixtures.* Industrial & Engineering Chemistry, 1950. **42**(8): p. 1508-1511.
153. Minter, C.C., *Thermal conductivity of binary mixtures of gases. I. Hydrogen-helium mixtures.* The Journal of Physical Chemistry, 1968. **72**(6): p. 1924-1926.

154. Chen, Z. and C. Lu, *REVIEW Humidity Sensors: A Review of Materials and Mechanisms* Sensor Letter, 2005. **3**: p. 274-295.
155. Leo, A., S. Liu, and J.C. Diniz da Costa, *Production of pure oxygen from BSCF hollow fiber membranes using steam sweep.* Separation and Purification Technology, 2011. **78**(2): p. 220-227.
156. Geffroy, P.M., et al., *Rational selection of MIEC materials in energy production processes.* Chemical Engineering Science, 2013. **87**(0): p. 408-433.
157. Evdou, A., V. Zaspalis, and L. Nalbandian, *La(1−x)SrxMnO3−δ perovskites as redox materials for the production of high purity hydrogen.* International Journal of Hydrogen Energy, 2008. **33**(20): p. 5554-5562.
158. Tan, X., et al., *Enhancement of oxygen permeation through La0.6Sr0.4Co0.2Fe0.8O3−δ hollow fibre membranes by surface modifications.* Journal of Membrane Science, 2008. **324**(1–2): p. 128-135.
159. Pino, L., et al., *Catalytic partial-oxidation of methane on a ceria-supported platinum catalyst for application in fuel cell electric vehicles.* Applied Catalysis A: General, 2002. **225**(1–2): p. 63-75.
160. Souza, M.M.V.M. and M. Schmal, *Combination of carbon dioxide reforming and partial oxidation of methane over supported platinum catalysts.* Applied Catalysis A: General, 2003. **255**(1): p. 83-92.
161. Ballarini, A., et al., *Platinum supported on alkaline and alkaline earth metal-doped alumina as catalysts for dry reforming and partial oxidation of methane.* Applied Catalysis A: General, 2012. **433–434**(0): p. 1-11.
162. Deutschmann, O. and L.D. Schmidt, *Modeling the partial oxidation of methane in a short-contact-time reactor.* AIChE Journal, 1998. **44**(11): p. 2465-2477.

Appendices

A.1 Error Propagation

Based on the GCA and GCB readings, the mole fraction obtained for the water splitting coupled methane reforming reported in section 3.3.3 is as follows (refer Table 3.3).

Appendix 1: Mole fractions of the inlet and outlet gases for the water splitting coupled methane experiment. The shell side was fed with 30mlmin^{-1} of 5% methane balance in argon and the lumen side was fed with 30mlmin^{-1} of 4% water balance in argon.

	Lumen side/ Mole fraction (%)	Shell side/ mole fraction (%)				
	H_2	H_2	CO	CH_4	CO_2	H_2O
Inlet	-	-	-	5.00± 0.50	-	-
Outlet	0.16± 0.02	0.42± 0.04	0.16± 0.02	4.71± 0.47	0.02± 0.002	-

Following Equation 3.3, the calculation of the OP_{SS} rate is as follow;

$$OP_{SS} = \frac{[(0.16-0)+2(0.02-0)]}{100}\left(30\text{mLmin}^{-1} \times \frac{1}{24465\text{mLmol}^{-1}} \times \frac{1\text{min}}{60\text{s}}\right)$$

$$= 0.04\ \mu\text{molO}.\text{s}^{-1}$$

Using the 10% error level explained and described before in section 3.2.4, the $OP_{SS_{min}}$ can be calculated as follows (refer Equation 3.6);

$$OP_{SS_{min}} = \frac{[(0.14-0)+2(0.02-0)]}{100}\left(27\text{mLmin}^{-1} \times \frac{1}{24465\text{mLmol}^{-1}} \times \frac{1\text{min}}{60\text{s}}\right)$$

$$= 0.03\ \mu\text{molO}.\text{s}^{-1}$$

And the $OP_{SS_{max}}$ can be calculated using Equation 3.7. Example for calculation is as follows;

$$OP_{SS_{max}} = \frac{[(0.18-0)+2(0.02-0)]}{100}\left(33\text{mLmin}^{-1} \times \frac{1}{24465\text{mLmol}^{-1}} \times \frac{1\text{min}}{60\text{s}}\right)$$

$$= 0.05\ \mu\text{molO}.\text{s}^{-1}$$

The deviation between the OP_{SS} and $OP_{SS_{min}}$ is 0.01μmolO.s^{-1}. The same deviation value is also obtained between OP_{SS} and $OP_{SS_{max}}$. This makes the largest deviation for the error associated to OP_{SS} is 0.01 μmolO.s^{-1}. Thus the value reported for the OP_{SS} for water splitting coupled methane reforming is (0.04 ± 0.01) μmolO.s^{-1}

In certain cases where there is a larger deviation of either from the min or max readings, the largest amount of deviation will be considered as the new error level to be reported together with the oxygen permeation rates in the thesis.